UNIVERSITA' DEGLI STUDI DI PISA

DIPARTIMENTO DI FARMACIA

SCUOLA DI DOTTORATO DI RICERCA IN "FISIOPATOLOGIA CLINICA E SCIENZA DEL FARMACO"

PROGRAMMA: "SCIENZA DEL FARMACO E DELLE SOSTANZE BIOATTIVE"

TESI DI DOTTORATO

The endocannabinoid system:

1. Design, synthesis and biological evaluation of heterocyclic derivatives as potential MAGL inhibitors.

2. Study of the ischemic damage effects in cannabinoid receptors knockout mice.

Direttore del corso di Dottorato di Ricerca:

Prof. Adriano Martinelli

Autore:

Dr. Francesca Castelli

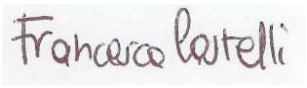

A thesis submitted in fulfillment of the requirements for the degree of Doctor of Clinic Phisiopathology and Science of Drugs, University of Pisa, 2013.

Index

8. REFERENCES

Ad Alessandro ed Andrea …

4 INTRODUCTION

1.1 Endocannabinoid system (ECS)

The ECS is constitute by the two cannabinoid receptors (CBRs), the central CB1 (CBR1 or CB1R) and the peripheral CB2 (CB2R or CBR2), together with their endogenous ligands or endocannabinoids and the enzymes responsible for their metabolism fatty acid amide hydrolyze (FAAH) and monoglyceride lipase (MAGL or MGL). However, more recent data has suggested that this is an oversimplification, in fact some studies demonstrated the presence of non-neuronal CB1R, furthermore other projects showed that CB2R has a limited central nervous system distribution. Moreover there is evidence for additional CB-like receptors (such as GPR55, GPR18, TRPV channels…), but currently the evidence is not considered sufficiently strong for them to be formally included in the CB receptor family.[1] The proposed endogenous ligands (Fig. 1) are arachidonic acid derivatives in which the acid chain is bound to a polar head group (ethanolamine or glycerol) by amide (such as anandamide or *N*-arachidonoylethanolamine (**1**), AEA), ester (2-arachidonoylglycerol or 2-AG (**2**) and virodhamine (**3**)) or ether functionalities (2-arachidylglycerol or noladin ether (**4**)).

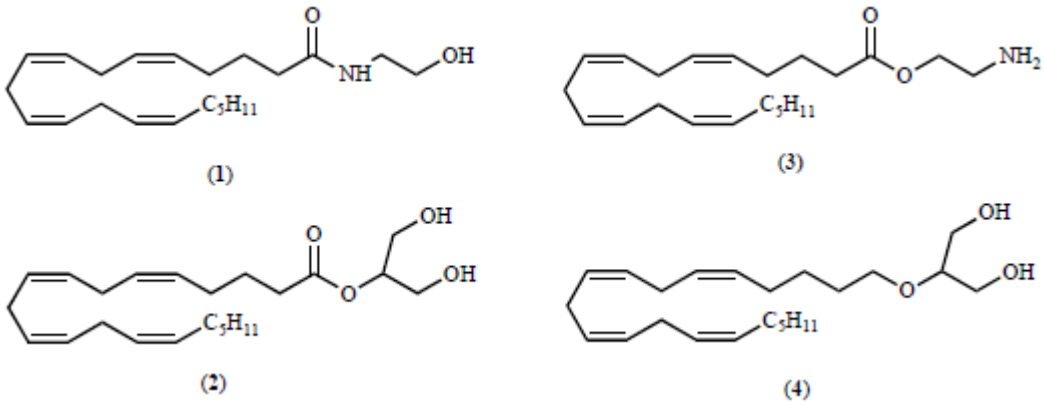

Fig. 1. Structures of the cannabinoid receptor ligands anandamide (**1**), 2-arachidonoylglycerol (**2**), virodhamine (**3**) and noladin ether (**4**)

1.2 Endocannabinoid receptors

Within the CNS, CB1 receptors are mainly expressed in the basal ganglia, cerebellum, hippocampus, and cortex [2, 3, 4], and their activation has been associated with most of the psychotropic and behavioral actions of cannabinoid drugs. By contrast, CB2 receptors are primarily localized in cells involved inimmune and inflammatory

responses.[5] CB2 receptors are also expressed in the cerebellum and brain stem [6, 7] and they modulate the mobility and function of microglial cells in vitro and in vivo.

Both receptor subtypes are $G_{i/o}$-coupled and, when activated, they initiate signaling events typically associated with this class of G-proteins, e.g., inhibition of cAMP accumulation and cAMP dependent protein kinase (PKA).[9] Noteworthy, CB1 receptors are also constitutively active in the absence of exogenously applied agonists [8] and distinct cannabinoid ligands have been shown to promote CB1 coupling to different G_i isoforms [9]. CB1 receptors may also couple to Gs proteins and form heterodimers with dopamine D2 and mu-opioid receptors. Agonist-dependent activation of different signaling pathways has been also described for CB2 receptors .

Consistent with their proposed modulatory role of inhibitory and excitatory neurotransmission, CB1 receptors are located presynaptically on GABAergic neurons and interneurons and on glutamatergic terminals. CB1 expression and activity is regulated via multiple mechanisms.

In particular, extracellular signal-regulated kinase (ERK) and focal adhesion kinase (FAK) have been shown to affect CB1 gene expression in neurons and to participate in changes in synaptic plasticity observed after administration of cannabinoid agonists.[10]

The development of CB1 and CB2 knockout mice on different backgrounds (CD1, C57BL), and of mutant mice lacking the CB1 receptors in neuronal subpopulations has improved our understanding of the biological roles played by these receptors in vivo and showed that some of the effects of cannabinoid agonists persist after the ablation of CB1 and CB2 genes. These non-CB1/CB2 targets include other G-protein-coupled receptors (GPCR), ion channels (TRPV receptors) and nuclear receptors (PPAR).

1.3 Endocannabinoids and metabolizing enzymes

The endocannabinoids are a family of endogenous signaling lipids that activate cannabinoid and non-CB1/CB2 receptors.

Unlike classic neurotransmitters, endocannabinoids are not stored in synaptic vesicles, but are produced on demand by stimulus dependent cleavage of membrane phospholipid precursors . To date, arachidonoyl ethanolamide (anandamide, AEA) and 2-arachidonylglycerol (2-AG) are the best-characterized examples (Fig. 2) [11, 12, 13]

.

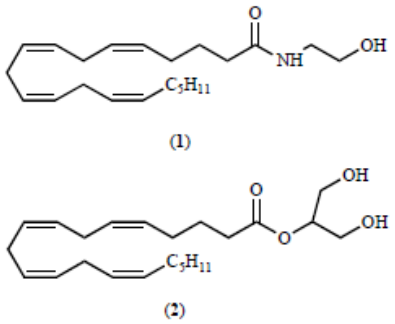

Fig. 2. Structures of the cannabinoid receptor ligands anandamide (**1**), 2-arachidonoylglycerol (**2**)

AEA acts as partial agonist at CB1 and CB2 receptors and mimics most of the pharmacological effects produced by cannabinoid drugs in vitro (inhibition of adenylyl cyclase activity) and in vivo (e.g., analgesia, hypomotility, hypothermia). AEA is synthesized from the deacylation of the phospholipid precursor N-arachidonoyl phosphatidylethanolamine (NAPE) via a Ca^{2+}-dependent process involving a NAPE-specific PLD activity. In rat hippocampus, NAPE-PLD is located pre-synaptically on excitatory terminals, in the proximity of intracellular calcium stores. The location of the biosynthetic machinery of AEA is remarkably different from that of 2-AG (post-synaptic), suggesting distinct physiological roles for these two endocannabinoids. Interestingly, no significant changes in the levels of brain AEA have been found in NAPE-PLD knockout mice, indicating the existence of additional biosynthetic pathways, such as those initiated by the recently identified α/β-hydrolase 4 (ABHD 4). [14]

The biological actions of AEA are terminated via a two-step process consisting of facilitated diffusion into cells via a carrier mediated transport, followed by enzymatic hydrolysis via a fatty acid amide hydrolase (FAAH).[14]

Enzymes other than FAAH can metabolize AEA. For example, AEA is a substrate for cycloxygenase-2 (COX-2) (Fig. 3). [15]

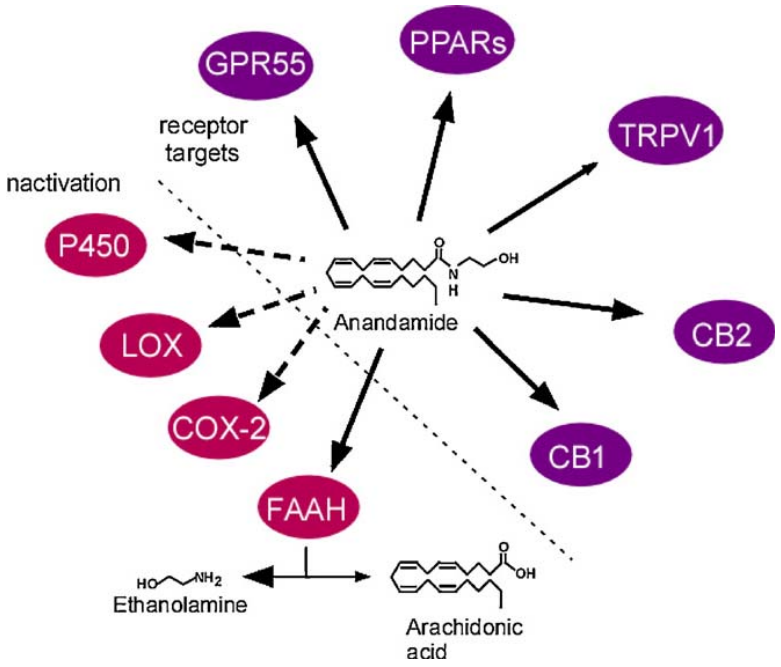

Fig. 3. Receptor targets and metabolic enzymes of anandamide. Anandamide can activate GPCR receptors, suchasCB1, CB2 and GPR55, ionotropic (TRP) receptors, such TRPV1 and the nuclear receptors PPARs (alpha and gamma subtypes). Anandamide is hydrolyzed into ethanolamine and arachidonic acid by fatty acid amide hydrolase (FAAH) and can serve as a substrate, although with low affinity, for cycloxygenase-2 (COX-2), 12- and 15-lipoxygenases (LOXs) and P450.

The result of this cyclooxygenation is the formation of prostaglandin-like compounds (prostamides), which have weak effects at prostanoid receptors. Administration of exogenous AEA to FAAH−/− mice leads to the production of detectable levels of prostamides, suggesting that the COX-2 metabolic pathway becomes physiologically relevant under conditions affecting FAAH activity or promoting COX-2 upregulation, as in the case of neurodegenerative diseases or tissue damage. In addition, lipoxygenases (12-LOX and 15-LOX) and P450 (Fig. 3), including its major brain isoform CYP2D6 [128], convert AEA into biologically active metabolites that exert their biological actions via cannabinoid, PPAR and TRPV1 receptors.[16] However, the functional role of these substances in the CNS has not been determined.

2-AG is a full agonist at cannabinoid receptors, although less potent than AEA, stimulates GPR55 receptors in transfected cells, acts as a retrograde messenger on pre-synaptic CB1 receptors located on excitatory and inhibitory synapses to inhibit neurotrasmitter release, and is an autocrine mediator of post-synaptic slow self-inhibition (SSI) of neocortical interneurons . In the brain, 2-AG is synthesized via a receptor/Gq-initiated sequential hydrolysis of inositol phospholipids containing arachidonic acid by diacylglycerol lipase (DAGL).

Experimental evidence suggests that 2-AG is accumulated intracellularly by the same carrier protein mediating AEA re-uptake and that this putative carrier is not regulated by 2-AG metabolizing enzymes, at least in vitro. Although 2-AG can be

metabolized by FAAH [150] and the serine hydrolase MAGL is the major hydrolyzing enzyme in intact neurons (Fig. 4). [17, 18]

As in the case of AEA, other enzymes, including COX-2 and LOX, can metabolize 2-AG. The COX-2-derived metabolite, PGE2 glycerol ester has been shown to modulate miniature inhibitory currents and to affect long-term potentiation (LTP) in mouse hippocampus in a CB1-independent fashion (Fig. 4).

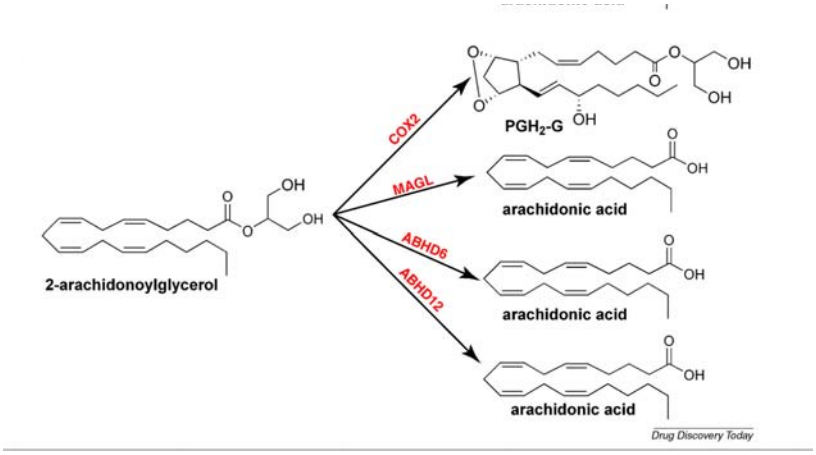

Fig. 4. Schematic representation of 2-AG inactivating pathways. 2-Arachidonoylglycerol signaling is terminated by MAGL, ABHD6 or ABHD12- mediated hydrolysis or by COX2 oxidation into PGH2-G. Note that arachidonic acid, PGH2-EA and PGH2-G can be further transformed into other bioactive lipids, such as prostaglandins and endocannabinoid-derived prostaglandins, respectively.

Unlike AEA, 2-AG does not directly activate TRPV1 or PPAR receptors but can bind to non-CB1/CB2 targets as suggested by the observation that the behavioral effects induced by N-arachidonyl maleimide (NAM), a selective MAGL inhibitor with in vivo efficacy, are only partially reversed by the CB1 antagonist Rimonabant.

In summary, the endocannabinoids are emerging as important signaling lipids in the CNS that modulate excitatory and inhibitory neurotransmission and synaptic plasticity. These lipids do not bind metabotropic cannabinoid receptors exclusively, but display significant promiscuity as they activate ionotropic and nuclear targets (TRPV1 and PPAR receptors) as well as other non-CB1/CB2 receptors.

The characterization of the endocannabinoid biosynthetic and metabolic pathways has led to the discovery of novel molecular entities, such as NAPE-PLD, FAAH and MAGL, which can be targeted pharmacologically not only to manipulate endocannabinoid levels, but also to investigate the role of the endocannabinoid system in physiological and pathological conditions. In this regard, the development of more selective FAAH/MAGL inhibitors with significant in vivo activity is crucial to understand the specific biological actions of AEA, 2-AG and their metabolites in living animals.

Part 1: DESIGN, SYNTHESIS AND BIOLOGYCAL EVALUATION OF HETEROCYCLIC DERIVATIVES AS POTENTIAL MAGL INHIBITORS

2. MAGL

2.1 MAGL: Structure and most important residues[19]

As reported before MAGL is the enzyme that catalyzed the hydrolysis of 2-AG.

In 2005, the first homology model of MAGL was presented based on 3D structure of chloroperoxidase from Streptomyces lividans as the template. As a result of poor sequence homology between MAGL and chloroperoxidase, the homology model offered limited insights into the overall structure and organization of MAGL protein. However, as the central core of the α/β hydrolase superfamily members is highly conserved, the model offered first insights into the MAGL active site with the catalytic triad: serine 122 (S122), aspartic acid 239 (D239) and histidine 269 (H269), previously identified based on mutagenesis studies (Fig. 5). The model also suggested that two cysteine residues (C208 and C242) were located within a close distance from the active site and it was suggested that one or both of these cysteines were potential targets of the maleimide-based inhibitor NAM (Fig. 7, Fig. 8). Site-directed mutagenesis studies have provided experimental support for these predictions.[20]

The crystal structure of MAGL was recently solved and this was achieved independently by two laboratories. Labar et al. solved the structure of human MAGL at 2.2 Å resolution and interestingly, MAGL crystallized in this study as a dimer. Bertrand et al. resolved the crystal structure of human MAGL both in its apoenzyme form and in complex with the potent covalent inhibitor SAR629 (for more details about the compound see below). As expected, protein folds conserved in the α/β hydrolase superfamily were present also in the MAGL structure. These include an eight-stranded β-sheet, composed of seven parallel strands and one antiparallel strand, surrounded by α helices. Moreover, a flexible cap domain covers the structurally conserved β-sheet and a lid domain guards the entrance of a relatively large, occluded hydrophobic tunnel (approx. 25 Å in length and approx. 8 Å in width), and the active site is buried at the bottom of the tunnel (Fig. 5 B). [20]

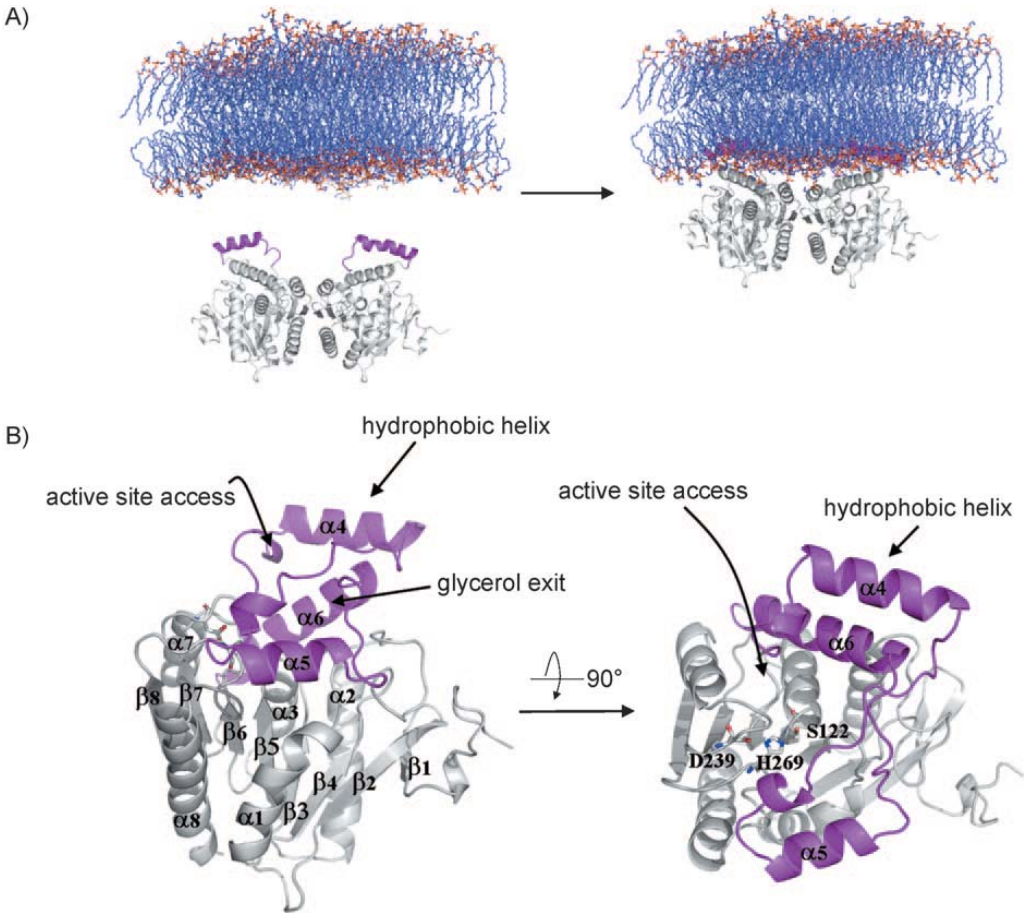

Fig. 5. Overall structure of *h*MAGL. A) MAGL asymmetric unit. α4 helix is colored magenta. Membrane representation is a palmitoyloleoylphosphatidylethanolamine bilayer minimized using molecular dynamics simulation. B) Left: Side view of a MAGL monomer, with catalytic triad represented as sticks, and cap domain colored magenta. Right: Top view (908 rotation) of the same MAGL subunit.[19]

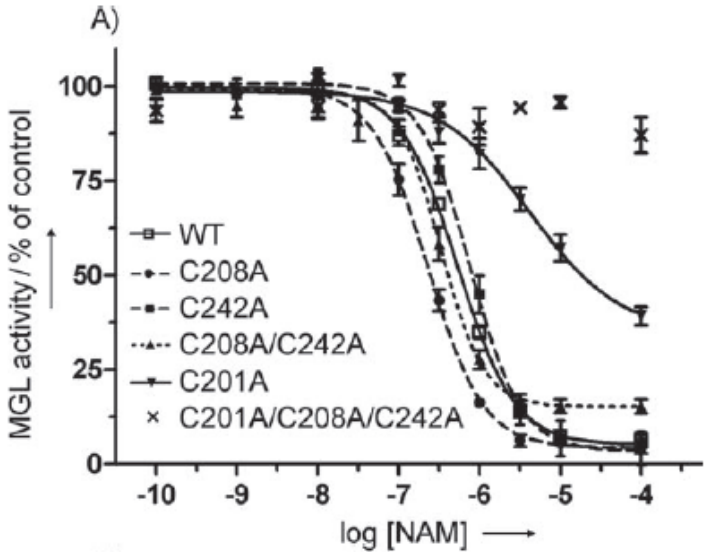

Fig. 6. NAM inhibits human MAGL by targeting Cys201. A) Dose-dependent inhibition of wild-type and mutant MAGL by NAM. Values are expressed as percent of control and represent mean ±SEM of at least four experiments done in duplicate.[19]

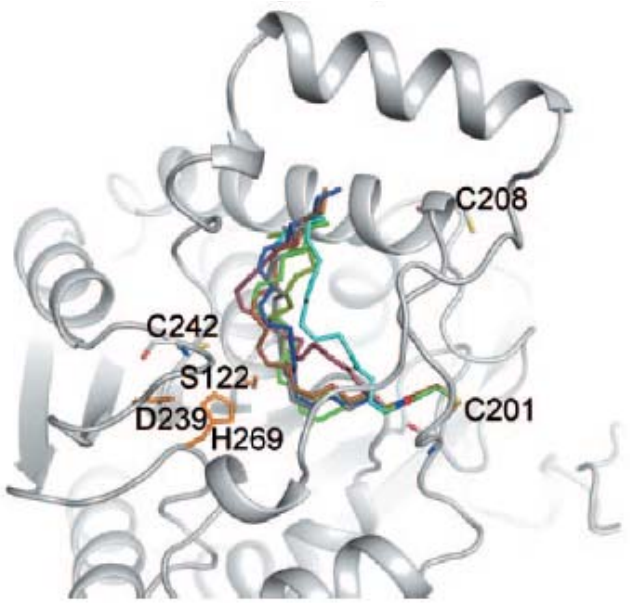

Fig. 7. Docking of NAM in the active site of MAGL, bound to Cys201. The main conformations found by using Gold software are represented with different colours. Catalytic triad is coloured in orange, and Cys201, Cys208 and Cys242 are represented.[20]

2.2 Binding of the natural substrate

Elucidation of the MAGL structure provides the first structural basis for rational drug design. To illustrate this and to highlight some key structural features of the active site, 2-AG has been docked in MAGL (Fig. 8, Fig.9). This reveals a cavity able to accommodate the long and flexible lipid chain of the substrates. The near environment of the catalytic triad (Ser122, Asp239 and His269) presents a more hydrophilic character than the channel pointing towards the enzyme surface. Besides the backbone NH from Met123 and Ala51, which form the "oxyanion hole," the Tyr58 hydroxyl group, the NH from the His121 and His272 side chains, the guanidinium from Arg57, the carboxylate from Glu53, and the backbone carbonyl from Ala51 delimit a polar cavity that accommodates the polar glycerol head group of 2-AG. A positive electron density feature was apparent in the vicinity of the oxyanion hole at the end of the structure-refinement process. This was located at the entry of this polar cavity and precisely at the same place as the glycerol moiety in 2-AG docking results. [21]

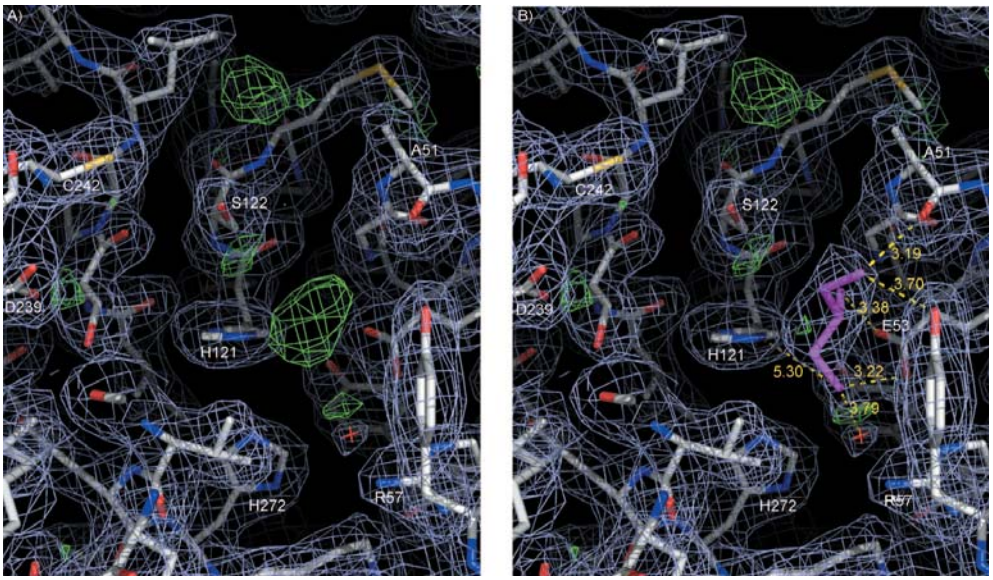

Fig. 8. Docking of 2-AG in the active site of MAGL.[21]

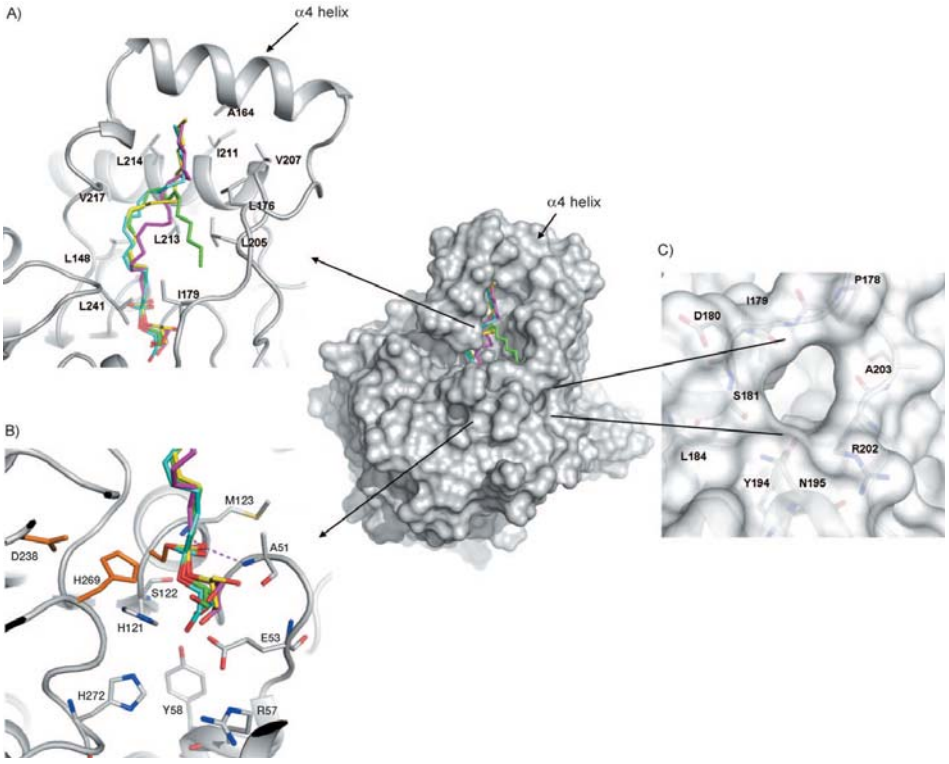

Fig. 9. Docking of 2-AG in the active site of MAGL. The natural substrate is bound in the tetrahedral intermediate state to Ser122. The four first conformations found by using Gold software are represented using different colours. A) Acyl-binding and B) alcohol-binding sites are highlighted, as well as C) the glycerollexit channel. Side chains of residues interacting with the 2-AG acyl moiety or lining the hydrophilic cavity are represented as sticks. The interactions in the oxyanion hole are represented with dashed lines. The a4 helix is also indicated by arrows.[21]

2.3 Catalytic mechanism

The kinetics of lipolytic enzymes can be considered as a two-phase process that includes a first binding step followed by hydrolysis of the substrate. As a general feature of lipases, they can hydrolys monomeric substrate molecules, but only after binding to the substrate interface, conversion of the aggregated substrate can take place. Once the substrate reaches the active site, its ester bond is hydrolysed in a mechanism similar to that of serine proteases. Catalysis is initiated by nucleophilic attack of the serine hydroxyl on the susceptible carbonyl carbon of the substrate. This attack is facilitated by a general acid-base mechanism in which the serine is activated by a hydrogen bond in relay with histidine and aspartate or glutamate. Afterwards, a tetrahedral acyl-enzyme is formed, which is stabilized by the "oxyanion hole". In general, the "oxyanion hole" is not preformed but is created by the opening of the lid and the exposure of a substrate-binding pocket. Collapse of the tetrahedral adduct in the forward direction involves expulsion of the leaving group (corresponding to the alcohol moiety) and generation of a second acyl-enzyme complex. Finally, the deacylation step involves the attack of a water molecule at the active site. Similarly to the catalytic serine, the water molecule is activated as a more effective nucleophile due to the proton shuttling of the charge-relay system (Fig. 10).[19, 21]

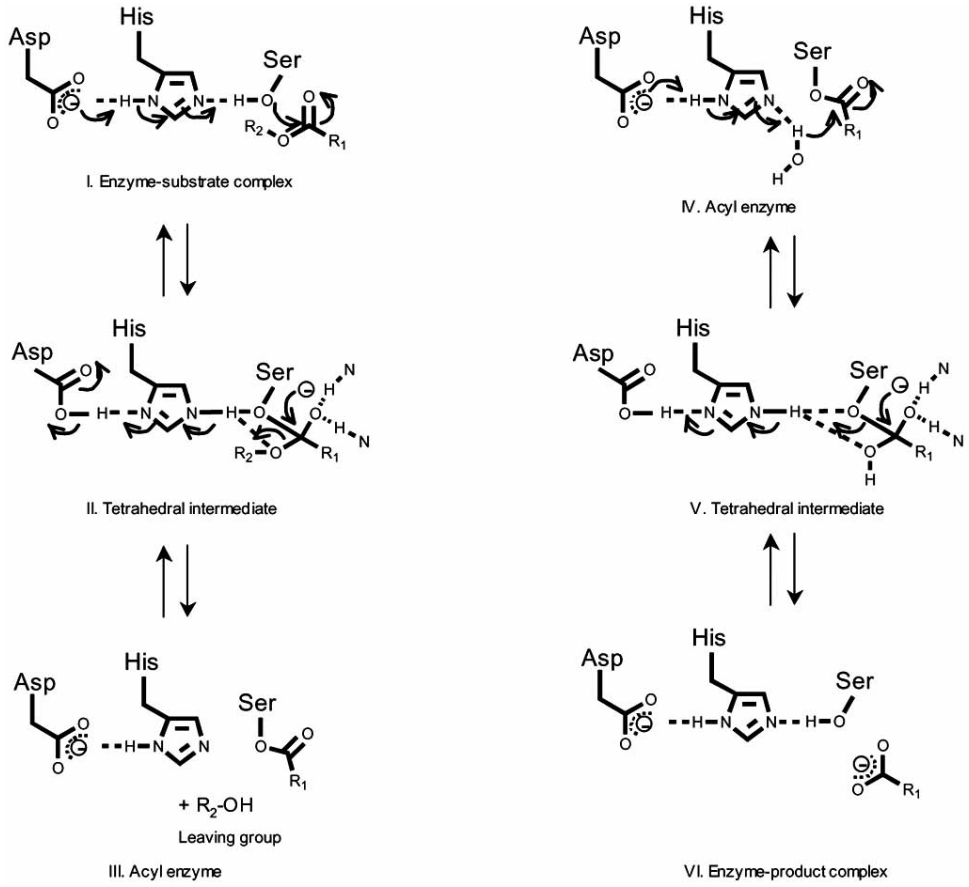

Fig. 10. Schematic representation of the catalytic mechanism based on a catalytic triad of serine (nucleophile), histidine and aspartate. In MAGL the catalytic triad is formed by Ser122, His269 and Asp269.

3. MAGL INHIBITORS

3.1 General serine hydrolase inhibitors

Since mechanistically MAGL is a serine hydrolase, the first wide group of inhibitors are the general serine-hydrolase inhibitors. This series of mechanistically based inhibitors binds in either a reversible or irreversible covalent manner to the nucleophilic serine disrupting its catalytic activity. Chemically, we can distinguish three main reactive groups: fluorophosphonates, trifluoromethylketones and sulfonylfluorides (Table 1, Table 2). As the most representative compound within each of these classes we can mention methyl arachidonylfluorophosphonate (MAFP), arachidonyltrifluoromethylketone (ATFMK) and phenylmethylsulfonylfluoride (PMSF). All these compounds are not new to the ECS field, since they are old known FAAH inhibitors. Considering the similarity between the mechanism and the structure of the substrate between MAGL and FAAH, it is clear that one of the first aspects to consider when identifying potential MAGL inhibitors is the selectivity between the two hydrolytic enzymes FAAH and MAGL.[19]

Table 1. Inhibition of 2-AG and AEA Hydrolysis by General Serine Hydrolase Inhibitors

Compound	Structure	IC_{50} MAGL (μM)	IC_{50} FAAH (μM)
MAFP	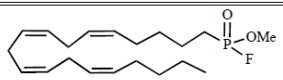	0.0022 ± 0.0003[a]; 0.8 ± 0.05[b]; 0.10 ± 0.02[c]	0.0025[e]
ATFMK	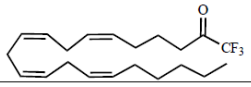	2.5 ± 0.04[b]; 66 ± 9[d]	1.9[e]
HDSF	CH_3-$(CH_2)_{15}$-SO_2F	0.241 ± 0.017[a]; 6.2 ± 0.1[b]	0.0102[f]
PMSF	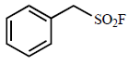	155 ±7[a]	0.9[e]

Table 2. Inhibition of 2-AG and AEA Hydrolysis by Trifluoromethylketones

Compound	Structure	IC_{50} MAGL (μM)	IC_{50} FAAH[c] (μM)
ATFMK	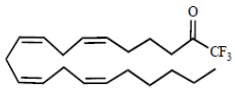	66[a] 2.5 ± 0.04[b] 2.9[c]	0.55
OTMK	$CH_3(CH_2)_7CH{=}CH(CH_2)_7COCF_3$	1.0[c]	0.076
PTMK	$CH_3(CH_2)_{14}COCF_3$	7.8[c]	0.073

Further modification of the trifluoromethylketone moiety with the introduction of a sulfide (R-S-) group in the α position, structural motif known to inhibit esterases, has

been also analysed in a brief SAR study aimed at the search of new antitumor agents acting as MAGL inhibitors (Fig. 11). From the experimental values of this series of compounds, it is observed that the inhibition of degradation of 2-AG and 2-OG is increased with the length of the alkyl chain (R). [19]

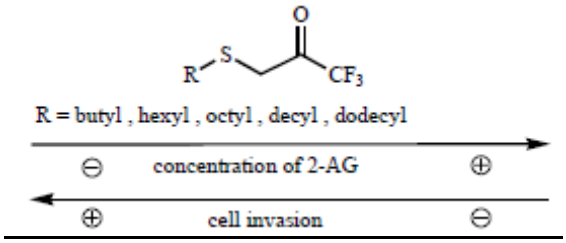

Fig. 11. Effect of the introduction of a α-sulfide group (R-S-) in trifluoromethylketones on 2-AG hydrolysis and invasion of prostate cancer cells.

3.2 Inhibitors inspired by the endogenous substrate: 2-AG analogues

In the structure of 2-AG we can distinguish three main parts susceptible to modifications: i) fatty acid chain, ii) linker and iii) glycerol moiety (Fig. 12). Based on this, the abilities of a series of analogues of 2-AG have been examined (Table 4) in their ability to inhibit cytosolic MAGL activity. With respect to the fatty acid chain, the experimental data reveal that both isomers 2-AG and 1-AG are equipotent in disrupting MAGL activity (IC_{50} = 13 and 17 μM, respectively). [19]

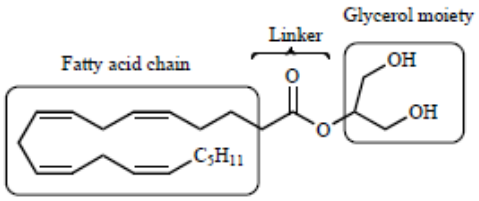

Fig. 12. 2-AG structure: points of structural modification.

Table 4. Inhibition of MAGL and FAAH by 2-AG Analogues

Compound	Structure	IC_{50} (μM) MAGL[a]	IC_{50} (μM) FAAH[a]
2-AG	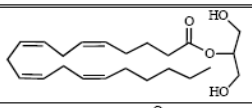	13	37%[b]
1-AG	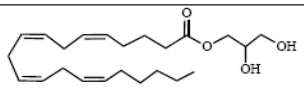	17	42%[b]
2-OG	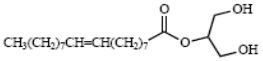	15	2.5
2-LG	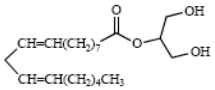	12	22
O2204	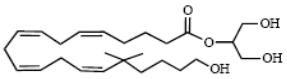	14[c]	35
Arachidonoylserinol	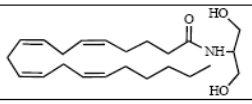	73	78
Noladin ether	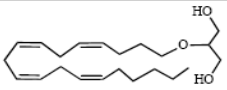	36	3
O1502	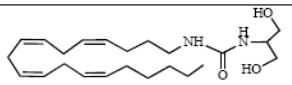	39%[b]	19
CAY10402	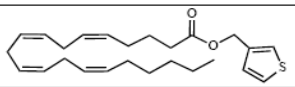	14%[b]	10
VDM11	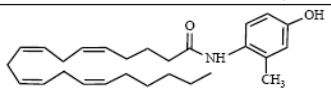	20	2.6

3.3 Inhibitors inspired by the endogenous substrate: 1-AG Homologues

Since 1-AG shows comparable potency to 2-AG as MAGL inhibitor (IC_{50} (1-AG) = 17 μM and IC_{50} (2-AG) = 13 μM, Table 4) but it is more stable in biological solutions, a group of analogues of 1-AG have been examined as MAGL inhibitors. The structural study (Table 5) includes variations in length (14-22 carbons) and number of unsaturations (0-5) of the fatty acid chains. The main conclusions of this study indicate that for cytosolic MAGL the number of unsaturations does not affect significantly the interaction as the IC_{50} values range between 4.5 and 21 μM. However, a decay of inhibition is observed for the monounsaturated compounds (O3908 and O4066) and a total loss of activity for the saturated C-20, 1-arachidinoylglycerol. In contrast, shorter fully saturated compounds such as 1-palmitoylglycerol (C-16) and 1-myristoylglycerol (C-14) inhibit MAGL.[20]

Table 5. Inhibition of MAGL and FAAH by a Series of 1-AG Analogues

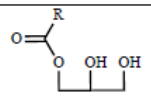

Compd	R	IC_{50} (μM) MAGL[a]	IC_{50} (μM) FAAH[a]
1-AG	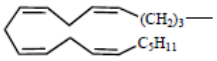	7.1; 17[b]	6.2; 42%[b,c]
O3832	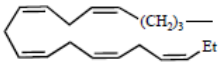	8.2	7.6
O3872	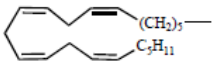	4.5	14
O3846	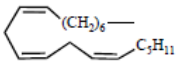	7.5	23
O3907	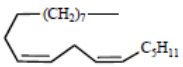	5.1	5.7
O3908	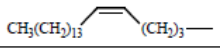	21	11
O4066		19	10
1-arachidinoylglycerol	CH_3-$(CH_2)_{18}$-	19±%[c]	10±3%[c]
1-palmitoylglycerol	CH_3-$(CH_2)_{14}$-	12	8.0
1-myristoylglycerol	CH_3-$(CH_2)_{12}$-	32	18
O1428	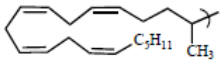	15	28±3%[b]
O4081	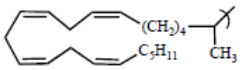	5.8	5.1
O3973	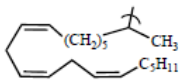	4.2	2.4

3.4 *De novo* inhibitors

Two inhibitors of MAGL have been recently described whose structures (Table 6) do not resemble any endogenous cannabinoid. URB754 was reported to inhibit 2-AG degradation through a non competitive and irreversible mechanism with an IC_{50} value of 200 nM measured in rat brain MAGL expressed in HeLa cells. Besides, it showed a high degree of selectivity towards FAAH of about 150 fold (IC_{50} = 31.8 μM). The other MAGL inhibitor identified, URB602, showed a lower capacity to disrupt MAGL hydrolysing activity (IC_{50} = 28-75 μM depending on the source of enzyme) but did not affect the FAAH catalytic activity. [19]

Table 6. Inhibitory Potencies of URB754 and URB602 Towards MAGL and FAAH

Compound	IC_{50}MAGL[a]	IC_{50}FAAH[b]
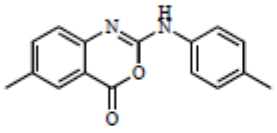 URB754	200±16nM	318±38μM
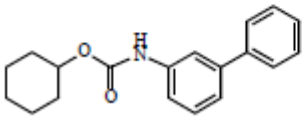 URB602	75 ± 7 μM 28 ± 4 μM[c]	No inhibition

Another inhibitor of this class of compounds is SAR629, a derivative of the triazolo-carboxamide series (Fig.13). It shows a nanomolar activity range and its mechanism of inhibition mimics the pathway of 2-AG hydrolysis by MAGL by making a relatively stable carbamate adduct with the catalytic serine instead of the relatively labile ester adduct (Fig. 14).[22]

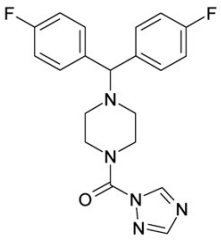

SAR629

Fig. 13. SAR 629: *De novo* MAGL inhibitor.

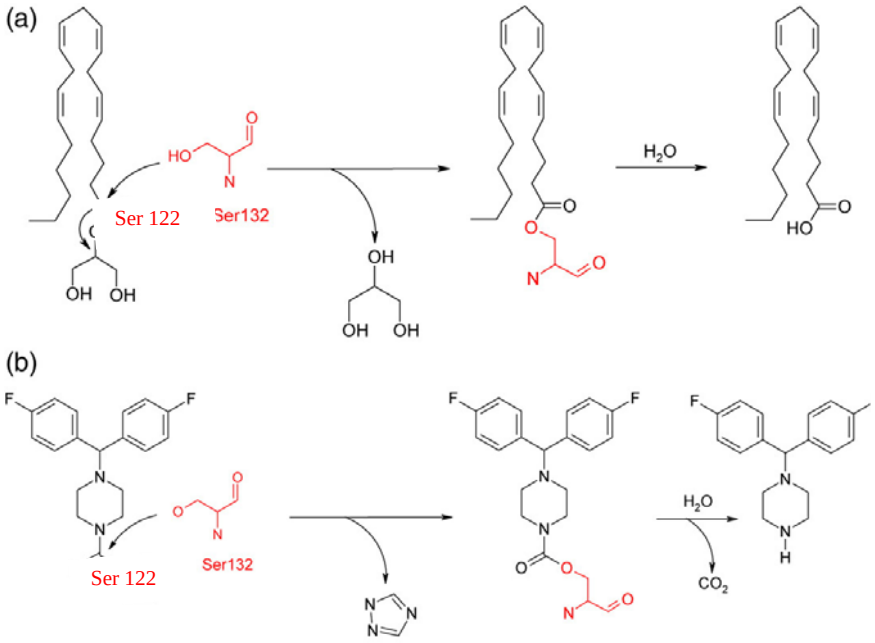

Fig. 14. a) hydrolysis of 2-AG by MAGL. b) hydrolysis of SAR 629 by MAGL.

In the analysis of model in which SAR629 and MAGL bound covalently, the compound adopts a Y shape with its two fluorophenyl moieties pointing toward opposite directions and perpendicular to each other. These moieties are perpendicular to the piperidine linker that adopts a chair conformation. In addition to the covalent bond with Ser122, SAR629 interacts with MAGL essentially by hydrophobic interactions and few polar interactions. Water-mediated interactions occur between the inhibitor nitrogen piperazine or oxygen atoms of its carbamate function and His269 side-chain or Ala61 main-chain carbonyl oxygen (Fig. 15).[22]

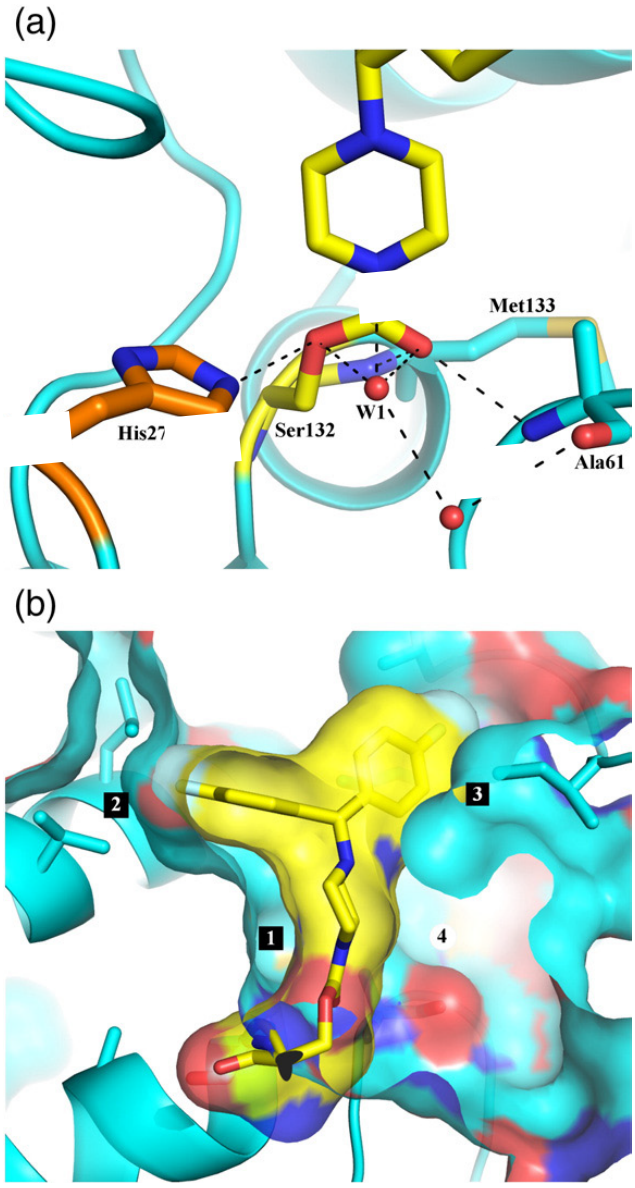

Fig. 15. Docking study of SAR629 into the active site of the enzyme.[22]

The piperazine moiety is in contact with the protein only via van der Waals interactions on one side (Fig. 15b, square 1), but makes no contact on the other side. The nitrogen atoms of the piperazine are not involved in any polar contacts with the protein. One of the fluorophenyl moieties of SAR629 fits in a pocket consisting of Leu158, Leu223, and Leu224, creating van der Waals interactions (Fig. 15b, square 2). The other fluorophenyl ring is sandwiched between Leu186, Ile189, and Leu215 side chains (Fig. 15b, square 3) and points toward a pocket rich in polar atoms (namely, main-chain carbonyl oxygen atoms of Leu186, Gly187, and Pro188 and main chain nitrogen of Ile189). The only direct polar contact between protein and inhibitor occurs between main-chain nitrogen atoms of Ala61 and Met133 (oxyanion hole) and the carbonyl oxygen of SAR629 (Fig. 17). The covalent bond formation between Ser122 and the carbon of the carbamate function is thought not to be fully

irreversible. It is supposed that a water molecule is able to hydrolyze the carbamate function connecting the catalytic serine and the inhibitor; however, this process is supposed to be slow. [22]

According to this knowledge is possible to affirm that the carbonyl oxygen of the urea function seems necessary to create the only polar interaction between the inhibitor and the protein. One of the fluorophenyl groups is positioned just above a "plateau" of hydrophobic residues. The role of the piperazine is to orient the other moieties toward pharmacophoric points, and it could probably be replaced by other moieties. [22]

The reported MAGL inhibitor JZL184 has a chemical structure very close to that of SAR629 (Fig. 16). Its mechanism of inhibition and its mode of recognition should be similar (Fig. 14).[22]

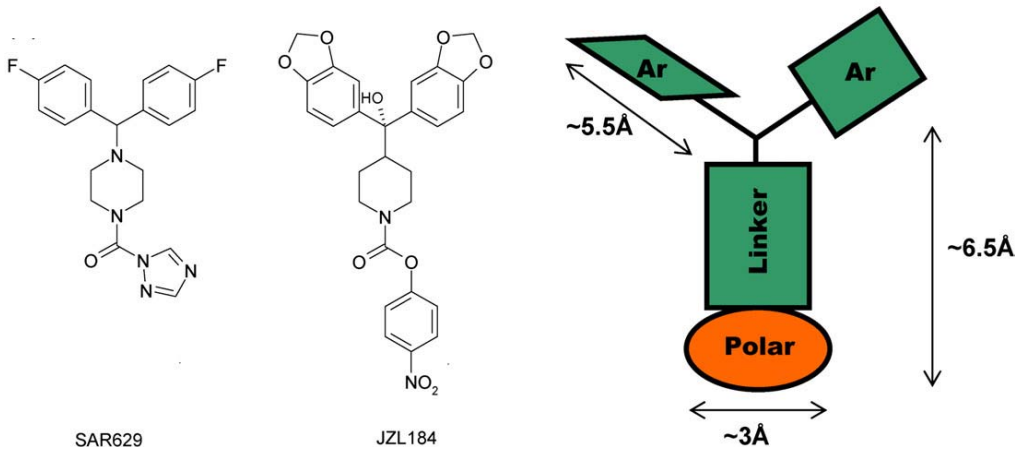

Fig 16. Pharmacophoric model of SAR629 and JZL184. (Dark green elements depict flat and hydrophobic pharmacophoric points, whereas the orange element depicts a polar pharmacophore. Ar, aromatic).[22]

3.5 Organophosphoric (OP) derivatives as MAGL inhibitors

Organophosphorus (OP) derivatives with general structure showed in figure 17, as reported in literature, are another class of potential MAGL inhibitors and could interact with several components of the cannabinoid system. [22, 23, 24, 25]

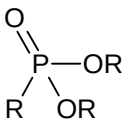

Fig. 17. General structure of OP derivatives

In particular Casida et al. indicated that some OP derivatives inhibit MAGL activity *in vitro* and that this inhibition leads to elevation of 2-AG levels in mice brain,[19 d] furthermore they showed that most OP compounds posses little or no selectivity for MAGL versus FAAH. One of the most representative compounds of this class of derivatives is UP101 which showed, as we can see from table 6a, a high inhibition activity of the ECS enzyme but not selectivity towards MAGL. Other OP derivatives which did not showed high selectivity for MAGL versus FAAH are CPO and Paraox reported in figure 18. [26]

Tab. 6a. Inhibition activity of UP101

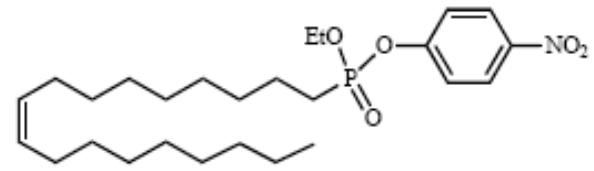

Target	IC_{50} (μM)[a]
MAGL (COS cell cytosol)	3.2 ± 0.17
DAGLα (human recombinant)	3.7 ± 0.2
FAAH (rat brain membranes)	0.18 ± 0.14

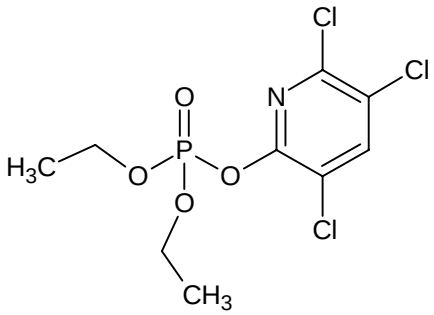

CPO

IC50 MAGL= 10 nM

IC50 FAAH= 460 nM

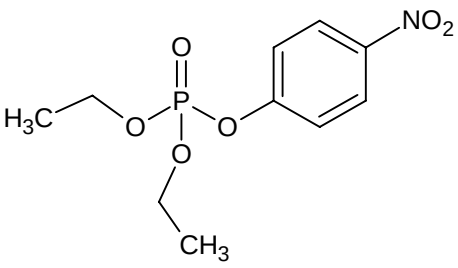

Paraox

IC50 MAGL= 1.2 mM

IC50 FAAH= 5.9 mM

Fig. 18

Moreover Nomura et al. demonstrated that several of the non-cholonergic OP effects are mediated by the ECS and that the inhibition of the metabolic enzyme by OP compounds is due for the phosphorylation of the catalytic site serine (S122 for MAGL and S241 for FAAH). [19 b]

3.6 Inhibitors targeting the essential sulfhydril group of MAGL

The presence of some thiol groups close to the catalytic site of the enzyme led to the design of NEM analogues as MAGL inhibitors (Table 7). Maleimide analogues behave as Michael acceptors toward thiol residues, binding irreversible to the enzyme .[19]

Table 7. Inhibition of MAGL by Maleimide and Succinimide Derivatives in Rat Cerebellar Membranes

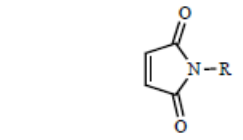

R	IC_{50} (μM)[a]
H	70 ± 6
Et	53 ± 7
Pr	53 ± 6
c-Hex	51 ± 6
Ph	44 ± 6
OH	413 ± 23
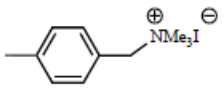	68 ± 7
	9.2 ± 0.8
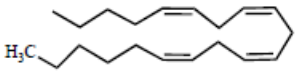	0.140 ± 0.005

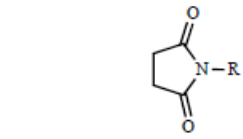

R	IC_{50} (μM)[a]
H	b
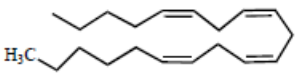	c

9. THERAPEUTIC APPLICATIONS OF MAGL TARGETING COMPOUNDS

In the last years, several studies have demonstrated the key physiological roles of 2-AG. Accordingly, the design and synthesis of compounds able to inhibit MAGL could offer new perspectives in the understanding and treatment of several disorders. Some of the most promising applications are discussed below.

Neuroprotection and Neurodegenerative Diseases: different studies suggest that endocannabinoids are neuroprotective in different *in vivo* and *in vitro* models. They can protect neurons from hypoxic injury and may represent endogenous neuroprotective molecules in cerebral ischemia. For example, 2-AG protects rat cerebral neurons from ischemia *in vitro* and increases cell viability when these cells are subjected to hypoxia and glucose deprivation. Additionally, levels of endogenous 2-AG were found significantly elevated in the closed head injury model in mice and 2-AG administration produced significant reduction of brain oedema and infarct volume, better clinical recovery, and reduced hippocampal cell death. The protection induced by 2-AG has been attributed to CB1 activation, since this effect was attenuated by the CB1 selective antagonist SR141716A and was absent in CB1(-/-) mice and this mechanism could involve inhibition of intracellular inflammatory signaling pathways. Furthermore, the relation between 2-AG and epilepsy has also received attention. Since cannabimimetic molecules including Δ9-(-)-tetrahydrocannabinol (Δ 9-THC) are known to depress neurotransmission and to exert anticonvulsant activities, endogenous 2-AG produced during neural excitation could play a regulatory role in calming the enhanced synaptic transmission. In this regard, 2-AG inhibits the depolarization-induced increase in intracellular calcium in NG108-15 cells, thereby modulating several neural functions in this cell type. Hence, 2-AG could prevent the excessive excitability that takes place in epilepsy. Another interesting aspect is the possible implication of 2-AG in neurodegenerative diseases, such as multiple sclerosis (MS). For instance, in areas associated with nerve damage in the MS model of chronic relapsing experimental autoimmune encephalomyelitis (CREAE), increased levels of AEA and 2-AG were detected, suggesting a protective role of these endocannabinoids. In a different animal model of MS, experimental autoimmune encephalomyelitis (EAE), AEA and 2-AG levels were found to be decreased in brain motor related regions (striatum, midbrain). Recently studied showed that in EAE the protective role of endocannabinoids can be disrupted by the action of interferon-α (IFN-α). The massive release of IFN-α by the primed T cells invading the CNS blocks the activation of purinergic P2X7 receptors, the key step that induces 2-AG production by microglia. The disruption of the endocannabinoid-

mediated neuroprotection induced by IFN-α occurs without affecting the functionality of the cannabinoid receptors, thus providing additional support for the use of an endocannabinoid-based medicine to treat MS.[19]

Feeding Behaviour: Marijuana and its major psychotropic component, Δ 9- THC, were found to stimulate appetite and increase body weight in wasting syndromes. Additionally, endocannabinoids have been involved in the control of energy balance and food intake and their effects have been described as mainly CB1–mediated, since they are antagonized by SR141716A. They may also stimulate lipogenesis and fat accumulation. Therefore, endocannabinoids add to the list of the numerous neurotransmitters and neuropeptides involved in the physiological control of appetite and satiety. In particular, 2-AG has been described to stimulate feeding in a potent and dose-dependent manner, effect blocked in part by the action of SR141716A.

Interestingly, the neurohormone leptin, which is the main regulator of the hypothalamic orexigenic and anorectic signals, exerts a negative control on the AEA and 2-AG levels. Considering the role played by endocannabinoids in the intricate network that regulates feed control, the manipulation of their levels could offer useful approaches to the treatment of eating disorders as well as metabolic syndromes.[19]

Cancer: The endocannabinoid system is implicated in cancer because it plays a fundamental role in the control of the cell survival/death decision. Although both endocannabinoids, AEA and 2-AG, have been found to inhibit proliferation of certain cancer cell lines, we will focus on the effects of the latter. 2-AG inhibits proliferation of human breast (EFM-19) and prostate (DU-145) cancer cell lines. 2-AG has been also involved in cancer cell invasion. Block of 2-AG metabolism increases endogenous 2-AG levels, which inhibits invasion of the androgen-independent prostate cancer cells PC-3 and DU-145. These effects have been linked to CB1 receptor activation, considering that CB1 is expressed in these prostate cancer cell lines as well as in the human prostate gland (at a level comparable with the CB1 expression in cerebellum) where it negatively regulates adenylyl cyclase activity. Because prostate cancer has become the most common cancer in men, identifying novel targets and new agents for its treatment has become an imperative issue. Supporting a more general role of 2-AG in tumoral processes, the 2-AG-mediated inhibition of cell proliferation can take place in other types of cancer cell lines such as colorectal carcinomas and C6 glioma cells. Also, tumors such as meningiomas show a massive enhancement in the levels of 2-monoacylglycerols including 2-AG.

Therefore, it has been suggested that endocannabinoids could act as endogenous anti-tumour mediators by stimulation of both cannabinoid and non-cannabinoid receptor mediated mechanisms. Considered together, all the above data have raised the view that the design and synthesis of new compounds that block 2-AG degradation may open new possibilities in the treatment of these types of cancer. [19]

Drug Dependence: The brain reward system constitutes another point of interest for 2-AG since it has demonstrated a remarkable capacity to attenuate the naloxone-precipitated withdrawal signs in morphine-dependent mice. This result is in agreement with the proposed upregulation of cannabinoid CB1 receptors in morphine dependence, and it supports the hypothesis that either accelerators of endocannabinoid synthesis or inhibitors of its degradation may have a therapeutic potential to treat opiate withdrawal symptoms. The profound changes that the ECS undergoes during the different phases of sensitization to morphine in rats provide a possible neurochemical basis for this cross-sensitization between opiates and cannabinoids. Moreover, 2-AG could play a role in alcohol addiction and in addictions to other drugs such as marijuana, nicotine, and cocaine by activation of the same or related reward pathways. [19]

Other Disorders: It is known that endocannabinoids induce analgesia. For example, when the MAGL inhibitor URB602 is microinjected into the periaqueductal grey matter, it induces in a CB1-dependent manner an increase in the levels of 2- AG, which has been related to an enhancement of the stressinduced analgesia. These effects, which run parallel to those observed after inactivation of anandamide degradation, suggest that 2-AG as well as anandamide could mediate opioid-independent stress-induced analgesia. Another aspect of interest is the presence of the CB1 receptor and both AEA and 2-AG in ocular tissues. Cannabinoids have shown capacity to reduce the ocular hypertension and, in particular, topical application of anandamide was shown to decrease the intraocular pressure in normotensive rabbits. Moreover, topical administration of 2- AG and noladin ether also decreased intraocular pressure in rabbits, reduction that has been attributed to the CB1 receptor. These effects could be of direct application in glaucoma, the disorder characterized by a pathological enhancement of the intraocular pressure. In this regard, the levels of 2-AG and *N*-palmitoyl ethanolamine have been found to be significantly decreased in the ciliary body in eyes from patients with glaucoma, further supporting the role of these endogenous compounds in the regulation of intraocular pressure.

Finally, the role of 2-AG in the immune system and in particular its effect on the motility of human natural killer cells should be noted, 2-AG induces the migration of KHYG-1 cells (a natural killer leukemia cell line) and human peripheral blood natural killer cells. This migration can be blocked by the presence of the CB2 antagonist SR144528, and interestingly, it does not occur in the case of AEA or Δ9- THC. Accordingly, it has been suggested that 2-AG could contribute to the host-defense mechanism against infectious viruses and tumor cells. [19]

10. EXPERIMENTAL PART

5.1 INTRODUCTION

Monoacylglycerol lipase (MAGL) is a metabolizing enzyme which belongs to the endocannabinoid system. The endocannabinoid system includes the endogenous ligands: anandamide (AEA) and 2-arachidonoyl glycerol (2-AG) (Fig.19), the cannabinoid receptors CB1 and CB2, the anandamide transporter protein, and two metabolizing enzymes: fatty acid amide hydrolase (FAAH) which is involved in the inactivation of AEA and monoglyceride lipase (MAGL or MGL) which is involved in the inactivation of 2-AG.[19]

2- AG is the natural ligand for CB1 and CB2 receptors even if it interacts predominantly with CB2 receptors, it exhibits lower affinity than AEA and it is considered the primary endogenous cannabinoid in the brain.

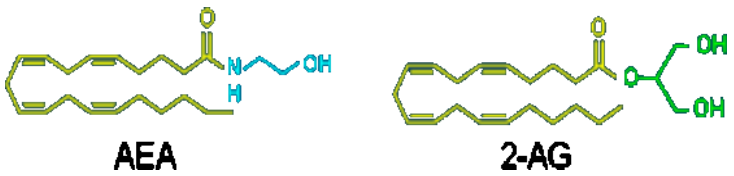

Fig. 19

Biological activities of 2-AG have been reported in: immune function, cell proliferation, embrio development, neuroprotection, immunomodulation, cardiovascular function and inflammatory responses.[20]

MAGL is a serine hydrolase belonging to the "α/β hydrolase fold" family characterized by a central β sheet core surrounded by a variable number of α helicals. The catalytic triad is formed by serine (S122), aspartic acid (D239) and histidine (H269) residues, in addition 3 cysteine residues appear to contribute to the regulation of its functions (Fig. 20).[19, 20]

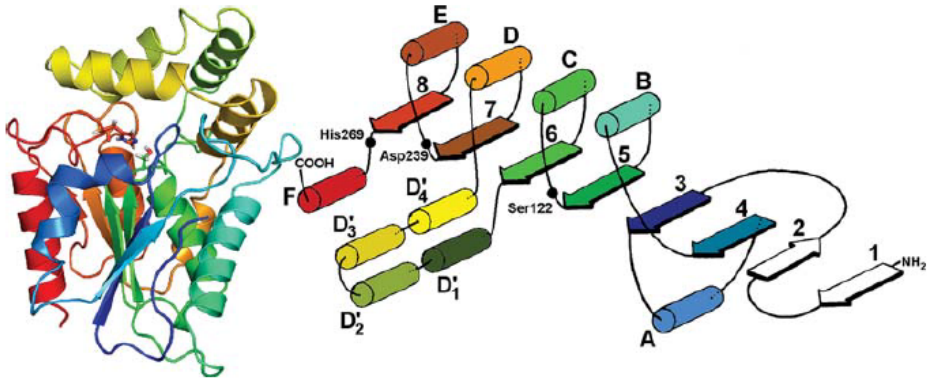

Fig. 20. Tertiary structure and schematic diagram of MGL. The catalytic triad S122, D239 and H269 is shown in stick representation. [21]

MAGL is involved in the inactivation of 2-AG, in particular it catalyses the hydrolysis of 2-AG to fatty acid and glycerol (Fig. 21).[19, 20]

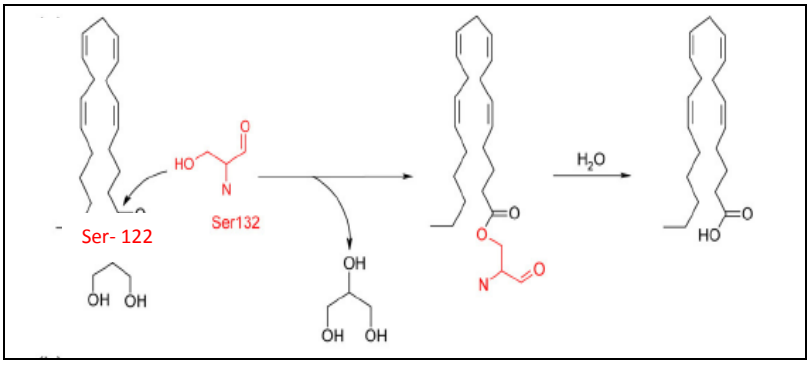

Fig. 21. Interaction between 2-AG and Ser-122 of the enzyme MAGL

MAGL Inhibitors

There are different kinds of MAGL inhibitors, the major-ones are: NON-SPECIFIC SERINE HYDROLASE INHIBITORS, INHIBITORS INSPIRED BY THE ENDOGENOUS SUBSTRATE and *De novo* INHIBITORS.[6]

The main therapeutic applications of MAGL inhibitors are:

1. NEUROPROTECTION : they can protect neurons from hypoxic injury and they can protect from cerebral ischemia;[19, 20]

2. FEEDING BEHAVIOUR: they can stimulate appetite, lipogenesis and fat accumulation;[19, 20]

3. Treatment of CANCER: they can inhibit the proliferation of certain cancer cell lines;[19, 20]

4. Treatment of GLAUCOMA: they can regulate intraocular pressure;[19, 20]

5. ANALGESIC EFFECTS.[19, 20]

5.1.1 Design, synthesis and biological evaluation of derivatives as potential MAGL *de novo* inhibitors

De novo Inhibitors

Some inhibitors of MAGL have been described whose structures do not resemble any endogenous cannabinoid: URB754, URB602 (Fig. 22), SAR629 and JZL184 (Fig. 13c).

- URB754 was reported to inhibit 2-AG degradation through a non competitive and irreversible mechanism;[19]
- URB602 have similar characteristics and mechanism of URB754 and it showed a lower capacity to disrupt MAGL hydrolysing activity;[19]
- Other de novo INHIBITORs are: JZL184 which is a piperidine derivate and SAR629 which is a piperazine derivative with interesting selectivity for MAGL over FAAH and which showed a similar mechanism of inhibition. In particular, it is reported that SAR629 mechanism of inhibition mimics the pathway of 2-AG hydrolysis by MAGL by making a relatively stable carbamate adduct with the catalytic serine instead of the relatively labile ester adduct (Fig. 23a and Fig. 23b).[19, 21] MAGL–SAR629 co-structure permits the identification of pharmacophoric points (Fig. 23c): the carbonyl oxygen of the urea function seems necessary to create the only polar interaction between the inhibitor and the Ser-122 of the protein. One of the fluorophenyl groups probably interacts with some hydrophobic residues and the piperazine group rapresent a linker use to orient the other moieties toward pharmacophoric points (carbonyl oxygen and aromatic substituent). This linker could be probably replaced by other moieties.[19, 21]

Compound	IC_{50} MAGL[a]
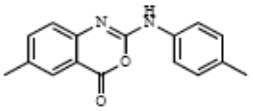 URB754	200±16nM
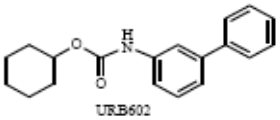 URB602	75 ± 7 μM 28 ± 4 μM[c]

Fig. 22

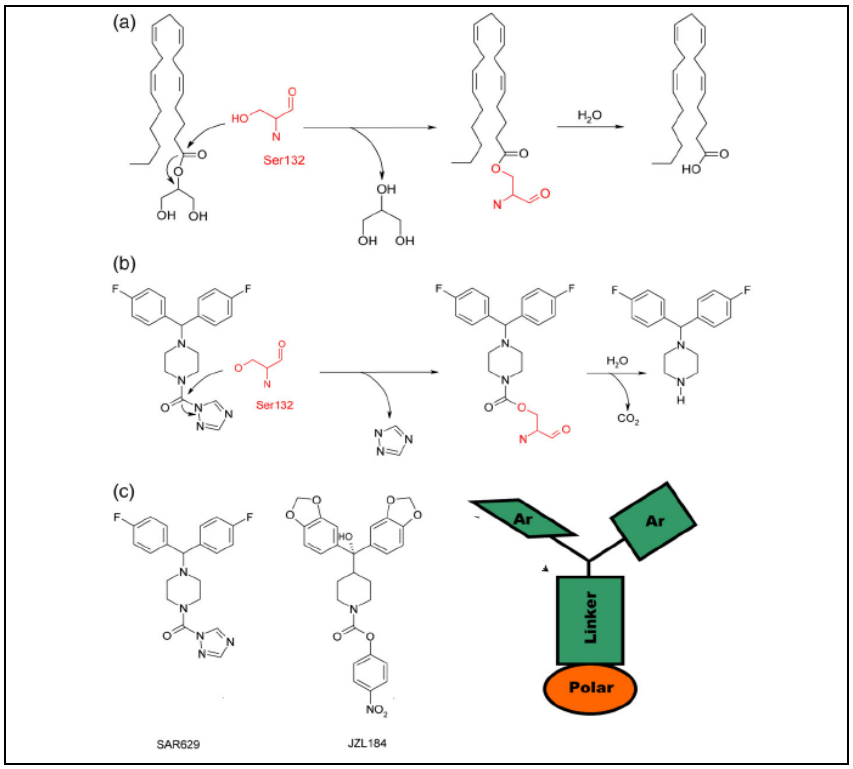

Fig. 13

During the first period of my PhD thesis we designed and synthesized compounds with general structure **A**, **B, C, D** and **E** as potential MAGL *de novo* inhibitors.

These compounds could have the same interactions of SAR-629 and JZL-184, with the active site of the enzyme, in fact they are characterize by:

- the carbamate carbonyl oxygen, which could create the only polar interaction between the ligand and Ser-122 of the protein,
- the aromatic substituent (R_2), which could interact with some hydrophobic residues of the protein,
- the heterocyclic nucleus as a linker between the other mojeties , which could orients them toward the pharmacophoric points.

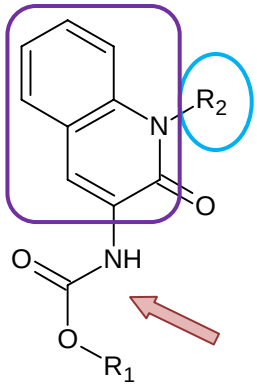

A

R_1= phenyl, *p*-nitro phenyl;
R_2= benzyl.

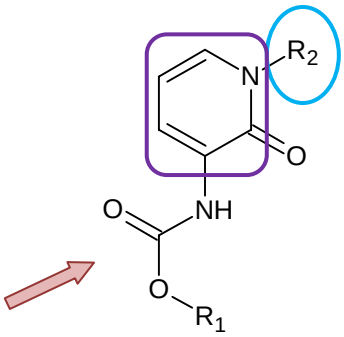

B, C

B: R_1= phenyl; R_2= benzyl.
C : R_1=R_2= phenyl.

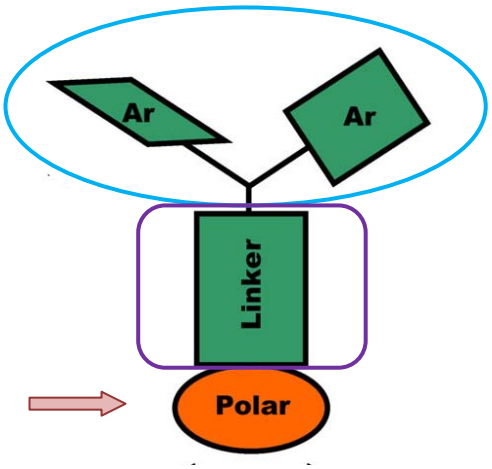

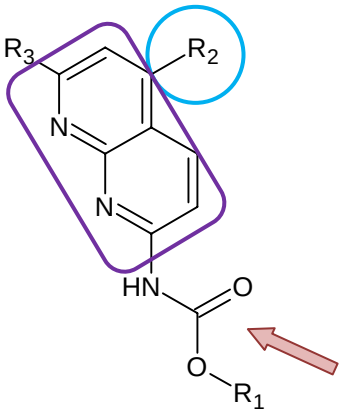

D

R_1, R_2= phenyl group; R_3=Cl, OMe.

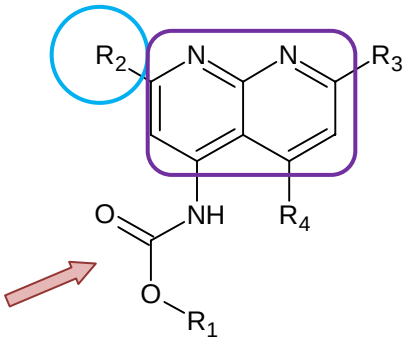

E

R_1, R_2= phenyl group; R_3=Me, Br, OMe; R_4= H, Me

Compounds with general structure **A** were obtained as reported in Scheme 1.

Scheme 1

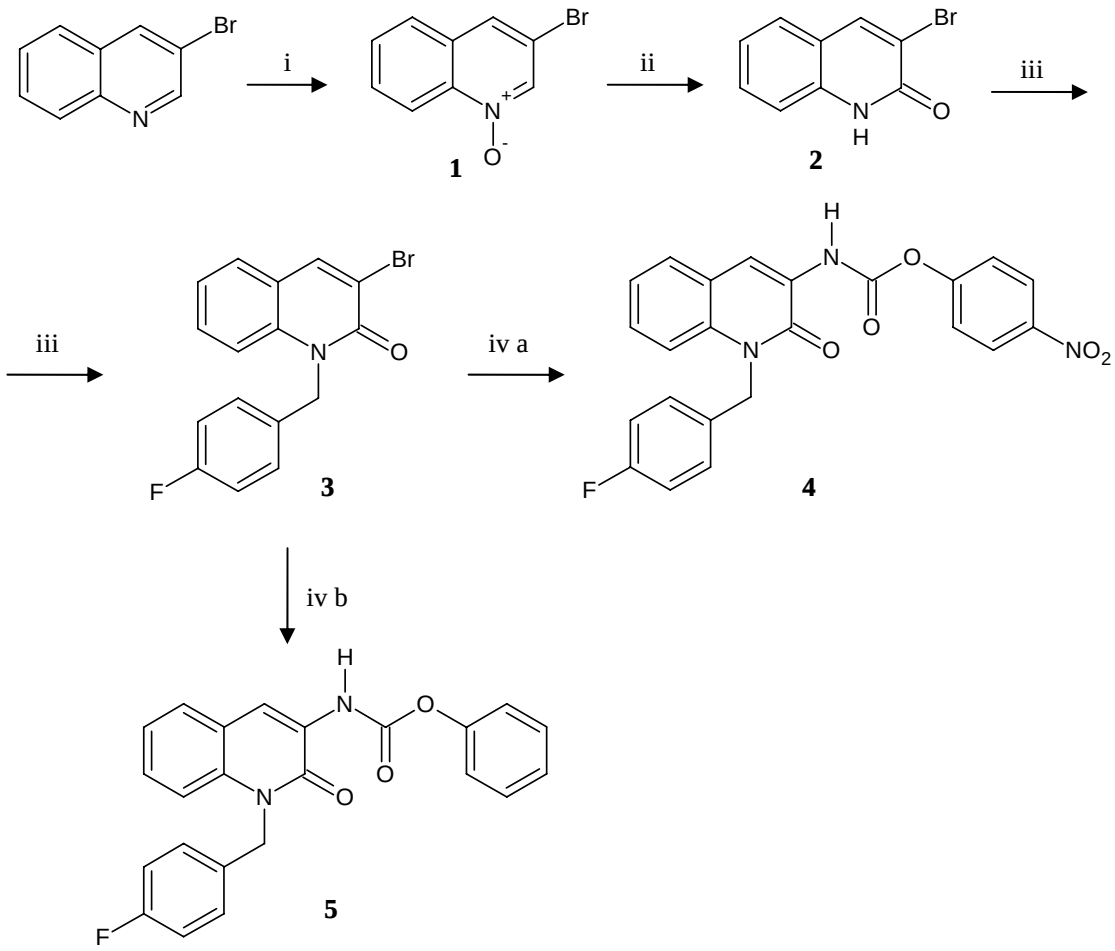

Reagents and conditions. i: m-CPBA, $CHCl_3$, r.t., 20h. ii: benzoyl chloride, NaOH/H_2O, CH_2Cl_2, 0°C, 2h. iii: NaH, anhydrous DMF, 50°C, 2h; 4-fluorobenzyl chloride, r.t., 24h. iv a: 4-nitrophenyl chloroformate, $Pd(OAc)_2$, Cs_2CO_3, Xantphos, dioxane, 100°C, 10h; or microwave conditions: 140°C, 125 Psi, 200 W, 38 min, stirring on, cooling on. iv b: phenyl chloroformate, $Pd(OAc)_2$, Cs_2CO_3, Xantphos, dioxane, 100°C, 10h; or microwave conditions:

The N-oxide **1** was obtained starting from 3-brome-quinoline treated with m-CPBA in $CHCl_3$ at room temperature for 20 hours. The reaction between compound **1** and benzoyl chloride, aqueous NaOH 1.5 M in CH_2Cl_2 at 0°C for 2 hours gave compound **2** as a crystalline pure solid. The bromo-quinoline **2** was treated with NaH in anhydrous DMF for 2 hours at 50°C and then with *p*-fluorobenzyl chloride, at room temperature for 24 hours, to afford compound **3.** The desired compounds **4** and **5** were obtained by palladium-catalyzed C–N coupling reaction between compound **3** and phenyl carbamate or *p*-nitrophenyl carbamate respectively, in 1,4-dioxane using palladium acetate as catalyst, Xantphos as ligand and Cs_2CO_3 as base at 100°C for 10 hours or using the microwave at 140°C for 38 minutes.

Compounds with general structure **B** were synthesized in order to evaluate the importance of linker lipophilicity and of its steric hindrance, for the interaction with the enzyme.

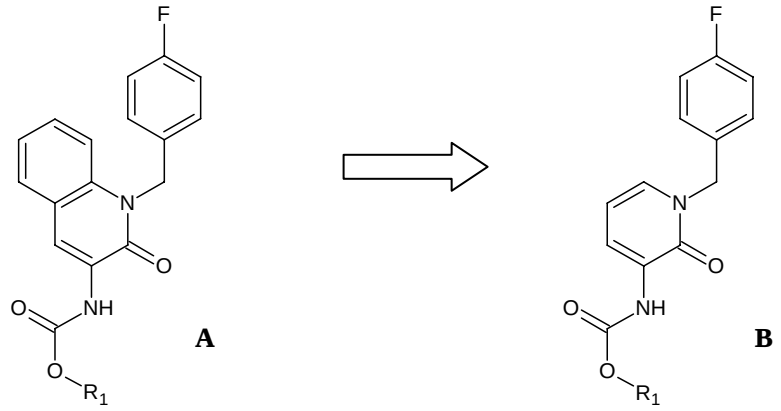

The synthesis of compounds with general structure **B** is depicted in the scheme 2.

Scheme 2

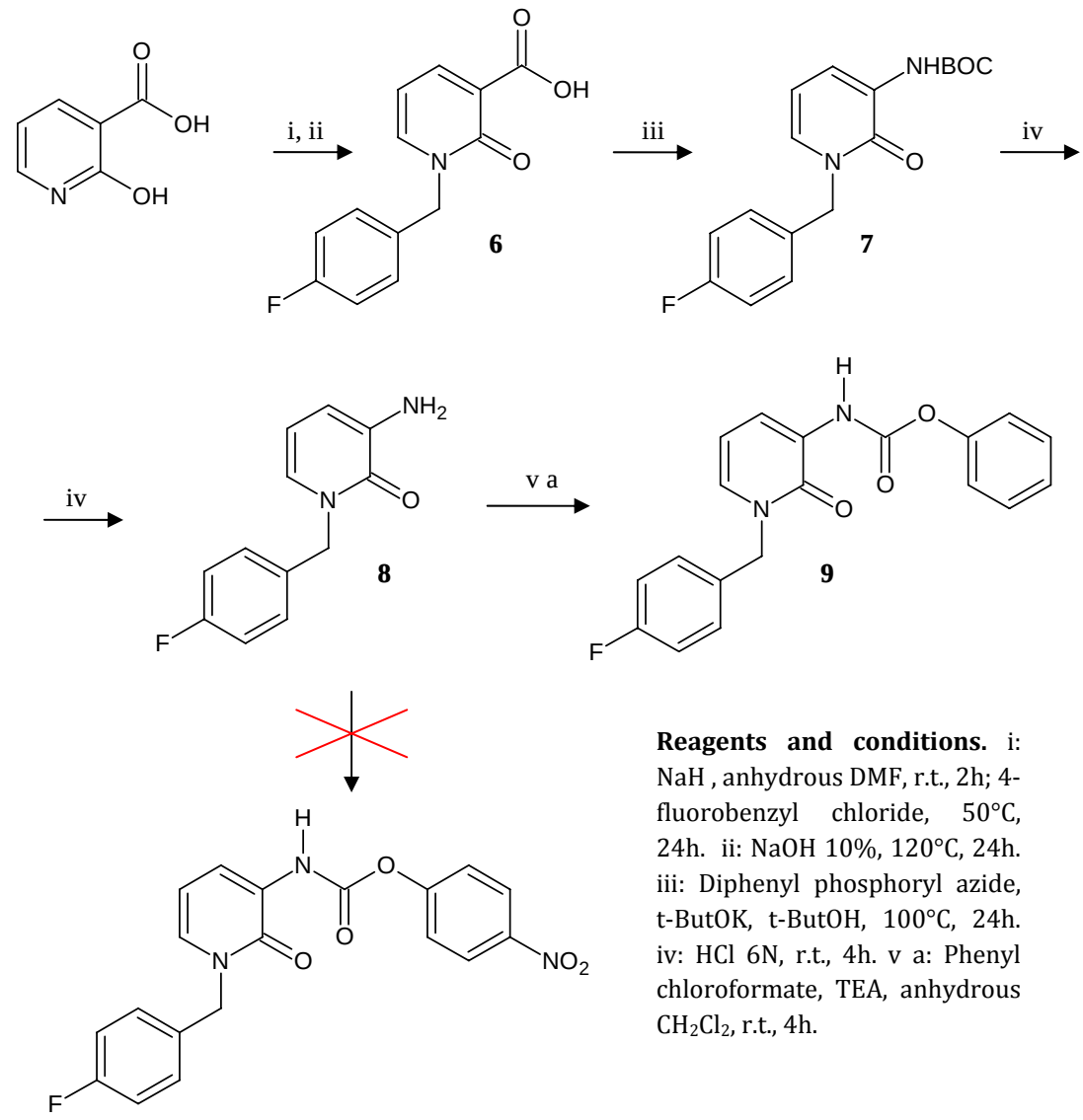

Reagents and conditions. i: NaH , anhydrous DMF, r.t., 2h; 4-fluorobenzyl chloride, 50°C, 24h. ii: NaOH 10%, 120°C, 24h. iii: Diphenyl phosphoryl azide, t-ButOK, t-ButOH, 100°C, 24h. iv: HCl 6N, r.t., 4h. v a: Phenyl chloroformate, TEA, anhydrous CH_2Cl_2, r.t., 4h.

The 2-hydroxy nicotinic acid was treated with NaH in anhydrous DMF for 2 hours at room temperature and then with *p*-fluorobenzyl chloride for 24 hours at 50°C to obtain a crude product which was treated with aqueous NaOH 10% under reflux for 4 hours to give, after acidification, the carboxylic acid **6.** The Curtius reaction between compound **6** and diphenyl-phosphorylazide, tBuOK in tBuOH at 100°C for 24 hours, afforded the corresponding BOC-derivative **7**, which was then hydrolyzed with HCl concentrate and then alkalized in order to obtain the amino-derivative **8**. The reaction between compound **8** and phenyl chloroformate, in presence of TEA in anhydrous CH_2Cl_2 at room temperature for 4 hours gave the desired compound **9**. Instead the reaction between compound **8** and *p*-nitro phenyl chloroformate, in the same conditions, did not yield the desired compound probably because at high temperature the reagent goes through degradation and at room temperature the substrate is poorly reactive.

Moreover in order to evaluate the importance of the distance between the carbonyl group of the molecules (which could interact with Ser-122) and the aromatic substituent R_2 (which could interact with some hydrophobic residues of the enzyme) we decided to synthesize compounds with general structure **C**, **D** and **E** which are characterized by different distance between these groups.

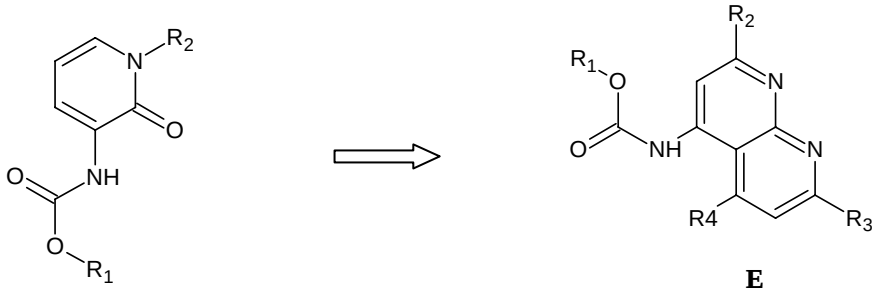

B

B: R_1= phenyl group
R_2= *p*- fluoro benzyl group.

E

E: R_1, R_2= phenyl group;
R_3=Me, Br, OMe; R_4= H, Me.

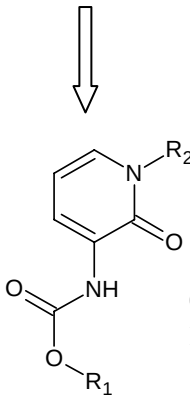

C

C: R_1= phenyl group;
R_2= *p*- fluorophenyl.

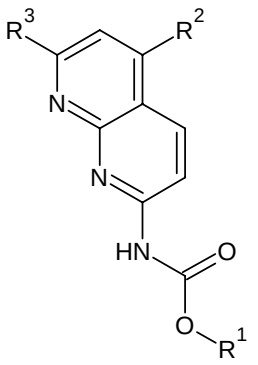

D

D: R_1, R_2= phenyl group;
R_3=Cl, OMe.

Compounds with general structure **C** were obtained as reported in scheme 3, starting from methyl 2-oxo-2*H*-pyran-6-carboxylate.

Scheme 3

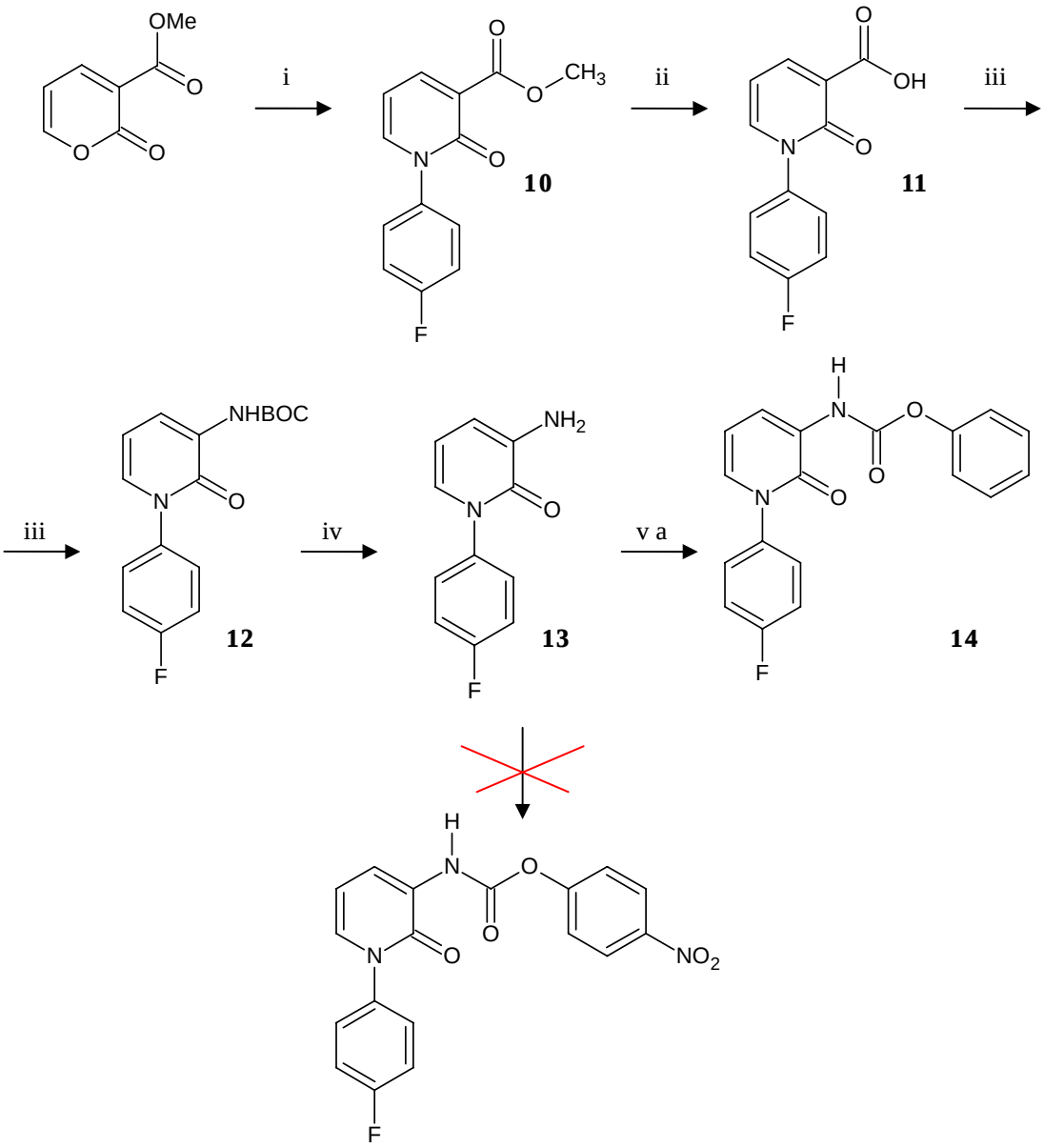

Reagents and conditions. i: 4-fluoroaniline, anhydrous DMF, 0°C, 7h; DMAP, EDCI hydrochloride, r.t., overnight. ii: NaOH 10%, reflux, 4h. iii: diphenyl phosphoryl azide, t-ButOK, t-ButOH, 100°C, 24h. iv: HCl 6N, r.t. , 4h. v a: Phenyl Chloroformate, TEA, anhydrous CH_2Cl_2, r.t., 4h.

The Michael addition of 4-fluoroaniline to pyranic ester, followed by intramolecular cyclization of the Michael adduct provided *p*-fluorophenyl-2-pyridone ester **10**, which was hydrolyzed using aqueous NaOH 10% at reflux for 4 hours to afford, after acidification, the *p*-fluorophenyl-2-pyridone acid **11**. The Curtius reaction of compound **11**, in the same conditions reported for compound **7**, afforded the

corresponding BOC-derivative **12**, which was then hydrolyzed with HCl concentrate at room temperature to give after alkalization the amino-derivative **13**. The reaction between compound **13** and phenyl chloroformate, in presence of TEA in anhydrous CH_2Cl_2 at room temperature for 4 hours gave the desired compound **14**. Also in this case the reaction between compound **13** and *p*-nitrophenyl chloroformate did not yield the corresponding *p*-nitro phenyl chloroformiate derivative.

The synthesis of compounds with general structure **D** is reported in scheme 4.

Scheme 4

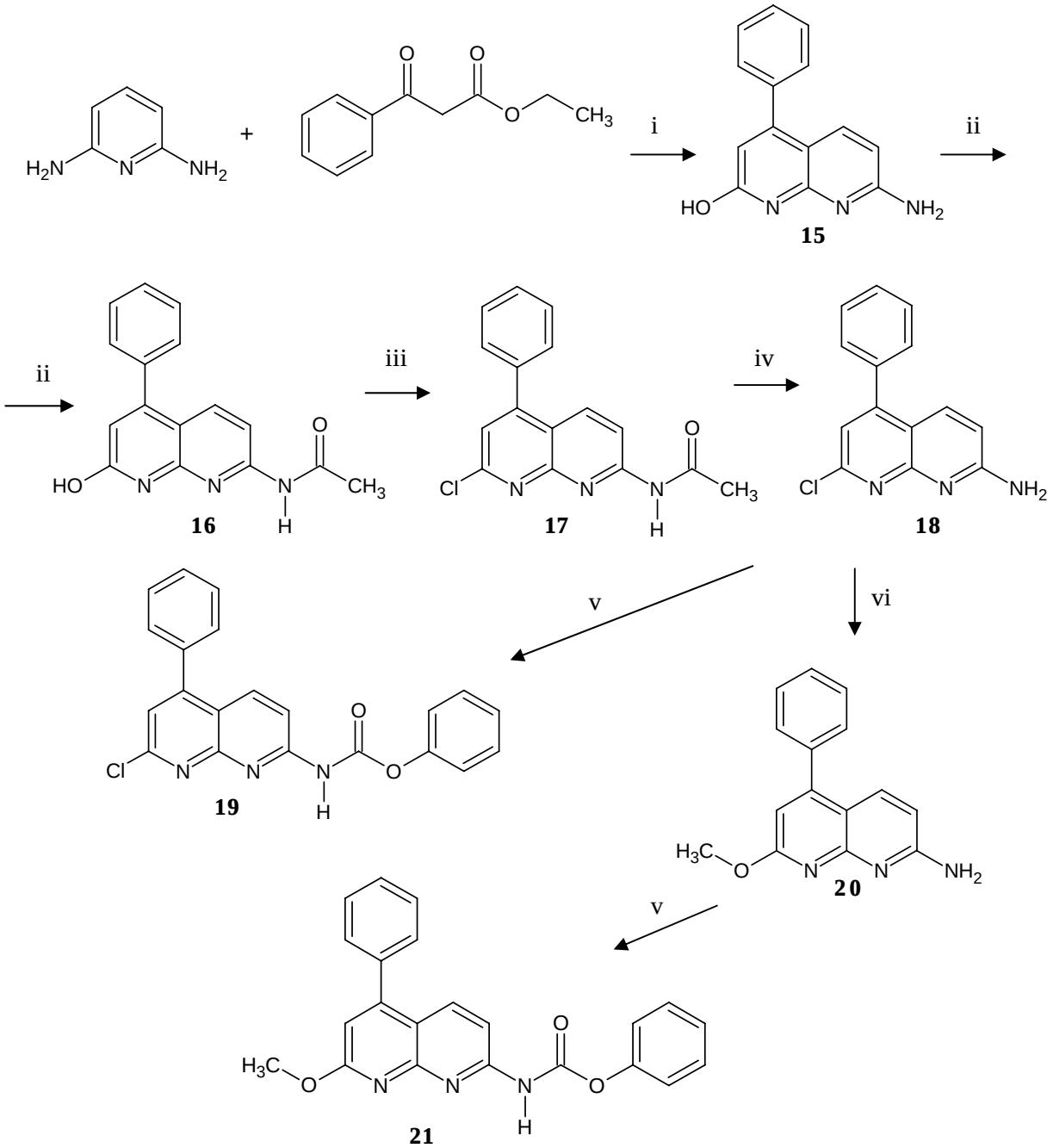

Reagents and conditions. i: 130°C, 30 min; H_2SO_4, 40°C, 16h. ii: Ac_2O, 140°C, 2h 30 min. iii: $POCl_3$, 100°C, 2h. iv: H_2SO_4, 100°C, 1h. v: dry CH_2Cl_2, TEA, phenylchloro formate, r.t., 12h. vi: MeONa, 80°C, 5h 30 min.

A mixture of 2,6-diamino pyridine and ethyl benzoyl acetoacetato was heated at 130°C until complete dissolution of the pyridine derivative, then was treated with H_2SO_4 at 40°C for 16 hours to yield compound **15,** [27] which was then acetylated by reaction with Ac_2O at 140°C for 2 hours and 30 minutes to obtain **16.** [27]The reaction of compound **16** with $POCl_3$ at 100°C for 2 hours gave the chloro derivative **17,**[27] which by treated with H_2SO_4 at 100 ° C for 1 hour to afford compound **18**. This compound by reaction with phenyl chloroformate, TEA at room temperature for 12 hours in dry CH_2Cl_2 gave the desired compound **19**. Moreover the reaction between **18** and MeONa at 80°C for 5 hours and 30 minutes yielded compound **20**, which by treatment with phenyl chloroformate, TEA at room temperature for 12 hours in dry CH_2Cl_2 gave the desired compound **21**.

Compounds belonging to the **E** series have been synthesized as shown in scheme 5.

Scheme 5

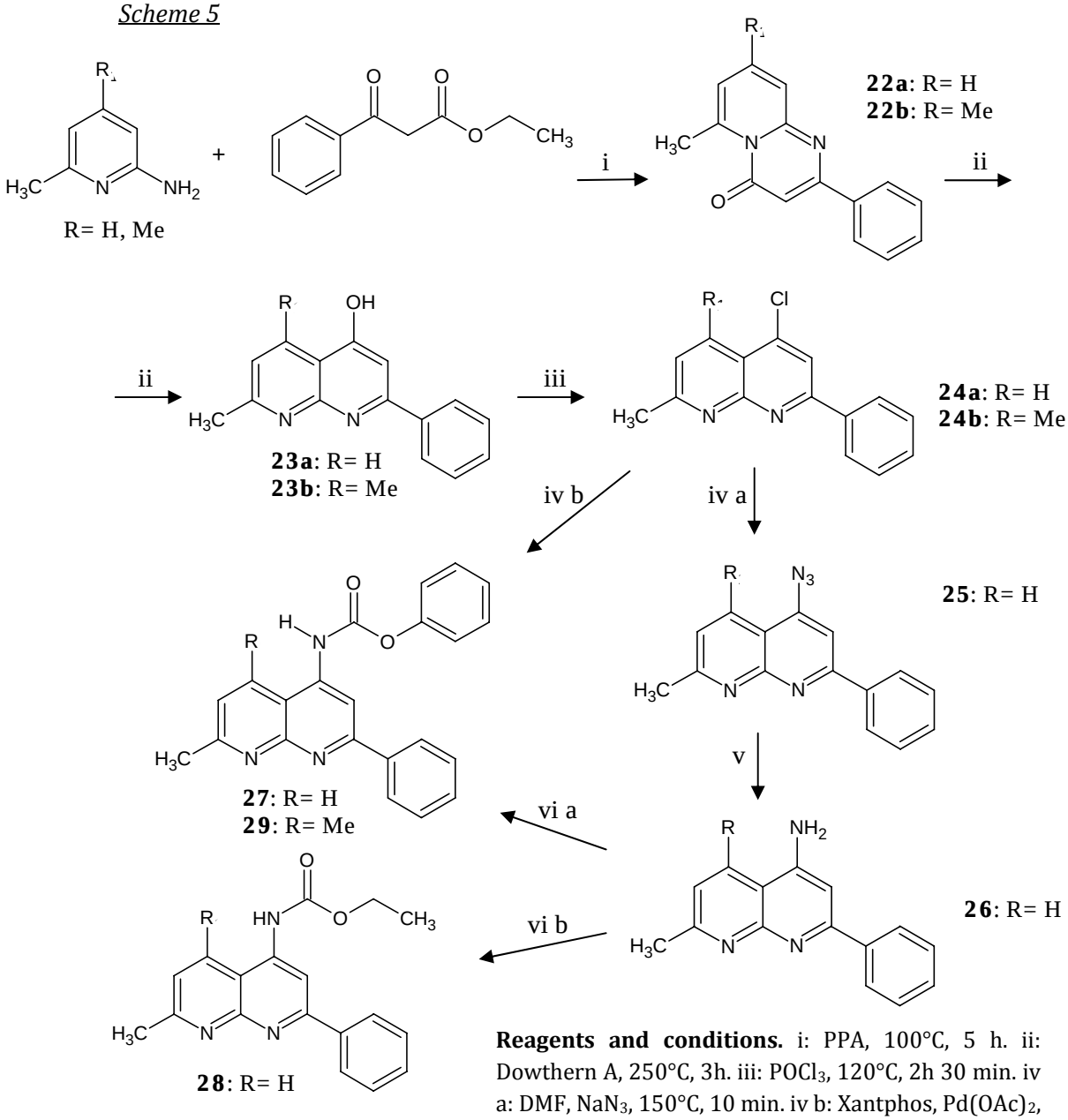

Reagents and conditions. i: PPA, 100°C, 5 h. ii: Dowthern A, 250°C, 3h. iii: $POCl_3$, 120°C, 2h 30 min. iv a: DMF, NaN_3, 150°C, 10 min. iv b: Xantphos, $Pd(OAc)_2$, Cs_2CO_3, phenyl acetylformiate, dioxane, 85°C, 24h. v: ethanol, H_2-Pd/C, r.t., 4h. vi a: dry CH_2Cl_2, TEA, phenyl chloroformate, r.t., 24h. vi b: dry CH_2Cl_2, TEA, ethyl chloroacetate, r.t., 24h.

The reaction between 2-amino-6-methyl pyridine or 2-amino-4,6-dimethyl pyridine and ethyl benzoyl acetoacetato at 100°C in PPA for 5 hours yielded compound **22a** or **22b** respectively , which by heating in Dowthern A at 250°C for 3 hours gave compounds **23a** or **23b** respectively**.** The reaction between compound **23a** or **23b** and $POCl_3$ at 120°C for 2 hours and 30 minutes yielded compound **24a** or **24b** respectively. Compound **24a** by a substitution reaction with NaN_3 at 150°C for 10 min gave the azide derivative **25,** which was then reduced by catalytic hydrogenation using H_2-Pd/C in ethanol at room temperature to afford the amino derivative **26**. The reaction between **26** and phenyl chloroformate, TEA in dry CH_2Cl_2 afforded compound **27** in very low yield instead the same reaction with ethyl chloroacetate gave compound **CV6** in good yield. Alternatively compound **28** was obtained by a palladium-catalyzed C–N coupling reaction between **24a** and phenyl carbamate, in 1,4-dioxane using palladium acetate as catalyst, Xantphos as ligand and Cs_2CO_3 as base at 85°C for 24 hours. Moreover the corresponding 5,7-dimethyl derivative **29** was obtained starting from compound **24a,** using the same conditions above reporte for the preparation of compound **28** (phenyl carbamate, in 1,4-dioxane using palladium acetate as catalyst, Xantphos as ligand and Cs_2CO_3 as base at 85°C for 24 hours).

5.1.2 Design, synthesis and biological evaluation of phenyl piperazine derivatives as MAGL inhibitors inspired by the endogenous substrate (2-AG).

As reported before another class of MAGL inhibitors are compounds inspired by the endogenous substrate 2-AG [19, 28, 28a] which are characterized by: a fatty acid chain (hydrophobic fragment), a linker and a polar substituent (Fig. 24).

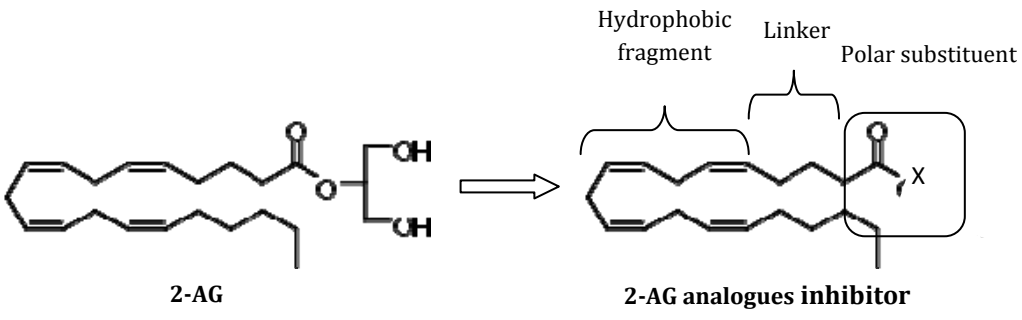

Fig 24. General structure of 2-AG analogues MAGL inhibitors

These compounds retain the arachidonic acid chain in their structure and this moiety could be oxidized in biological tissue, limiting the selectivity of the compounds. Moreover the arachidonic acid is a key metabolite in several pathways and therefore can be recognized by different enzymes, including lipases and cyclooxygenases. For this reason the arachidonic acid moiety was replaced by a suitable bioisostere such as biphenyl group.[29] In particular, recently, compounds of general structure **M** [30] were reported as potent inhibitors of human recombinant MAGL.

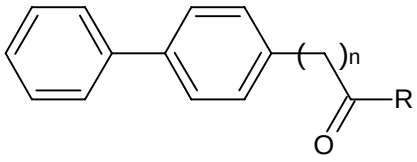

M

On the basis of these knowledge our research group decided to design and synthesize compounds with general structure **N**.

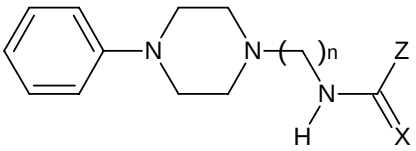

N

X= O, S. Z= NHR_1, R_1

As we can see from the structure reported above:

- the phenyl group of general structure **M** was replaced by the piperazine moiety, which is a characteristic group of other MAGL inhibitors such as SAR629 [19] (Fig.25.).

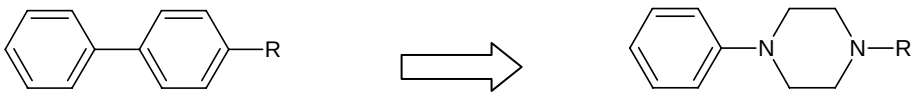

Fig. 25

- carbamate, thiocarbamate, urea, thiourea, and amide groups constituted the polar moiety, such as in other MAGL inhibitors just reported in literature.[31]
- the spacer is characterized by different chains of carbon atom in order to evaluate which is the best distance, between the hydrophobic fragment and the polar group, for the interaction with the enzyme.

In particular during my PhD project we synthesized urea, thiourea and amide derivatives with general structure **F**, **G** and **H**.

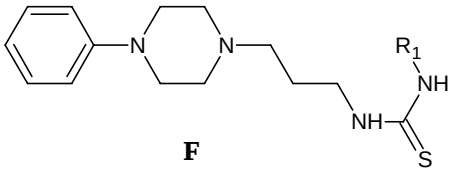

F

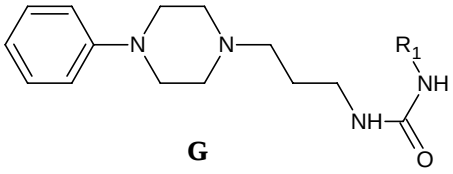

G

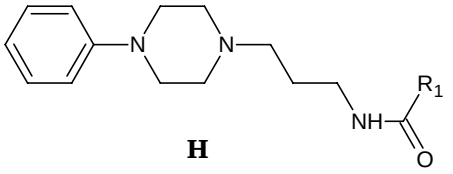

H

The synthesis of compounds with general structure **F**, **G**, **H** is reported in scheme 6.

Scheme 6

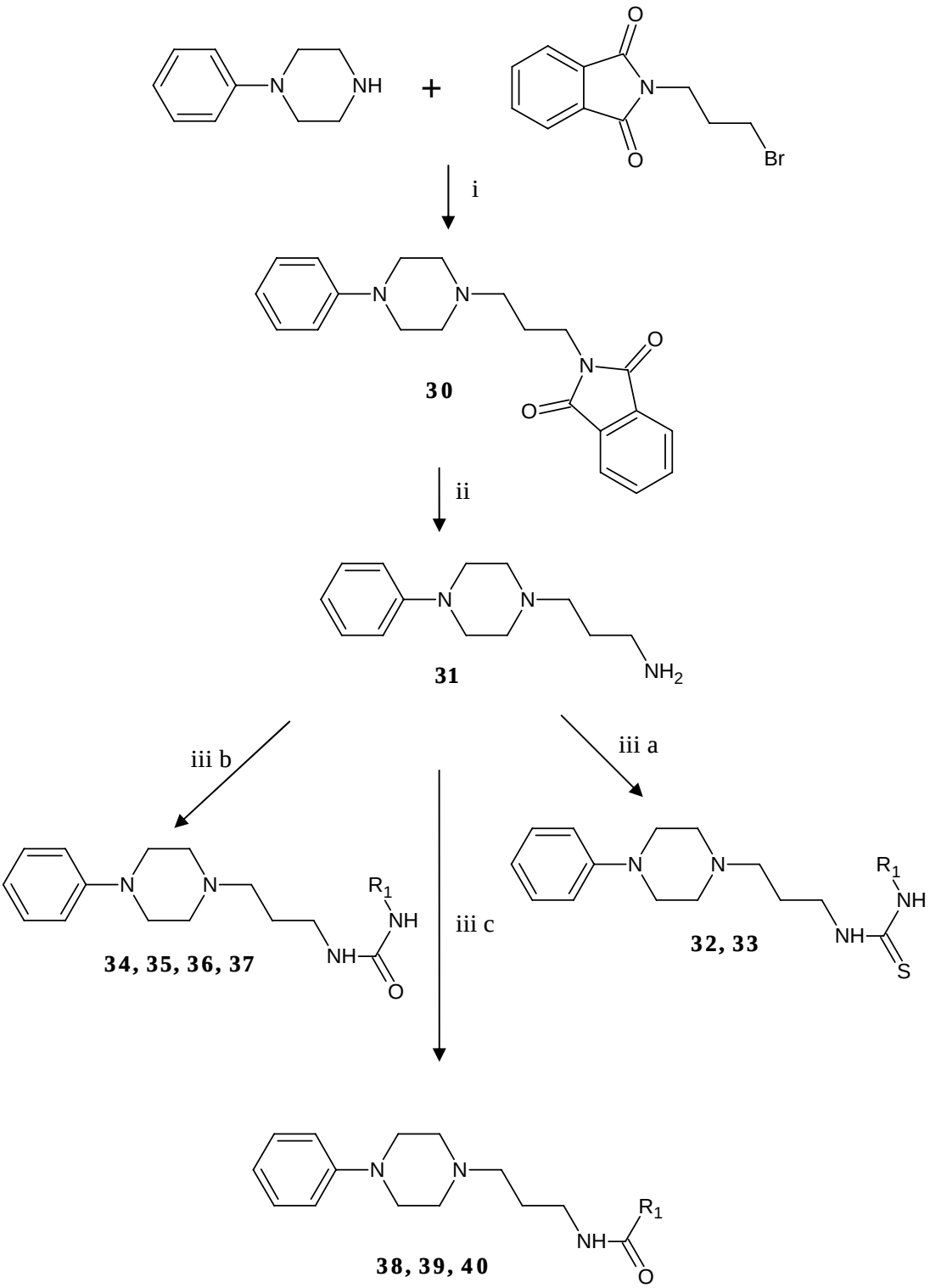

Reagents and conditions. i: dry CH_3CN, TEA, reflux, 16 h. ii: NH_2NH_2 acq., EtOH, 105°C, 5h. iii a: toluene, *p*-methoxy phenylisotiocyanate or *p*-chloro phenylisotiocyanate, r.t., 2h. iii b: toluene, phenyl isocyanate or *p*-methoxy phenylisocyanate or *p*-chloro phenylisocyanate or 2,4-dimethoxy phenylisotiocyanate, r.t., 2h. iii c: dry Ch_2Cl_2, benzoyl chloride or *p*-methoxybenzoyl chloride or *p*-fluorobenzoyl chloride, 0°C, 2h.

Tab 8. R_1 of compounds described in scheme 7.

COMPOUND	R1
32	*p*-chloro benzyl
33	*p*-methoxy benzyl
34	Benzyl
35	*p*-chloro benzyl
36	*p*-methoxy benzyl
37	2,4- dimethoxy benzyl
38	Benzyl
39	*p*-methoxy benzyl
40	*p*-fluoro benzyl

The reaction of N-(3- bromopropyl)phtalimide with phenylpiperazine, TEA in dry ACN at reflux for 16 hours yielded compound **30** which by reaction with hydrazine in ethanol at 150 ° C for 5 hours gave **31**. Compounds belonging to **F** series were obtained by reaction between **31** and *p*-methoxy phenylisotiocyanate or *p*-chloro phenylisotiocyanate respectively, in toluene at room temperature for 2 hours. Instead the reaction between **31** and phenyl isocyanate, *p*-methoxy phenylisocyanate, *p*-chloro phenylisocyanate or 2,4-dimethoxy phenylisotiocyanate respectively, in toluene at room temperature for 2 hours yielded the desired derivatives of series **G.** Moreover the amide derivatives of series **H** was obtained by the reaction between **31** and benzoyl chloride, *p*-methoxybenzoyl chloride or *p*-fluorobenzoyl chloride respectively, in dry CH_2Cl_2 at 0°C for 2 hours.

5.1.3 Design, synthesis and biological evaluation of orgaphosphoric derivatives as potential MAGL inhibitors.

Organophosphorus (OP) derivatives with general structure showed in figure 26, as reported in literature, are another class of potential MAGL inhibitors and could interact with several components of the cannabinoid system. [19 a, 19 b, 19 c]

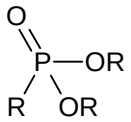

Fig. 26. General structure of OP derivatives

In particular Casida et al. indicated that some OP derivatives inhibit MAGL activity *in vitro* and that this inhibition leads to elevation of 2-AG levels in mice brain,[19 d] furthermore they showed that most OP compounds posses little or no selectivity for MAGL versus FAAH. One of the most representative compounds of this class of derivatives is UP101 which showed, as we can see from table 9, a high inhibition activity of the ECS enzyme but not selectivity towards MAGL (Table 9). Other examples of OP derivatives which did not showed high selectivity for MAGL versus FAAH are CPO and Paraox reported in figure 27. [19 d]

Tab. 9. Inhibition activity of UP101

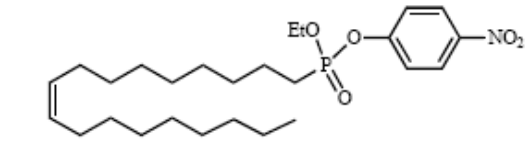

Target	IC_{50} (μM)[a]
MAGL (COS cell cytosol)	3.2 ± 0.17
DAGLα (human recombinant)	3.7 ± 0.2
FAAH (rat brain membranes)	0.18 ± 0.14

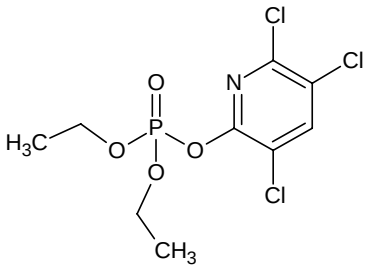

CPO

IC50 MAGL= 10 nM

IC50 FAAH= 460 nM

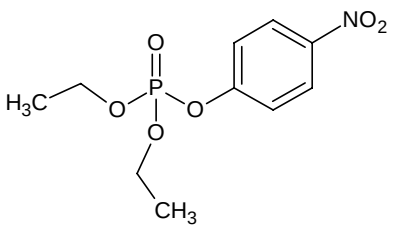

Paraox

IC50 MAGL= 1.2 mM

IC50 FAAH= 5.9 mM

Fig. 27

Moreover Nomura et al. demonstrated that several of the non-cholonergic OP effects are mediated by the ECS and that the inhibition of the metabolic enzyme by OP compounds is due for the phosphorylation of the catalytic site serine (S122 for MAGL and S241 for FAAH). [19 b]

On the basis of these knowledge we decided to design and synthesize OP derivatives with general structure **I** and **L** .

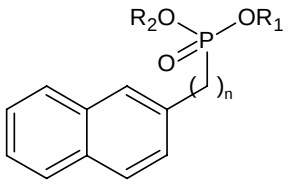

I

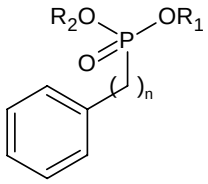

L

They are characterized by:

- a hydrophobic fragment, constitutes by naphthalene or benzyl group, in order to analyze the importance of the nucleus lypophilicity for the interaction with the enzyme.
- a spacer, constitutes by different chains of carbon atom in order to evaluate which is the best distance, between the hydrophobic nucleus and the polar group, for the interaction with the enzyme.
- a polar group, constitutes by a phosphonate moiety which present as R_1 and/or R_2 aromatic substituent, alkyl chains or H atoms.

During my PhD thesis we synthesized compound **41, 42, 43, 44** (n=1) as reported in scheme 7 and 8.

The synthesis of series **I** compounds is depicted in scheme 7.

Scheme 7

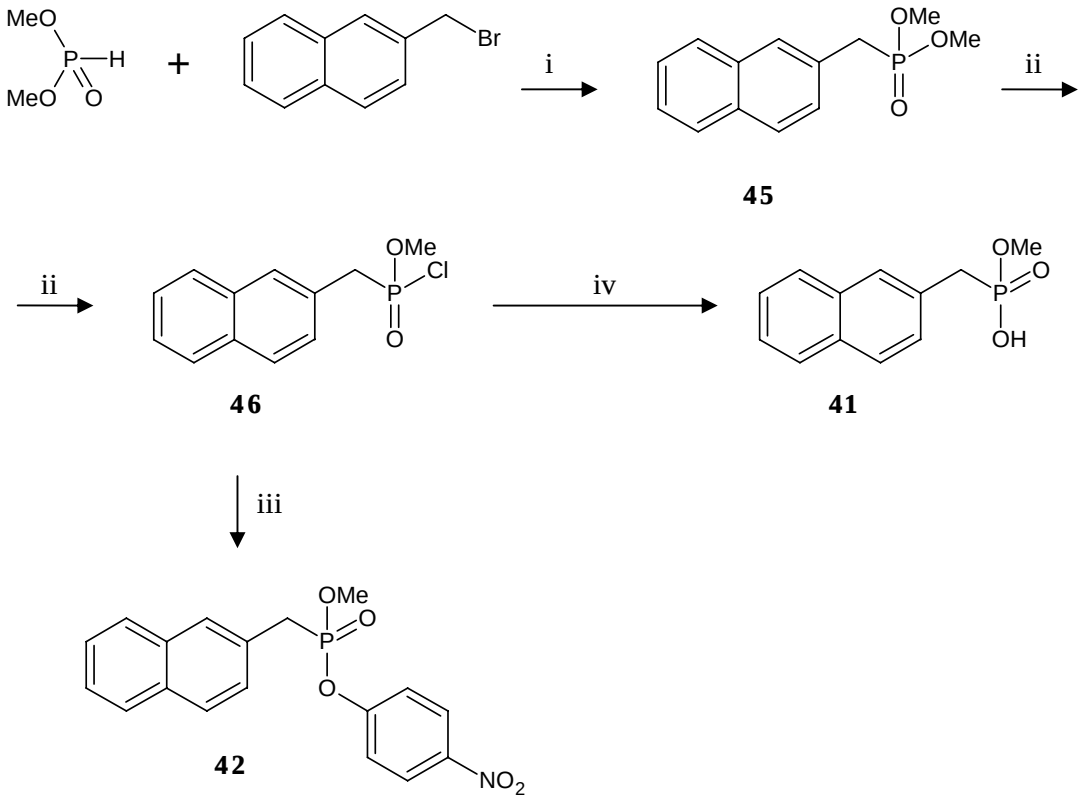

Reagents and conditions. i: Cs_2CO_3, TBAI, dry DMF, r.t., 24h. ii: $POCl_3$, 60°C, 3h. iii: 4-nitro phenol, TEA, dry CH_2Cl_2, 5h, from 0°C to r.t.. iv: NaOH 10%, r.t., 12h.

The reaction between dimethyl phosphite and 2-bromo methylnaphthalene with TBAI, Cs_2CO_3 in dry DMF at room temperature for 24 hours gave compound **45** which by reaction with $POCl_3$ at 60°C for 3 hours afforded **46.** The treatment of **46** with *p*-nitro phenol, TEA in dry CH_2Cl_2 for 5 hours yielded the desired final compound **42**. The desired compound **41** was obtained by reaction between **46** and NaOH 10% at room temperature for 12 hours.

Compounds with general structure **L** were synthesized, as reported in scheme 8, starting from diethyl benzylphosphonate which by treatment with NaOH 10% at room temperature for 12 hours gave the desired compound **43**; instead the reaction of diethyl benzylphosphonate with $POCl_3$ at 60°C for 3 hours yielded **47,** which by reaction with *p*-fluoro phenol, TEA, in dry CH_2Cl_2 for 5 hours led the desired final compound **44**.

Scheme 8

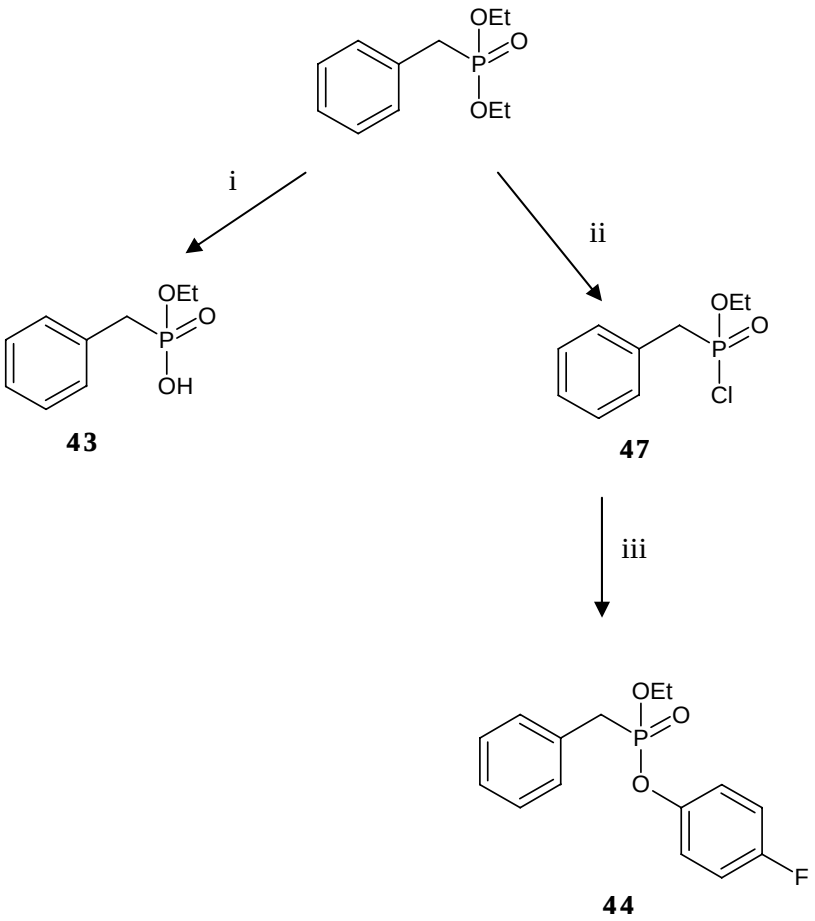

Reagents and conditions. i: NaOH 10%, r.t., 2 h- 30 min. ii: $POCl_3$, 60°C, 3h. iii: 4-fluoro phenol, TEA, dry CH_2Cl_2, 5h, from 0°C to r.t..

5.2 DISCUSSION AND CONCLUSIONS

The synthesized compounds were tested using a HPLC assay, developed in our research laboratory, using human recombinant MAGL as enzyme and 4-nitro phenylacetate (4-NPA) as enzymatic substrate. Several studies have been demonstrated that this compound (4-NPA) is a good MAGL substrate which, by enzymatic hydrolysis, causes the release of *p*-nitrophenol (PNP) (Fig. 28). [32]

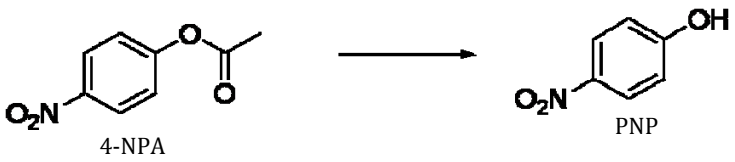

Fig. 28. Hydrolysis of 4-NPA and release of PNP.

The inhibitory activity of compounds tested, obtained from the residual enzymatic activity, was achieved from the quantitative analysis of PNP released.

As reported below, in the experimental part section, the best HPLC analysis conditions are:

- ✓ Stationary phase: VARIAN 150x4.6 mm INTERSIL 5µ;
- ✓ Mobile phase: composed of 53% MeOH and 47% 10mM ammonium acetate buffer at pH 4;
- ✓ Flow: 1.0 mL / min;
- ✓ Detector UV set at wavelengths of 315 nm;
- ✓ Synthesized compound concentration: 5 µM.

Moreover, in relation to the experimental experiences, all the compounds tested need a pre-incubation time, between the enzyme and inhibitor, of 30 minutes at 37°C and an incubation time of 10 minutes at 37°C after the substrate addition.

CARBAMATE DERIVATIVES

The MAGL percentage inhibition of carbamate derivatives tested with general structure **A, C, D** and **E**, until now, is reported in table 10.

Tab. 10. MAGL inhibitory activity of **A**, **B**, **D** and **E** series compound.

Compound	**Structure**	**% of MAGL residual activity** **[comp.]= 5 µM**	**% of MAGL inhibition** **[comp.]= 5µM**
5 **(A series)**	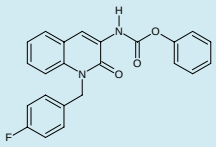	79.7%	20.3%
14 **(C series)**	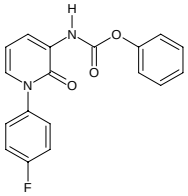	24.4%	75.6%
21 **(D series)**	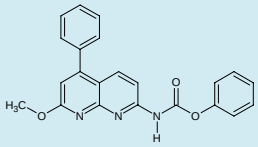	80.8%	19.2%
27 **(E series, R_1= H)**	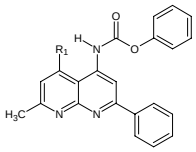	14.9%	85.1%
28 **(E series, R_1= H)**	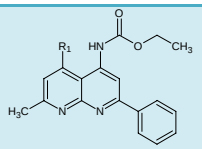	13%	87%
29 **(E series, R_1= Me)**	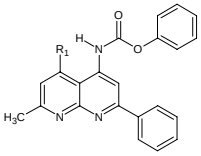	8.6%	91.4%

The data obtained using this assay showed that compound **14** (series **A**) posses higher MAGL inhibitory activity than compound **5** (series C). This result indicate that the more lipophilicity and/or steric hindrance of **5**, cause a reduction of compound-enzyme interaction. Moreover, the derivatives with greater MAGL inhibitory activity are **27**, **28** and **29**, which belongs to the **E** series. Thus is possible to assume that for this molecules the distance between the polar group (which could interact with Ser-122) and the aromatic substituent (which could interact with some hydrophobic residues of the enzyme) is better than in the other compounds tested.

PHENYL PIPERAZINE DERIVATIVES

The MAGL percentage inhibition of phenyl piperazine derivatives **F, G** and **H** tested is reported in table 11.

Tab. 11. MAGL inhibitory activity of some **F**, **G** and **H** series compound.

Compound	Structure	% of MAGL residual activity [comp.]= 5µM	% of MAGL inhibition [comp.]= 5µM
33	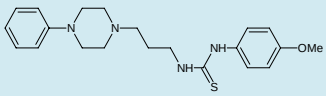	25.8%	74.2%
34	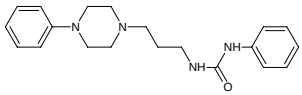	19.9%	80.01%
36	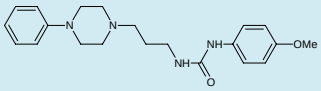	23.7%	76.3%
38	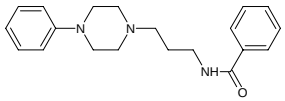	19.4%	80.6%
39	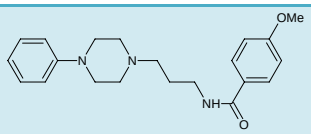	25.5%	74.5%

The results obtained showed that all compounds belonging have a good MAGL inhibitory activity, in fact the percentages of inhibition are between 74.5 to 80.6%, and the most potent inhibitor of these series is the amide derivative **38**, which inhibits the enzyme activity of 80.6%.

OP DERIVATIVES

Table 12 reported the percentage MAGL inhibition activity of compound **42,** which is the only OP derivatives tested until now using the HPLC assay.

Tab. 12. % of MAGL inhibitory activity of **42**.

Compound	Structure	% of MAGL residual activity [comp.]= 5 µM	% of MAGL inhibition [comp.]= 5µM
42	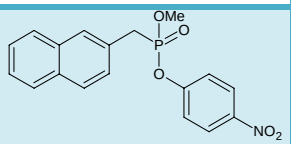	5.6%	94.4%

The inhibition curve was obtained analyzing five scalar concentrations of **42**, starting from a mother solution of 98,74 µM. The results obtained for each concentration are reported in table 13:

Tab.13

Concentration (µM)	% of MAGL residual activity	% of MAGL inhibition
10,97	5,6	94,4
5,49	7,4	92,6
0,00549	43,7	56,3
0,000549	89,3	10.7
0,0000549	98,8	1.2

The obtained data were elaborated in order to obtain the inhibition curve and the EC50 value (Fig. 29).

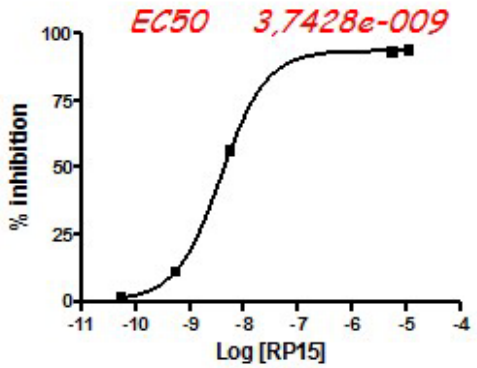

Fig.29. Inhibition curve of **42** and EC50 value.

Moreover some of the compounds synthesized were also tested, at the concentration of 1µM, by Dr. Chicca of the Institute of Biochemistry and Molecolar Medicine of Bern

University (Switzerland) using a radiometric assay with recombinant human MAGL and [^{3}H] 2-OG (2- oleyl glycerol) as enzymatic substrate.

Table 14, 15 and 16 reported the results obtained by the HPLC assay and the radiometric assay.

Tab. 14. MAGL inhibitory activity of **A**, **B**, **C**, **D** and **E** series compound.

Compound	**Structure**	**Radiometric assay** **% of MAGL inhibition [comp.]= 1µM**
5	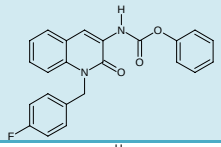	9.0%
9	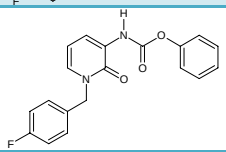	14.0%
14	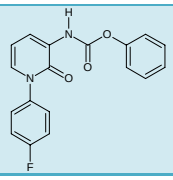	31.7%
19	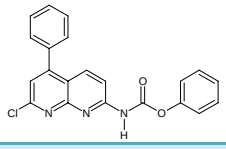	11.1%
21	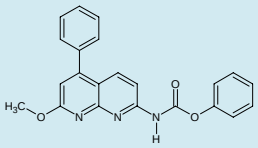	4.1%
27 **(R1= H)**	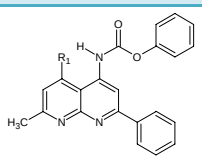	4.2%
28 **(R_1= H)**	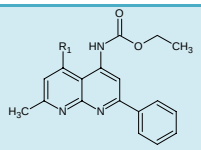	14.0%
29 **(R_1= Me)**	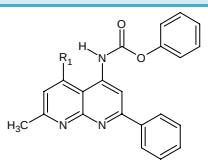	3.8%

Tab. 15. MAGL inhibitory activity of **F**, **G** and **H** series compound. (N.A.= no activity).

Compound	**Structure**	**Radiometric assay % of MAGL inhibition [comp.]= 1µM**
32	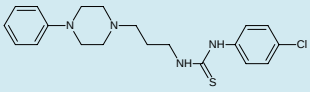	N.A.
34	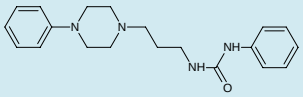	N.A.
36	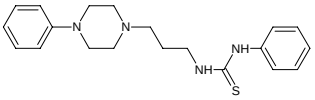	N.A.
37	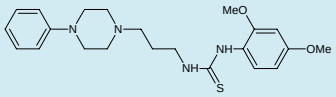	7.6%
38	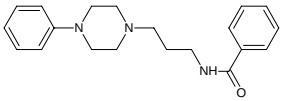	33.0%

The EC50 value was also calculated for compound RP15 (Tab. 16)

Tab. 16. % of MAGL inhibitory activity of compound **42**.

Compound	**Structure**	**Radiometric assay % of MAGL inhibition [comp.]= 1µM**
42	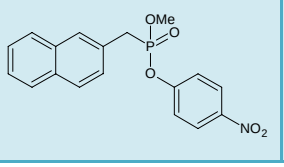	86.8% EC50=63.6 nM

The data reported in Table 14, 15 and 16 showed that there is a general correspondence between the results obtained using the radiometric assay and the HPLC assay. Furthermore compound **42** possess the highest MAGL inhibitory activity with a MAGL inhibition percentage of 86.8% and with EC50 of 63.6 nM (Fig.30).

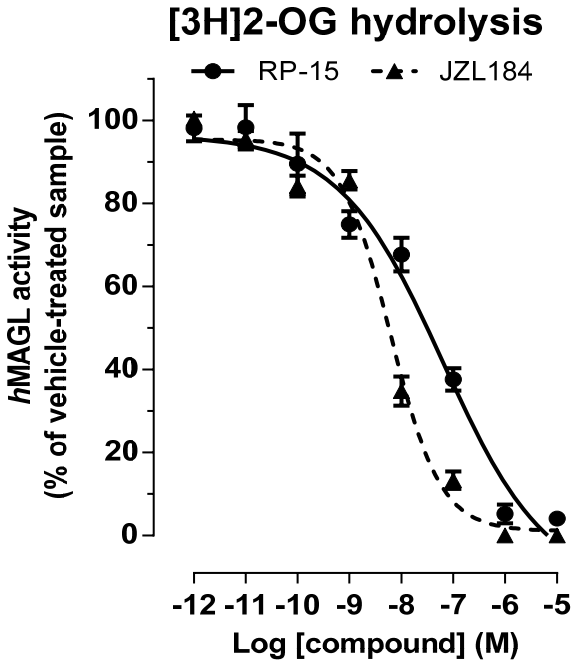

	RP15	JZL184
EC50	6.360e-008	6.238e-009

Fig. 30. EC50 of RP15 and comparison with the compound reported in literature JZL 184.

Furthermore Dr. Chicca evaluated also the FAAH and ABHD inhibitory activity of synthesized compounds and their interaction with the CB receptors using a method reported in literature. [33]

Receptor-binding experiments were performed with crude membrane expressing *h*CB1 or *h*CB2 receptors and co-incubated with 1 μM of synthesized compounds and [^{3}H]-CP-55940 as enzymatic substrate.[33] Instead FAAH activity was assessed using a cellular homogenate from fresh pig brains and the assay was done using 1 μM of synthesized compounds which were incubated with non-radioactive AEA and [ethanolamine-1-^{3}H]-AEAas enzymatic substrate.[33] Finally α,β-hydrolases (ABHD) -6 and -12 inhibition assays were performed using diluted pig brain homogenate preincubated with 1 μM of synthesized compound nonradioactive (2-OG) and [1,2,3-^{3}H]-2-OG as enzymatic substrate.[33]

Table 17 shows compound with most significant percentage of ECS enzyme inhibition or interaction with CB receptors.

Table 17. (N.A.= no activity)

Compound	% of MAGL inhibition [comp.]= 1µM	% of FAAH inhibition [comp.]= 1µM	% of ABHD inhibition [comp.]= 1µM	% of bound with CB1 [comp.]= 1µM	% of bound with CB2 [comp.]= 1µM
5 (A series)	9.0%	N.A.	N.A.	37.95%	68.8%
9 (B series)	14.0%	N.A.	N.A.	N.A.	N.A.
14 (C series)	31.7%	N.A.	N.A.	N.A.	N.A.
34 (G series)	N.A	29.7%	N.A.	N.A.	N.A.
38 (H series)	33.0%	N.A.	N.A.	21.2%	N.A.
36 (G series)	N.A.	10.2%	N.A.	N.A.	N.A.
42 (I series)	86.8%	97.8%	N.A.	23.0%	N.A.

Table 17 shows compounds with most significant percentage of ECS enzymes inhibition or interaction with the CB receptor. Analyzing the data we can assume that:

1. Compound **5** showed CB binding capacity.
2. None of the tested compounds showed ABHD inhibition activity.
3. Compound **14**, which is the greater MAGL inhibitor of **A**, **B** and **C** series using the radiometric assay, did not showed FAAH or ABHD inhibitory activity, and from these results we can conclude that the phenyl carbamate **14** is a low but selective MAGL inhibitor.
4. Compound **38,** which present good MAGL inhibitory capacity did not have any activity toward the other tested ECS enzymatic systems, while compound **34** showed a good FAAH inhibitory activity. We can also affirm that we have identified and characterized two new selective FAAH or MAGL inhibitors : **38** is a selective MAGL inhibit and **34** is a selective FAAH inhibitor.
5. **42**, as we expected, [23, 24] strongly inhibits both MAGL and FAAH enzyme.

Due to the high inhibitory activity of this compound, our research group is developing a project in order to obtain, with appropriate structural changes, fluorescent molecules that could be use as enzymatic substrates for the inhibitory activity assay.

5.4 CHEMISTRY

Melting points were determined on a Kofler® hot stage apparatus and are uncorrected. ^{1}H-NMR spectra were recorded with a Bruker AC-200® spectrometer in δ units with TMS as an internal standard. TLC was performed on silica gel sheets (Silica Gel 60 F254, Merck, Germany). Microwave-assisted reactions were run in a CEM microwave synthesizer. The system for isocratic flash chromatography includes a Buchi® Pump Module C-601 (continuous flow of solvents up to 250ml/min at max 10bar) and Buchi® prepacked cartridges (silica gel 60, particle size 40-63 µm).
The analytical HPLC system consisted of a Thermo Finnigan Spectra System SN4000 system controller, coupled to a P2000 pump, a SCM1000 degasser, and a UV2000 UV detector at an operation wavelength of 220 and 280 nm (Thermo Finnigan, Waltham, MA). Separation was performed on a 150 mm × 4.6 mm Luna column packed with 5 μm C18 particles. The mobile phase, delivered at isocratic flow, consisted of methanol (15-30%) and water (85-70%). HPLC grade methanol was acquired from Sigma-Aldrich (Sydney, Australia), and the water used was of Milli-Q grade purified by a Milli-Q UV purification system (Millipore Corporation, MA). For all compounds, 1.0 mg was dissolved in 2.0 mL of MeOH and an amount of 20 μL was injected in analytical HPLC. Comparing the chromatograms, we were able to estimate the purity of each compounds that appeared >96%.

3-bromoquinoline 1-oxide (1)

0.508 g (2.95 mmol) of m-CPBA was added to a solution of 0.600 g (2.88 mmol) of 3-bromo-quinoline in 10 ml of $CHCl_3$. The mixture was stirred at room temperature for 20 hours. Then the mixture was diluted with 10 ml of aqueous $NaHCO_3$ 1M and aqueous NaOH 1M and extracted with $CHCl_3$, the organic layer was dried with $MgSO_4$ and concentrated under reduced pressure to obtain a crude product. The crude was treated with petroleum ether and the precipitate obtained was collected by filtration and crystallized with petroleum ether high-boiling (p.e.= 100- 120°C) in order to obtain **1**.

Yield: 58%

Mp: 191-194°C

^{1}H-NMR: (DMSO) 8.70-8.63 (m, 2H, H_4, H_2); 7.90-7.67 (m, 4H, H_5, H_6, H_7, H_8);

3-bromoquinolin-2(1*H*)-one (2)

4 ml of aqueous NaOH 1.5N (3.00 mmol) and 0.20 ml (1.68 mmol) of benzoyl chloride was added to a solution of 0.300 g (1.40 mmol) of **1** in 5 ml of CH_2Cl_2. After that the mixture was stirred at 0°C for 2 hours, the precipitate obtained was collected

by filtration and crystallized with petroleum ether high-boiling (p.e.= 100- 120°C) in order to obtain **2.**

Yield: 80%

Mp: 215-217°C

^{1}H-NMR: (DMSO) δ 8.26 (s, 1H, H_4); 7.56 (d, 1H, H_5); 7.43 (d, 1H, H_8); 7.28 (m, 2H, H_6, H_7); 1.47 (s, 1H, NH)

3-bromo-1-(4-fluorobenzyl)quinolin-2(1*H*)-one (3)

0.083 g (3.47 mmol) of NaH was added to a solution of 0.500 g (2.89 mmol) of **2** in 20 ml of anhydrous DMF and the mixture was stirred at 50°C for two hours. After that 0.38 ml of 4-fluorobenzyl chloride (3.47 mmol) was added dropwise and the mixture was stirred at room temperature for 24 hours. The solution was then concentrated under vacuum, the crude product was treated with water and the precipitate obtained was purified by flash-chromatography using as eluent ethyl-acetate/ hexane (4/1) in order to obtain compound **3** as a crystalline solid.

Yield: 57%

Mp: 224-227°C

^{1}H-NMR: (DMSO) δ 8.21 (s, 1H, H_4); 7.50 (m, 2H, H_5, H_8); 7.27 (m, 4H, phenyl group); 7.05 (m, 2H, H_6, H_7); 5.58 (s, 2H, CH_2)

4-nitrophenyl [1-(4-fluorobenzyl)-2-oxo-1,2-dihydroquinolin-3-yl]carbamate (4)

0.124 g (0.370 mmol) of **3** was added, under nitrogen flow, to a suspension of 0.005 g (0.030 mmol) of $Pd(AcO)_2$, 0,010 g (0.020 mmol) of Xantphos, 0,150 g (0,820 mmol) of 4-nitrophenyl carbamate and 0,294 g (0.900 mmol) of Cs_2CO_3 in 7 ml of dioxane. The mixture was heated at 100°C for 10 hours, after that it was cooled, filtered and concentrated under reduced pressure. The crude product obtained was purified by flash-chromatography using as eluent CH_2Cl_2 to obtain compound **4** as a light brown solid.

The same reaction was also done using the microwave with the following conditions: T= 140°C, t= 38 min, P= 5 Bar, stirring on, cooling on. The mixture was then cooled, filtered and concentrated under reduced pressure. The crude product obtained was purified by flash-chromatography using as eluent CH_2Cl_2 to obtain compound **4** as a light brown solid.

Yield: 35%

Mp: 238-241°C

^{1}H-NMR: (DMSO) δ 8.32 (s, 1H, NH carbamate); 7.85 (s, 1H, H_4); 7.81 (s, 1H, H_8); 7.57 -7.45 (m, 4H, phenyl group); 7.38 -7.13 (m, 7H, phenyl group, H_5, H_6, H_7); 5.61 (s, 2H, CH_2)

Phenyl [1-(4-fluorobenzyl)-2-oxo-1,2-dihydroquinolin-3-yl]carbamate (5)

0.124 g (0.370 mmol) of **3** was added, under nitrogen flow, to a suspension of 0.005 g (0.030 mmol) of $Pd(AcO)_2$, 0.010 g (0.020 mmol) of Xantphos, 0.112 g (0.820 mmol) of phenyl carbamate and 0.294 g (0.900 mmol) of Cs_2CO_3 in 7ml of dioxane. The mixture was heated at 100°C for 10 hours, after that it was cooled, filtered and concentrated under reduced pressure. The crude product obtained was purified by flash-chromatography using as eluent CH_2Cl_2 to obtain compound **5** as a light brown solid.

The same reaction was also done using the microwave with the following conditions: T= 140°C, t= 38 min, P= 5 Bar, stirring on, cooling on. The mixture was then cooled, filtered and concentrated under reduced pressure. The crude product obtained was purified by flash-chromatography using as eluent CH_2Cl_2 to obtain compound **5** as a light brown solid.

Yield: 33%

Mp: 231-233°C

^{1}H-NMR: (DMSO) δ 8.31 (s, 1H, NH carbamate); 7.83 (s, 1H, H_4); 7.81 (s, 1H, H_8); 7.57-7.40 (m, 4H, phenyl group); 7.33-7.10 (m, 7H, phenyl group; H_5; H_6; H_7); 5.51 (s, 2H, CH_2).

4-fluorobenzyl 1-(4-fluorobenzyl)-2-oxo-1,2-dihydropyridine-3-carboxylate (6)

0.650 g (12.9 mmol) of NaH was added to a solution of 1.50 g (10.8 mmol) of 2-hydroxy nicotinic acid in 20 ml of anhydrous DMF and the mixture was stirred at room temperature for two hours. After that 1.50 ml (12.9 mmol) of 4-fluorobenzyl chloride was added dropwise and the mixture was stirred at 50°C for 24 hours. Furthermore the solution was concentrated under vacuum and the crude product obtained was washed with water and collected by filtration. The crude mixture was added to a solution of NaOH 10% and heated under reflux for 4 hours. Then the solution was cooled into ice bath and acidified until acid pH. The precipitate obtained was collected by filtration and treated with petroleum ether high-boiling (p.e.= 100-120°C) in order to obtain compound **6** as a crystalline solid.

Yield: 75%

Mp: 221-224°C

^{1}H-NMR: (DMSO) δ 14.40 (s, 1H, COOH); 8.40 (m, 2H, H_4, H_6); 7.41 (d, 2H, phenyl group); 7.18 (d, 2H, phenyl group); 6.48 (t, 1H, H_5); 5.28 (s, 2H, CH_2)

Tert-butyl [1-(4-fluorobenzyl)-2-oxo-1,2-dihydropyridin-3-yl]carbamate (7)

1.05 ml (4.85 mmol) of diphenyl phosphoryl azide was added to a solution of 1.00 g (4.05 mmol) of **6** and 0.590g (4.85 mmol) of t-ButOK in 25 ml of t-ButOH. The mixture was heated under reflux for 24 hours, after that the mixture was diluted with CH_2Cl_2, washed with water and dried with $MgSO_4$. The organic layer was concentrated under reduced pressure to give a crude product as a brown oil. The crude product was purified by flash-chromatography using as eluent hexane/ethyl acetate (3/1) to obtain **7** as a crystalline solid.

Yield: 25%

Mp: 230-233°C

^{1}H-NMR: (DMSO) δ 8.60 (s, 1H, NH carbamate); 7.81 (d, 1H, H_4); 7.55 (d,1H, H_6); 7.37 (m, 2H, phenyl group); 7.16 (m, 2H, phenyl group); 5.15 (s, 2H, CH_2); 1.46 (s, 9H, t-butyl)

3-amino-1-(4-fluorobenzyl)pyridin-2(1*H*)-one (8)

0.300 g (0.940 mmol) of **7** was added to 16 ml of HCl 6N and the mixture was stirred at room temperature for 4 hours. After that the solution was alkalized with $NaHCO_3$ 1 M and the product was extracted with CH_2Cl_2. The organic layer was dried with anhydrous $MgSO_4$ and evaporated under reduced pressure to give **8** as a brown oil.

Yield: 95%

^{1}H-NMR: (DMSO) δ 7.32 (m, 2H, phenyl group); 7.29 (m, 2H, phenyl group); 7.17 (d, 1H, H_4); 6.42 (d, 1H, H_6); 5.11 (s, 1H, NH_2); 5.05 (s, 2H, CH_2).

Phenyl [1-(4-fluorobenzyl)-2-oxo-1,2-dihydropyridin-3-yl]carbamate (9)

0.44 ml (2.73 mmol) of phenyl chloroformate was added dropwise to a solution of 0.300 g (1.05 mmol) of **8** and 0.38 ml of TEA (2.73 mmol) in 10 ml of anhydrous CH_2Cl_2. After that the mixture was stirred at room temperature for 4 hours, it was evaporated under vacuum and the crude product obtained washed with water, treated with diethyl ether and collected by filtration.

Yield: 65%

Mp: 135-138°C

^{1}H-NMR: (DMSO) δ 8.95 (s, 1H, H carbamate); 7.83 (d, 1H, H_4); 7.80 (d, 1H, H_6); 7.61-7.17 (m, 8H, phenyl group); 6.75 (m,1H, phenyl group); 6.32 (t, 1H, H_5); 5.16 (s, 2H, CH_2)

Methyl 1-(4-fluorophenyl)-2-oxo-1,2-dihydropyridine-3-carboxylate (10)

0.37 ml (3.90 mmol) of 4-fluoroaniline was added to a solution of 1.00 g (3.25 mmol) of methyl 2-oxo-2*H*-pyran-6-carboxylate in 10 ml of anhydrous DMF. The solution was stirred at 0°C for 7 hours, after that was added 0.100g (0.810 mmol) of DMAP and 0,810 g (4.22 mmol) of EDCI hydrochloride. The mixture was stirred overnight at room temperature, then the solution was concentrated under reduced pressure to obtain a crude product. The crude was washed with water and the organic layer and the product was extracted with ethyl acetate. The organic layer was dried with $MgSO_4$ and was concentrated under reduced pressure to obtain a product, which was purified by flash-chromatography, using as eluent ethyl acetate/hexane (3/1) to obtain **10** as a crystalline solid.

Yield: 57%

Mp: 219-221°C

^{1}H-NMR: (DMSO) δ 8.10 (dd, 1H, H_4); 7.92 (dd, 1H, H_6); 7.45 (m, 2H, phenyl group); 7.33 (m, 2H, phenyl group); 6.37 (t, 1H, H_5); 3.71 (s, 3H, OCH_3)

1-(4-fluorophenyl)-2-oxo-1,2-dihydropyridine-3-carboxylic acid (11)

0,450 g (1.82 mmol) of **10** was added to a solution of NaOH 10%, and the mixture was heated under reflux for 4 hours, the mixture was acidified at 0°C and the precipitate obtained was collected by filtration and use as crude product for further reactions.

Yield: 80%

^{1}H-NMR: (DMSO) δ 14.23 (s, 1H, COOH); 8.47 (dd, 1H, H_4); 8.20 (dd, 1H, H_6); 7.51 (m, 2H, phenyl group); 7.41 (m, 2H, phenyl group); 6.77 (t, 1H, H_5)

Tert-butyl [1-(4-fluorophenyl)-2-oxo-1,2-dihydropyridin-3-yl]carbamate (12)

0.40 ml (1.80 mmol) of diphenyl phosphoryl azide was added to a solution of 0.350 g (1.50 mmol) of **11** and 0.133 g (1.80 mmol) of t-ButOK in 25 ml of t-ButOH. The mixture was heated under reflux for 24h. After that the solution was diluted with CH_2Cl_2, washed with water and the organic layer was dried with $MgSO_4$, concentrated under reduced pressure and crystallized with petroleum ether high-boiling to obtain compound **12** as a crystalline solid.

Yield: 43%

Mp: 229-231°C

^{1}H-NMR: (DMSO) δ 8.76 (s, 1H, NH carbamate); 7.81 (dd, 1H, H_4); 7.55 (dd,1H, H_6); 7.37- 6.93 (m, 4H, phenyl group); 6.33 (t, 1H, H_5); 1.43 (s, 9H, t-Butyl)

3-amino-1-(4-fluorophenyl)pyridin-2(1*H*)-one (13)

0.150 g (0.490 mmol) of **12** was added to a solution of HCl 6N and the mixture was stirred at room temperature for 4 hours. After that the solution was alkalized with $NaHCO_3$ and the product was extracted with CH_2Cl_2. The organic layer was dried with anhydrous $MgSO_4$ and evaporated under reduced pressure in order to obtain **13** as a brown oil.

Yield: 90%

^{1}H-NMR: (DMSO) δ 7.41 (m, 2H, phenyl group); 7.36 (m, 2H, phenyl group); 6.75 (dd, 1H, H_4); 6.58 (dd, 1H, H_6); 6.15 (t, 1H, H_5); 4.31(s, 1H, NH_2)

Phenyl [1-(4-fluorophenyl)-2-oxo-1,2-dihydropyridin-3-yl]carbamate (14)

0.10 ml (0.610 mmol) of phenyl chloroformate was added dropwise to a solution of 0.050 g (0.250 mmol) of **14** and 0.085ml of TEA (6.21 mmol) in 10 ml of anhydrous CH_2Cl_2. After that the mixture was stirred for 4 hours at room temperature, evaporated and the crude product obtained was washed with water, treated with diethyl ether and collected by filtration to give **B2a.**

Yield: 62%

Mp: 145-148°C

^{1}H-NMR: (DMSO) δ 8.99 (s, 1H, H carbamate); 8.18 (dd, 1H, H_4); 7.90 (dd, 1H, H_6); 7.49-7,17 (m, 9H, phenyl group); 6.38 (t, 1H, H_5)

7-amino-4-phenyl-1,8-naphthyridin-2-ol (15)

2.50 g (22.9 mmol) of 2,6-diamino pyridine was heated with 6 ml of ethyl benzoyl acetoacetate until complete dissolution (130°C for about 30 minutes). After cooling, 6 ml of H_2SO_4 were added and the mixture was heated at 40°C for 16 hours. Furthermore the mixture was treated with water/ice, alkalized until pH= 8 using NH_4OH and the precipitate obtained was collected by filtration pure enough for further reactions.

Yield: 45%

^{1}H-NMR: (DMSO) δ 11.67 (1H, OH); 7.49-7.34 (m, 6H, Ar, 1H); 6.84 (NH_2); 6.31 (d, 1H); 6.01 (s, 1H).

N-(7-hydroxy-5-phenyl-1,8-naphthyridin-2-yl)acetamide (16)

3.00 g (12.6 mmol) of **15** were added to 40 ml of Ac_2O and heated at 140°C for 2 hours and half. After that the mixture was cooled and the precipitate obtained was collected by filtration and washed for a few times with ethanol to obtain **16** as a white solid (pure enough for further reactions).

Yield: 95%

^{1}H-NMR: (DMSO) δ 11.67 (1H, OH); 7.82 (NH); 7.49-7.34 (m, 6H, Ar, H_5); 6.31 (d, 1H,); 6.01 (s, H_6); 4.08 (s, 3 H, CH_3).

N-(7-chloro-5-phenyl-1,8-naphthyridin-2-yl)acetamide (17)

1.0 g of **16** (3.57 mmol) was added to 10 ml of $POCl_3$ and heated at 100°C for 2 hours. After cooling the mixture was treated with NH_4OH until pH= 8 and the precipitate obtained was collected by filtration and washed for a few times with water to obtain a white solid (pure enough for further reactions).

Yield: 95%

^{1}H-NMR: (DMSO) δ 11.2 (s, 1H, NH); 8.38 (d, 1H, H_5); 8.25 (d, 1H, H_6); 7.59 (s, 5H, Ar); 7.53 (s, 1H, H_3); 2.17 (s, 3H, CH_3).

7-chloro-5-phenyl-1,8-naphthyridin-2-amine (18)

1.50 g (5.04 mmol) of compound **17** was hydrolyzed with 15 ml of H_2SO_4 at reflux for 1 hour. After cooling the mixture was treated with water, alkalized with NH_4OH until pH= 8 and the precipitate obtained was collected by filtration.

Yield: 95%

^{1}H-NMR: (DMSO) δ 7.77 (d, 1H, H_5); 7.59-7.48 (m, 5H, Ar); 7.13 (s, 3H, NH_2, H_3); 6.81 (d, 1H, H_6).

Phenyl (7-chloro-5-phenyl-1,8-naphthyridin-2-yl)carbamate (19)

0.500 g (1.96 mmol) of **18** was solubilized in 15 ml of dry CH_2Cl_2, was added 0.71 ml (5.10 mmol) of TEA and 0.64 ml (5.10 mmol) of phenyl chloroformate. The mixture was stirred at room temperature for 12 hours, after that the solvent was evaporated under reduce pressure to obtain a crude product which was purified by flash chromatography using as eluent AcOEt/ hexane(1/3) to get **19** as a light yellow solid.

Yield: 62%

Mp: 98-101 °C

^{1}H-NMR: (DMSO) δ 11.46 (s, 1H, NH); 7.25-8.29 (m, 13H, Ar)

^{13}C-NMR: ($CDCl_3$) δ 154.24; 154.09; 152.44; 151.74; 150.31; 138.27; 135.85; 129.75; 129.66; 129.53; 129.22; 126.40; 121.96; 121.81; 117.97; 113.83

7-methoxy-5-phenyl-1,8-naphthyridin-2-amine (20)

A mixture of 0.700 g (2.74 mmol) of **18** and MeONa (53.2 ml of MeOH and 0.627 g of Na) was heated at 80°C for 5 hours and half. After that the solvent was evaporated under reduce pressure, was added water and the mixture was treated with HCl 10%

until pH= 8. The precipitate obtained was collected by filtration and dried under reduce pressure.

Yield: 92%

Mp: 174-180°C

^{1}H-NMR: (DMSO) δ7.65 (d, 1H, H_5); 7.50-7.42 (m, 5H, Ar); 6.70 (s, 2H, NH_2); 6.60 (d, 1H, H_6); 6.54 (s, 1H, H_3); 3.93 (s, 3H, OCH_3).

Phenyl (7-methoxy-5-phenyl-1,8-naphthyridin-2-yl)carbamate (21)

To a solution of 0.210 g (0.837 mmol) of **20** in 10 ml of dry CH_2Cl_2, was added 0.30 ml (2.18 mmol) of TEA and 0.27 ml (2.18 mmol) of phenyl chloroformate dropwise. The mixture was stirred at room temperature for 12 hours and then the solvent was evaporated under reduce pressure to obtain a crude product which was purified by flash chromatography using as eluent AcOEt/hexane (1/3).

Yield: 62%

Mp: 93-95 °C

^{1}H-NMR: (DMSO) δ 11.26 (s, 1H, NH); 8.14-8.10 (d, 1H, H_3); 7.94-7.98 (d, 1H, H_4); 7.21-7.53 (m, 10H, Ar); 6.91 (s, 1H, H_6); 4.01 (s, 3H, OCH_3)

^{13}C-NMR: ($CDCl_3$) δ 163.60; 153.84; 153.00; 151.40; 150.52; 149.56; 136.45; 135.59; 128.80; 128.60; 128.38; 128.26; 128.16; 125.07; 121.34; 114.54; 110.17; 52.91

6-methyl-2-phenyl-4*H*-pyrido[1,2-a]pyrimidin-4-one (22a)

6,4-dimethyl-2-phenyl-4*H*-pyrido[1,2-a]pyrimidin-4-one (22b)

A mixture of 5.00 g (0.046 mol) of 2-amino 6-methylpyridine or (0.042 mol) 2-amino 4,6-dimethylpyridine, 10.7 g (0.019 mol) of ethyl-benzoyl acetate and 50 g of PPA are heated at 100°C for 5 hours. Water and ice were added after cooling and the precipitate obtained was collected by filtration. The water was alkalized until pH=4 using NH_4OH and the precipitate was collected by filtration to obtain **22a** or **22b** respectively like a dark-yellow solid pure enough for further reactions.

Yield 22a: 85%

Yield 22b: 80%

4-chloro-7-methyl-2-phenyl-1,8-naphthyridine (23a)

4-chloro-5,7-dimethyl-2-phenyl-1,8-naphthyridine (23b)

1g of **22a**(4.23 mmol) or of **22b** (4.10 mmol) in 15 ml of Dowtherm A was heated at 250°C for 3 hours. After cooling the precipitate obtained was collected by filtration and washed with petroleum ether for five times to obtain **23a** or **23b** respectively like a brown solid.

Yield 23a: 80%

Yield 23b: 88%

Mp 23a: 122-124°C

Mp 23b: 125-127°C

^{1}H-NMR 23a: (DMSO) δ 11.67 (1H, OH); 7.38-7.24 (m, 6H, Ar, 1H); 6.10 (d, 1H); 5.95 (s, 1H); 3.25 (s, 3H, CH_3).

^{1}H-NMR 23b: (DMSO) δ 11.55 (1H, OH); 7.32-7.18 (m, 5H, Ar); 6.50 (s, 1H); 5.90 (s, 1H); 3.25 (s, 3H, CH_3); 3.15 (s, 3H, CH_3).

7-methyl-2-phenyl-1,8-naphthyridin-4-ol (24a)

5,7-dimethyl-2-phenyl-1,8-naphthyridin-4-ol (24b)

1g of **23a** (4.01 mmol) or **23b** (3.98 mmol) in 10 ml of $POCl_3$ was heated at 120°C for 2 hours and half. After cooling to the mixture was added water/ice and the solution was alkalized with NH_4OH until pH= 8. The precipitate obtained was collected by filtration and dried under vacuum to obtain **24a** or **24b** like a dark-white solid.

Yield 24a: 80%

Yield 24b: 88%

Mp 24a: 118-120°C

Mp 24b: 122-124°C

^{1}H-NMR 24a: (DMSO) δ 7.42-7.34 (m, 6H, Ar, 1H); 6.25 (d, 1H,); 5.80 (s, 1H); 3.30 (s, 3H, CH_3).

^{1}H-NMR 24b: (DMSO) δ 7.40-7.28 (m, 5H, Ar); 6.10 (s, 1H); 5.85 (s, 1H); 3.25 (s, 3H, CH_3); 3.18 (s, 3H, CH_3).

4-azido-7-methyl-2-phenyl-1,8-naphthyridine (25)

To a solution of 1g (4.23 mmol) of **24a** in 10 ml of dry DMF, was added 1g of NaN_3 and the mixture was heated at 150°C for 10 minutes. After cooling water/ice were added and the precipitate obtained was collected by filtration and washed for a few times with water to obtain **25** as a light-grey solid.

Yield: 78%

Mp: 119-121°C

^{1}H-NMR: (DMSO) δ 7.42-7.34 (m, 6H, Ar, 1H); 6.48 (d, 1H,); 5.65 (s, 1H); 3.20 (s, 3H, CH_3).

7-methyl-2-phenyl-1,8-naphthyridin-4-amine (26)

The azide group of compound 0.400 g (1.69 mmmol) of **25** was reduced, in absolute Ethanol, by catalytic hydrogenation using Pd/C at room temperature. After 4 hours the catalyst was eliminated by filtration, the ethanol was evaporated under reduce pressure and the crude obtained was purified by crystallization using ethyl acetate .

Yield: 72%

Mp: 1125-127°C

^{1}H-NMR: (DMSO) δ 10.05 (s, 2H, NH_2); 7.42-7.34 (m, 6H, Ar, 1H); 6.48 (d, 1H,); 5.65 (s, 1H); 3.20 (s, 3H, CH_3).

Ethyl (7-methyl-2-phenyl-1,8-naphthyridin-4-yl)carbamate (28)

0.100 g (4.27 mmol) of **26** was solubilized in 10 ml of dry CH_2Cl_2 and 0.15 ml (1.11 mmol) of TEA and ethyl-chloroacetate were added dropwise. After 24 hours at room temperature the mixture was filtered and the solvent was evaporated under reduce pressure to obtain a crude product which was purified by flash chromatography usibg as eluent CH_2Cl_2/ AcOEt (10/1) to get **28** as a light yellow solid.

Yield: 45%

Mp: 125-128°C

^{1}H-NMR: ($CDCl_3$) δ 8.68 (s, 1H, NH carbamate); 8.32 (s, 1H, H_3); 8.12-8.16 (d, 1H, H_5); 7.27-7.75 (m, 5H, H Ar); 7.31-7.47 (d, 1H, H_6); 4.30-4.33 (q, 2H, OCH_2); 2.79 (s, 3H, CH_3 Ar); 1.26-1.36 (t, 3H, CH_3)

^{13}C-NMR: ($CDCl_3$) δ 163.18; 160.99; 156.52; 153.26; 142.57; 138.95; 130.17; 129.12; 128.78; 128.17; 121.83; 11.45; 106.92; 62.43; 29.99; 25.67

Phenyl (7-methyl-2-phenyl-1,8-naphthyridin-4-yl)carbamate (27)

27 was obtained by a cross-coupling reaction between 0.046 g (0.079 mmol) of Xantphos, 0.009 g (0.004 mmol) of $Pd(OAc)_2$, 0.802 g (2.46 mmol) of Cs_2CO_3 and 0.250 g (0.984 mmol) of **24a** in dioxane. The mixture was heated at 85°C for 24 hours. After the mixture was filtrated, the solvent was eliminated under reduce pressure and the crude obtained was purified by flash chromatography using as eluent hexane/ AcOEt (2/1) to get **27** as a light yellow solid.

Yield: 37%

Mp: 130-132 °C

^{1}H-NMR: ($CDCl_3$) δ 8.59 (d, 1H, H_5); 8.10-8.55 (m, 2H, H_6, NH); 7.25-7.50 (m, 10H, Ar); 7.21 (s, 1H, H_3); 2.84 (s, 3H, CH_3)

^{13}C-NMR: ($CDCl_3$) δ 164.00; 162.98; 161.03; 157.50; 154.46; 131.57; 130.63; 130.09; 128.73; 127.96; 126.03; 122.17; 121.12; 102.29; 25.98.

Phenyl (5,7-DImethyl-2-phenyl-1,8-naphthyridin-4-yl)carbamate (29)

29 was obtained by a cross-coupling reaction between 0.046 g (0.079 mmol) of Xantphos, 0.009 g (0.004 mmol) of $Pd(OAc)_2$, 0.802 g (2.46 mmol) of Cs_2CO_3 and 0.250 g (0.824 mmol) of **24b** in dioxane. The mixture was heated at 85°C for 24 hours. After the mixture was filtrated, the solvent was eliminated under reduce pressure and the crude obtained was purified by flash chromatography using as eluent hexane/AcOEt (2/1) to get **29** as a light yellow solid.

Yield: 37%

Mp: 130-132 °C

^{1}H-NMR: ($CDCl_3$) δ 8.59 (d, 1H, H_5); 8.10-8.55 (m, 2H, H_6, NH); 7.25-7.50 (m, 10H, Ar); 7.21 (s, 1H, H_3); 2.84 (s, 3H, CH_3)

^{13}C-NMR: ($CDCl_3$) δ 164.00; 162.98; 161.03; 157.50; 154.46; 131.57; 130.63; 130.09; 128.73; 127.96; 126.03; 122.17; 121.12; 102.29; 25.98.

2-[3-(4-phenylpiperazin-1-yl)propyl]-1*H*-isoindole-1,3(2H)-dione (30)

1.34 g (5.00 mmol) of N-(3- bromopropyl)phtalimide was solubilized in 25 ml of dry ACN and 1.4 ml (10 mmol) of TEA and 0.76 ml (5 mmol) of phenylpiperazine were added. The mixture was heated under reflux for 16 hours. After that the mixture was cooled, was added water and the product was extracted with CH_2Cl_2. The organic layer was dried over $MgSO_4$ and then the solvent was evaporated under reduce pressure to obtain **30** as a yellow solid pure enough for further reactions.

Yield: 62%

^{1}H-NMR: ($CDCl_3$) δ 7.82-7.86 (m, 2H, Ar); 7.67-7.71 (m, 2H, Ar); 7.20-7.26 (m, 2H, Ar); 6.80-6.88 (m, 3H, Ar); 3.77-3.84 (t, 2H, CH_2); 3.03-3.07 (m, 4H, H piperazine); 2.45-2.57 (m, 6H, H piperazine, CH_2); 1.85-1.98 (m, 2H, CH_2)

3-(4-phenylpiperazin-1-yl)propan-1-amine (31)

To a solution of 2 g (5.73 mmol) of **30** in 40 ml of EtOH, was added 0.53 ml (1.72 mmol) of NH_2NH_2 acq. and the mixture was heated under reflux for 5 hours. After cooling, the mixture was alkalized with NaOH 5% until pH=8, the solvent was evaporated under reduce pressure and the product was treated with CH_2Cl_2. The organic layer was washed with water, dried over $MgSO_4$ and evaporated to dryness. The product obtained was crystallized with petroleum ether high-boiling.

Yield: 88%

Mp: 75-77 °C

^{1}H-NMR: ($CDCl_3$) δ 7.26-7.22 (t, 2H, Ar); 6.93-6.82 (m, 3H, Ar); 3.21-3.12 (m, 4H, H piperazine); 2.79-2.43 (m, 8H, H piperazine, 2 CH_2); 2.03 (s, 2H, NH_2); 1.72-1.65 (m, 2H, CH_2)

Phenyl-[3-(4-phenylpiperazin-1-yl)propan]-1-amide (38)

To a solution of 0.270 g (1.23 mmol) of **31** in 5 ml of dry CH_2Cl_2, was added 0.20 ml (1.48 mmol) of TEA and 0.17 ml (1.48 mmol) of benzoylchloride at 0°C. The mixture was stirred at 0°C for 2 hours, after that the solvent was evaporated under vacuum and the crude oil obtained was treated with ice and water. The precipitate obtained was collected by filtration and triturated with Et_2O for a few times, furthermore the solid was crystallized with hexane to obtain **38** as a white solid.

Yield: 54%

Mp: 89-92°C

^{1}H-NMR: ($CDCl_3$) δ 8.12 (s, 1H, NH); 7.81-7.84 (m, 2H, Ar); 7.26-7.45 (m, 5H, Ar); 6.86-6.94 (m, 3H, Ar); 3.77-3.84 (t, 2H, CH_2); 3.03-3.07 (m, 4H, H piperazine); 2.45-2.57 (m, 6H, H piperazine + CH_2); 1.85-1.98 (m, 2H, CH_2)

^{13}C-NMR: ($CDCl_3$) δ 167.49; 151.29; 134.97; 131.44; 129.53; 128.62; 127.18; 120.26; 116.44; 58.46; 53.66; 49.49; 40.86; 24.83.

p-methoxy phenyl-[3-(4-phenylpiperazin-1-yl)propan]-1-amide (39)

To a solution of 0.250 g (1.14 mmol) of **31** in 10 ml of CH_2Cl_2, was added 0.19 ml (1.37 mmol) of TEA and 0.15 ml (1.37 mmol) of *p*-methoxy benzoylchloride at 0°C. The mixture was stirred at 0°C for 2 hours, after that the solvent was evaporated under vacuum and the crude oil obtained was treated with ice and water. The precipitate obtained was collected by filtration and triturated with Et_2O at reflux for a few times to obtain **39** as a yellow-white solid.

Yield: 58%

Mp: 95-97°C

^{1}H-NMR: (DMSO) δ 8.39 (s,1H, NH); 7.79-7.83 (m, 3H, Ar); 7.22-6.75 (m, 7H, Ar); 3.77 (s, 3H, OCH_3); 3.29-3.26 (m, 2H, CH_2); 3.13-3.01 (m, 6H, H piperazine + CH_2); 2.57-2.53 (m, 4H, H piperazine); 1.75-1.69 (t, 2H, CH_2)

^{13}C-NMR: (DMSO) δ 164.93; 160.70; 150.21; 128.24; 126.20; 118.19; 114.71; 112.74; 54.89; 54.69; 51.96; 47.34; 44.86; 22.9.

p-fluoro phenyl-[3-(4-phenylpiperazin-1-yl)propan]-1-amide (40)

To a solution of 0.250 g (1.14 mmol) of **31** in 10 ml of CH_2Cl_2, was added 0.19 ml (1.37 mmol) of TEA and 0.16 ml (1.37 mmol) of *p*-fluoro benzoylchloride at 0°C. The

mixture was stirred at 0°C for 2 hours, after that the solvent was evaporated under vacuum and the crude oil obtained was treated with ice and water. The precipitate obtained was collected by filtration and triturated with Et_2O at reflux for a few times to obtain **40** as a pure white solid.

Yield: 43%

Mp: 93-95°C

^{1}H-NMR: (DMSO) δ 8.12 (s,1H, NH); 7.85-7.52 (m, 3H, Ar); 7.01-6.65 (m, 7H, Ar); 3.19-3.12 (m, 2H, CH_2); 3.08-3.01 (m, 6H, H piperazine + CH_2); 2.57-2.53 (m, 4H, H piperazine); 1.75-1.69 (t, 2H, CH_2)

^{13}C-NMR: (DMSO) δ 161.93; 157.70; 148.21; 12974; 126.80; 116.19; 111.71; 110.74; 54.69; 51.96; 47.34; 44.86; 22.9

Phenyl-[3-(4-phenylpiperazin-1-yl)propan]-1-urea (34)

To a solution of 0.219 g (1.00 mmol) of **31** in 3 ml of toluene, 0.13 ml (1.20 mmol) of phenylisocyanate were added and the mixture was stirred at room temperature for 2 hours. After that the solution was filtered, the solvent was eliminated under vacuum and the crude oil obtained was crystallized with diisopropyl ether to obtain **34** as a light yellow solid.

Yield: 55%

Mp: 79-81°C

^{1}H-NMR: (DMSO) δ 8.6 (s,1H, NH); 8.4 (s, 1H, NH); 7.15-7.39 (m, 7H, Ar);6.71-6.99 (m, 3H, Ar); 3.37-3.40 (m, 2H, CH_2); 3.04-3.06 (m, 4H, H piperazine); 2.46-2.58 (m, 6H, H piperazine + CH_2); 1.70-1.76 (t, 2H, CH_2)

^{13}C-NMR: (DMSO) δ 154.55; 150.38; 139.91; 139.09; 128.24; 128.11; 127.95; 121.15; 120.26; 118.06; 117.55; 116.98; 114.65; 54.86; 52.22; 47.59; 35.39; 26.44.

p-chloro phenyl-[3-(4-phenylpiperazin-1-yl)propan]-1-urea (35)

To a solution of 0.200 g (0.913 mmol) of **31** in 10 ml of toluene, 0.14 ml (1.10 mmol) of *p*-chloro phenylisocyanate were added and the mixture was stirred at room temperature for 2 hours. After that the solution was filtered and the solid obtained was crystallized with diisopropyl ether to obtain **35** as a light yellow solid.

Yield: 51%

Mp: 82-85°C

^{1}H-NMR: ($CDCl_3$) δ 7.31-7.16 (m, 7H, Ar); 6.96-6.84 (m, 3H, Ar); 5.94 (s, 1H, NH); 3.30-3.32 (m, 2H, CH2); 3.10-3.14 (m, 4H, H piperazine); 2.44-2.59 (m, 6H, H piperazine + CH_2); 2.29 (s, 1H, NH) 1.68-1.74 (t, 2H, CH_2)

^{13}C-NMR: ($CDCl_3$) δ 156.39; 151.23; 137.72; 129.35; 129.26; 128.64; 122.05; 120.10; 116.24; 56.62; 53.46; 39.76; 26.67

p-methoxy phenyl-[3-(4-phenylpiperazin-1-yl)propan]-1-urea (36)

To a solution of 0.250 g (1.14 mmol) of **31** in 10 ml of toluene, 0.18 ml (1.37 mmol) of *p*-methoxy phenylisocyanate were added and the mixture was stirred at room temperature for 2 hours. After that the solution was filtered and the solid obtained was crystallized with toluene to obtain **36** as a light yellow solid.

Yield: 68%

Mp: 89-92°C

^{1}H-NMR: ($CDCl_3$) δ 7.27-7.15 (m, 4H, Ar); 6.89-6.77 (m, 5H, Ar); 6.57 (s, 1H, NH); 3.61 (s, 3H, OCH_3); 3.36-3.38 (m, 2H, CH_2); 2.98 -3.03 (m, 4H, H piperazine); 2.43-2.56 (m, 6H, H piperazine + CH_2); 1.92 (s, 1H, NH); 1.68-1.74 (t, 2H, CH_2)

^{13}C-NMR: ($CDCl_3$) δ 154.82; 153.16; 150.36; 133.08; 128.22; 118.75; 114.62; 113.20; 54.91; 54.51; 52.22; 47.56; 37.00; 26.47

2,4-dimethoxy phenyl-[3-(4-phenylpiperazin-1-yl)propan]-1-urea (37)

To a solution of 0.200 g (0.913 mmol) of **31** in 10 ml of toluene, 0.197 g (1.10 mmol) of 2,4-dimethoxy phenylisocyanate were added and the mixture was stirred at room temperature for 2 hours. After that the solution was filtered and the solid obtained was crystallized with diisopropyl ether to obtain **37** as a light yellow solid.

Yield: 71%

Mp: 96-98°C

^{1}H-NMR: ($CDCl_3$) δ 7.23-7.25 (m, 2H Ar); 6.86-6.92 (m, 3H, Ar); 6.41-6.45 (m, 3H, Ar); 5.8 (s, 1H, NH); 3.69 (s; 6H, OCH3); 3.33-3.30 (m, 2H, CH_2); 2.98 -2.95 (m, 4H, H piperazine); 2.59-2.56 (m, 6H, H piperazine + CH_2); 1.92 (s, 1H, NH); 1.68-1.74 (t, 2H, CH_2)

^{13}C-NMR: ($CDCl_3$) δ 156.82; 155.16; 153.36; 133.08; 128.22; 118.75; 114.62; 113.20; 54.91; 54.51; 52.22; 47.56; 37.00; 26.47

p-chloro phenyl-[3-(4-phenylpiperazin-1-yl)propan]-1-tiourea (32)

To a solution of 0.250 g (1.14 mmol) of **31** in 10 ml of toluene, 0.232 g (1.37 mmol) of *p*-chloro phenyl isotiocyanate were added and the mixture was stirred at room temperature for 2 hours. After that the solution was filtered and the solid obtained was crystallized with toluene to obtain **32** as a light yellow solid.

Yield: 83%

Mp: 84-86°C

^{1}H-NMR: (DMSO) δ 9.55 (s, 1H, NH); 7.87 (s, 1H, NH); 7.13-7.44 (m, 7H, Ar); 6.70-6.77 (m, 2H, Ar); 3.05-3.08 (m, 2H, CH2); 2.47-2.27 (m, 6H, H piperazine + CH2); 2.06-2.08 (m, 4H, H piperazine); 1.68-1.74 (t, 2H, CH2)

^{13}C-NMR: ($CDCl_3$) δ 181.23; 151.05; 132.37; 130.30; 129.28; 120.12; 116.29; 77.96; 77.35; 76.71; 58.23; 53.47; 48.83; 48.10; 25.35

p-methoxy phenyl-[3-(4-phenylpiperazin-1-yl)propan]-1-tiourea (33)

To a solution of 0.250 g (1.14 mmol) of **31** in 10 ml of toluene, 0.19 ml (1.37 mmol) of *p*-methoxy phenyl isotiocyanate were added and the mixture was stirred at room temperature for 2 hours. After that the solution was filtered and the solid obtained was crystallized with toluene to obtained **33** as a light yellow solid.

Yield: 79%

Mp: 91-93°C

^{1}H-NMR: (DMSO) δ 9.28 (s, 1H, NH); 7.53 (s, 1H, NH); 7.15-7.19 (m, 4H, Ar); 6.73-6.88 (m, 5H, Ar); 3.63 (s, 3 H, OCH3); 3.33-3.30 (m, 2H, CH_2); 2.98 -2.95 (m, 4H, H piperazine); 2.59-2.56 (m, 6H, H piperazine + CH_2); 1.68-1.74 (t, 2H, CH_2)

^{13}C-NMR: (DMSO) δ 180.23; 155.84; 151.05; 132.37; 130.30; 129.28; 120.12; 116.29; 74.96; 74.35; 70.71; 58.23; 51.47; 47.83; 46.10; 23.35

Dimethyl (naphthalen-2-yl methyl)phosphonate (45)

To a solution of 0.500 g (4.54 mmol) of dimethyl phosphite in 15 ml of dry DMF, were added 4.44 g (13.6 mmol) of CS_2CO_3 and 5.030 g (13.6 mmol) of TBAI. The mixture was stirred at room temperature for 30 minutes and then were added 3.015 g (13.6 mmol) of 2-bromo methylnaphthalene. After 24 hours at room temperature the mixture was diluted with AcOEt and washed with water for few times. The organic layer was then dried with Mg_2SO_4 and the solvent was eliminated under vacuum to obtain a crude product which was purified by flash chromatography (eluent: 1 AcOEt/ 1 hexane).

Yield: 65%

Mp:105-107°C

^{1}H-NMR: ($CDCl_3$) δ 7.85-7.78 (m, 4H, H Ar); 7.50-7.28 (m, 3H, H Ar); 3.72 (s, 3H, CH_3); 3.67 (s, 3H, CH_3); 3.41-3.30 (s-s, 2H, CH_2)

Methyl (naphthalen-2-yl methyl) phosphonochloridonate (46)

To a solution of 0.1 ml (0.84 mmol)of $POCl_3$ was added to 0.200 g (0.80 mmol) of **45** and the mixture was stirred at 60°C for 3 hours. After that $POCl_3$ was eliminated

under vauum and the crude product was purified by flash chromatography (eluent: 2 hexane/3 AcOEt) to obtain **46** as a yellow-brown oil.

Yield: 86%

^{1}H-NMR: ($CDCl_3$) δ 7.80-7.78 (m, 4H, H Ar); 7.52-7.38 (m, 3H, H Ar); 3.82 (s, 3H, CH_3); 3.42-3.38 (s-s, 2H, CH_2)

Methyl 4-nitrophenyl (naphthalen-2-yl methyl) phosphonate (42)

To a solution of 0.300 g (1.82 mmol)of **46** in 15 ml of dry CH_2Cl_2, 0.05 ml (0.364 mmol) of TEA and 0.253 g (1.82 mmol) of 4-nitro phenol were added at 0°C and the mixture was stirred at room temperature. After 5 hours the solution was diluted with CH_2Cl_2, washed with water and with HCl 10%, the organic layer was then dried with Mg_2SO_4 and the solvent was eliminated under vacuum to obtain a crude product which was purified by flash chromatography using as eluent hexane/AcOEt (1/1).

Yield: 68%

Mp: 112-114°C

^{1}H-NMR: ($CDCl_3$) δ 8.13-8.16 (m, 2H, H Ar), 7.86-7.78 (m, 4H, H Ar); 7.43-7.52 (m, 3H, H Ar); 7.21-7.25 (m, 2H, H Ar); 3.78-3.77 (s-s, 3H, OMe); 3.62-3.51 (s-s, 2H, CH_2)

Methyl hydrogen (naphthalen-2-yl methyl) phosphonate (41)

2.30 ml (5.18 mmol) of NaOH 10% were added to 0.240 g (0.96 mmol) of **45** and the mixture was stirred at room temperature overnight. After that the solution was acidified with HCl conc, extracted with CH_2Cl_2, the organic layer was dried with Mg_2SO_4 and the solvent was eliminated under vacuum to obtain **41** as a pure solid.

Yield: 92%

Mp: 109-111°C

^{1}H-NMR: ($CDCl_3$) δ 7.85-7.78 (m, 4H, H Ar); 7.50-7.28 (m, 3H, H Ar); 3.67 (s, 3H, CH_3); 3.41-3.40 (s-s, 2H, CH_2); 3.38 (s, 1H, OH)

Ethyl hydrogen benzylphosphonate (43)

15.0 ml (35.48 mmol) of NaOH 10% were added to 1.50 g (6.57 mmol) of diethyl benzylphosphonate and the mixture was stirred at room temperature for 2 hours and half. After that the solution was acidified with HCl conc, extracted with CH_2Cl_2, the organic layer was dried with Mg_2SO_4 and the solvent was eliminated under vacuum to obtain **43** as a pure solid.

Yield: 79%

Mp: 95-97°C

^{1}H-NMR: ($CDCl_3$) δ 8.66 (s, 1H, OH), 7.28-7.30 (m, 5H, H Ar); 3.85-3.88 (q, 2H, OCH_2); 3.10-2.99 (s-s, 2H, CH_2); 1.17-1.24 (t, 3 H, CH_3)

Ethyl benzylphosphono chloridonate (47)

0.43 ml (4.60 mmol) of $POCl_3$ was added to 0.91 ml (4.38 mmol) of diethyl benzylphosphonate and the mixture was stirred at 60°C for 3 hours. After that $POCl_3$ was eliminated under vacuum and the crude product was purified by flash chromatography (eluent: 2 hexane/3 AcOEt) to obtain **47** as a yellow-brown product.

Yield: 96%

Mp: 100-102°C

^{1}H-NMR: ($CDCl_3$) δ 7.18-7.25 (m, 5H, H Ar); 3.89-3.88 (q, 2H, OCH_2); 3.00-2.97 (s-s, 2H, CH_2); 1.17-1.24 (t, 3 H, CH_3)

Ethyl 4-fluorophenyl benzylphosphonate (44)

To a solution of 1.05 g (4.80 mmol) of **47** in 15 ml of dry $CHCl_3$, 1 ml (6.80 mmol) of TEA and 0.538 g (4.80 mmol) of 4-fluoro phenol were added at 0°C and the mixture was stirred at room temperature. After 5 hours the solution was diluted with CH_2Cl_2, washed with water and with acid water, the organic layer was then dried with Mg_2SO_4 and the solvent was eliminated under vacuum to obtain a crude product which was purified by flash chromatography using as eluent hexane/AcOEt (3/1).

Yield: 46%

Mp: 106-108°C

^{1}H-NMR: ($CDCl_3$) δ 7.18-7.25 (m, 4H, H Ar); 6.97 -7.08 (m, 3H, H Ar); 3.79-3.78 (q, 2H, OCH_2); 3.05-2.87 (s-s, 2H, CH_2); 1.20-1.24 (t, 3 H, CH_3)

5.5 BIOLOGICAL ASSAY

5.5.1 MAGL INHIBITION HPLC ASSAY

Materials and methods

Reagents

- 4-Nitrophenyl acetate (4-NPA), Sigma Aldrich ®;
- *p*-nitrophenol (PNP), Sigma Aldrich ®;
- Acetonitrile for HPLC, Sigma Aldrich ®;
- Acetic acid, Sigma Aldrich ®;
- Ammonium acetate (≥ 98%); Sigma Aldrich ®;
- EtOH absolute, Sigma Aldrich ®;
- anhydrous DMSO; Sigma Aldrich ®;
- Methanol for HPLC, Sigma Aldrich ®;
- MAGL Assay Buffer, Cayman Chemical ®;
- human recombinant MAGL, Cayman Chemical ®;
- MAGL Substrate (4-NPA), Cayman Chemical ®;
- CAY 10499, Sigma Aldrich ®;
- JZL 184, Sigma Aldrich ®;
- JW 642, Sigma Aldrich ®.

Analytical Instruments

For the analysis was used a HPLC Thermo Finingam SCM 1000, with P2000 Pump, UV 2000 detector and injector loop with 20 ml. The column used is a Varian (150x4.6 mm) INTERSIL 5 µ.

Instrumentation for the preparation of aqueous solutions

All aqueous solutions were obtained using water "bidistilled" (resistance of 18.0 MQ) with ion exchange resins, and subsequently microfiltered with the appliance MilliQ (Millipore Corporation, MA, USA).

Preparation of the mobile phase:

1. Preparation of Ammonium Acetate Buffer

For each liter of solution are dissolved 0.77 g of ammonium acetate (CH_3COONH_4, PM 77.08 g/mol) in 900 mL of MilliQ water under magnetic stirring. The pH is adjusted, using a pH-meter with glass electrode, to a value of 4 adding dropwise acetic acid (CH_3COOH, 2M). The solution is then brought to volume in a volumetric flask of one

liter, and then filtered through a microporous membrane made of polypropylene with an average diameter of 0.2 microns (PALL Corporation, Michigan, USA) using a vacuum pump. During the period of non-use, the solution was stored at 3°C, and at the time of reuse has been redissolved in warm water (30°C).

Calibration line:

1. Preparation of stock solutions of 4-nitrophenyl acetate and p-nitrophenol.

18.1 mg of 4-NPA (MW = 181.15 g/mol) were dissolved in 10 mL of ethanol in a volumetric flask. The same procedure is carried out also for PNP, of which 13.9 mg (MW = 139.1 g / mol) are dissolved in 10 mL of ethanol and brought to volume in a volumetric flask. The solutions of PNP are stored at 3°C, instead the 4-NPA are stored at -2 C to avoid their degradation.

2. Preparation of solutions for the calibration curves of the 4-nitrophenyl acetate and p-nitrophenol.

From the stock solution 10 mM (solution A) of 4-PNA and PN, were prepared the standard solutions intermediate used for the calibration curve (Table 18).

Tab.18 Dilution scheme of 4-NPA e PNP for the calibration curve.

Taken volume (mL)	Final volume (mL) EtOH	Final concetration	Dilution name
750 µL of A	1,0	7,5 mM	B
1 mL of A	2,0	5,0 mM	C
500 µL of C	1,0	2,5 mM	D
1 mL of A	10,0	1,0 mM	E
1 mL of E	2,0	500 µM	G
500 µL of E	4,0	125 µM	F
1 mL of E	3,0	250 µM	H
200 µL of F	1,0	25 µM	I
600 µL of F	1,0	75 µM	L
200 µL of H	1,0	50 µM	M

3. Calibration curve of p-nitrophenol

The standard solutions prepared according to Table 18 were analyzed to determine the area of the PNP at λ = 315nm. The calibration curve was constructed on thirteen points yielding a value of R^2=0994. (Table 19, Fig.31).

Tab.19. Results obtained from the PNP analysis for the calibration curve.

Conc. µM	A	B	C	Average area	DS	DS%
0,50	6491	6361	6874	6575	218	3,31
1,25	15274	16335	15095	15568	547	3,52
2,50	24428,00	23075,00	25629,00	24377,33	1043,28	4,28
5	48809	48440	48872	48707	190,54	0,39
10	101383	108700	111705	107263	4334,77	4,04
25	346897	355280	369978	357385,00	9539,62	2,67
50	572777	541058	586526	566787	19039,34	3,36
75	1654630	1589669	1611405	1618568	26999,56	1,67
125	2766606	2608907	2772444	2715985,67	75753,55	2,79
250	4414072	4552353	4600061	4522162	78873,74	1,74
500	9439234	9107413	9778205	9441617	273854,87	2,90
1000	17059012	17302843	17404175	17255343	144859,79	0,84
2500	36423361	39230009	38160849	37292105	1200838,07	3,22

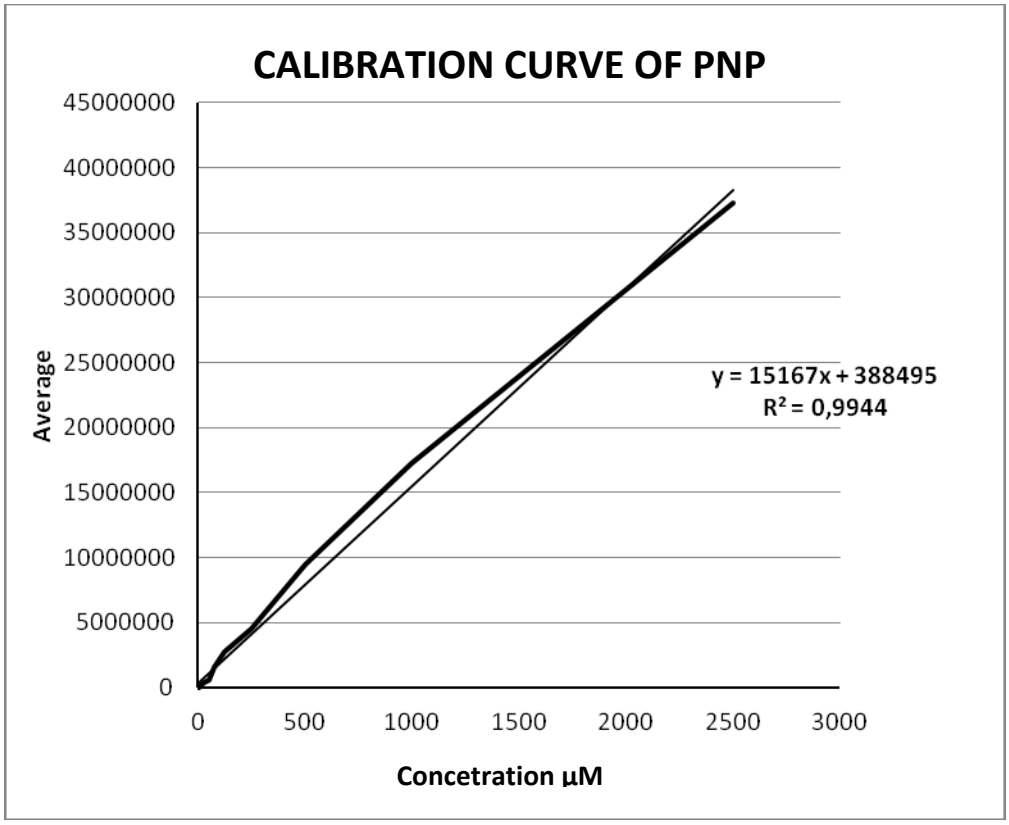

Fig.31. Calibration curve of the PNP.

The detection limit value (LOD) and quantification (LOQ), are respectively of 0.25 μM and 0.50 μM.

Preparation of solutions for the performance of the assay

The solutions used for the test were prepared in accordance with what is described by the kit Cayman Chemical ®. [37]

a) Incubation Buffer: 3 mL of "MAGL Assay Buffer" are brought to a volume of 30 mL using H_2O MilliQ filtered.

b) MAGL human ricomnbinante: 30 L of "MAGL Human Recombinant" are diluted with 570 mL of incubation buffer.

c) Substrate (4-NPA): It was originally used the sample provided by the company (1.2 mL concentration 4.25 mM). Subsequently the same sample was prepared by weighing 1.54 mg of 4-PNA and dissolved in 2 mL of EtOH.

Inhibitory activity of compounds tested

The screening of the compounds was done using the following chromatographic conditions:

- STATIONARY PHASE: VARIAN 150x4.6 mm INTERSIL 5μ;
- MOBILE PHASE: composed of 53% MeOH and 47% of buffer 10 mM ammonium acetate at pH 4;
- FLOW: 1.0 mL / min;
- DETECTOR UV: set at a wavelength of 270 nm for 4-postcode and 315 nm for PNP;

The screening protocol provides the following step (Table 20):

1. Analysis of the "BLANK": to 160 mL of incubation buffer were added 10 mL of EtOH and 10 mL of 4-PNA. After stirring were incubated for 10 minutes at 37°C and then 20 mL were analyzed by HPLC.
2. Initial determination (A.I) of the enzyme: to 150 mL of incubation buffer were added 10 mL of enzyme and 10 mL of EtOH; after stirring the sample is placed in pre-incubate for 30 minutes at 37 ° C and subsequently are added 10 L of 4-NPA and are incubated for 10 minutes at 37 ° C. 20 L were analyzed by HPLC.
3. Determination of compounds inhibitory activity: to 150 mL of buffer was added 10 mL of enzyme and 10 mL of inhibitor, were stirred and pre-incubated for 30 minutes at 37°C. After that were added 10 mL of 4-PNA , stirred and incubated for 10 minutes at 37°C. Finally, 20 mL were analyzed by HPLC.

Tab. 20. Summary table of the screening protocol.

	Buffer	MAGL	Solvent	Inhibitor	Substrate (4-NPA)
100% INITIAL ACTIVITY	150 µL	10 µL	10 µL	……	10 µL
BLANK	160 µL	……	10 µL	……	10 µL
INHIBITOR	160 µL	10 µL	……	10 µL	10 µL

Screening of compounds synthesized

This method was applied for the screening of compounds synthesized during my PhD thesis. All compounds were tested in duplicate at a concentration of 5 µM. The results obtained for each tested compounds are reported in table 25.

Tab.25 MAGL inhibition of teste compound at a concetration of 5µM.

Compound	% MAGL activity Experiment 1	% MAGL activity Experiment 2	% Average MAGL activity	% MAGL inhibition
5	75,74	83,72	79,73	20,27
14	23,58	25,19	24,38	75,61
21	87,21	74,31	80,76	19,24
27	15,86	13,9	14,88	85,12
28	11,62	14,42	13,02	86,98
29	6,69	10,59	8,64	91,36
33	30,16	21,43	25,80	74,20
34	19,41	20,56	19,99	80,01
36	19,52	27,81	23,66	76,34
38	22,29	16,50	19,40	80,60
39	27,54	23,47	25,51	74,49
42	5,49	4,76	9,94	7,35

COMPOUND 42

1.41 mg (MW = 357 g/mol) were dissolved in 1 mL of ethanol to obtain a solution 3949.58 µM (A) which was diluted in order to obtain a concentration of 98.74 µM (D) (Tab.26).

Tab.26. 42 dilution scheme.

Taken volume (µL)	Final volume (mL) EtOH	Final concetration (µM)	Dilution name
400 µl of A	0,8	1974,8	B
100 µl of B	1,0	197,48	C
400 µl of C	0,8	98,74	D

The final concentration of **42** used in the assay was found to be (Tab.27):

Tab.27 Concentrazione finale di **42**

Comp.	Conc. (µM)	Experiment 1	Experiment 2	% Average activity	% Inhibition
42	5,49	4,76	9,94	7,35	92,65

The inhibition curve was obtained by analyzing five scalar concentrations from a stock solution of 98.74 µM (D) of **42** with the following dilutions (Tab.28):

Tab .28 Dilution scheme of **42** for the calibration curve

Taken volume (µL)	Final volume (mL) EtOH	Final concetration (µM)	Dilution name
100 µL of D	1,0	9,874	E
100 µL of E	1,0	0,9874	F
100 µL of F	1,0	0,09874	G
100 µL of G	1,0	0,009874	H
100 µL of H	1,0	0,0009874	I

After dilution with EtOH the final concentrations of each aliquot were found to be the following (Tab.29):

Tab.29. Final concetration of each **42** aliquote.

Starting concetration (µM)	nmol in 10 µL	Final concetration (µM)
197,48	1,9748	10,97
98,74	0,9874	5,49
9,874	0,09874	0,549
0,9874	0,009874	0,0549
0,09874	0,0009874	0,00549
0,009874	0,00009874	0,000549
0,0009874	0,000009874	0,0000549

The assay was performed according to the scheme reported above (Table 20). At the end of the analysis, the concentration of *p*-nitrophenol present in each aliquot was determined using the calibration curve equation. Each analysis was performed in duplicate and the inhibitory activity of different concentrations of **42** was found to be as reported in table 30:

Tab.30

Concentration 42 (µM)	Exp. 1	Exp. 2	% Average activity	% Inibhibition
10,97	3,13	8,05	5,59	94,41
5,49	4,76	9,94	7,35	92,65
0,00549	38,46	49,04	43,75	56,25
0,000549	99,19	79,42	89,31	10.69
0,0000549	99	98,6	98,8	1.2

The obtained data, at different concentrations of inhibitor, were processed to obtain the inhibition curve and the value of IC50 of the compound (Fig.33).

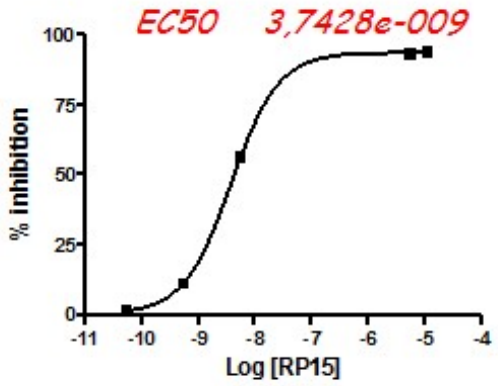

Fig.33. IC50 and inhibition curve of **42**

For compound **42** was also evaluated the importance of the pre-incubation time in absence of the substrate. The derivative was analyzed both in the absence of pre-incubation, either with a pre-incubation of 10, 20, 30 and 40 minutes. The data obtained show that after 30 minutes of pre-incubation between enzyme and inhibitor, the inhibitory activity does not show significant variations (Tab.31).

Tab.31

Pre-incubation (min)	% Enzymatic residual activity	% of Inhibition
0	68,77	31,23
10	29,61	70,39
20	16,20	83,80
30	7,98	92,02
40	4,96	95,04

Part 2. EFFECTS OF THE ISCHEMIC DAMAGE ON CB1/CB2 RECEPTOR DOUBLE KNOCKOUT MICE AND ON CB2 RECEPTOR KNOCKOUT MICE.

6. INTRODUCTION

Cerebral ischemia is a major cause of death or incapacitation in industrialized countries. In stroke treatment time is very important in order to restore the perfusion of the ischemic region to reduce neurodegeneration. There is a long list of symptoms and signs of stroke that are determined by the size and the location of the infarction. These range from neck stiffness, nausea and headache to blurred vision, vertigo, dizziness and convulsions; there are also a wide of motor and sensorimotor deficits. In addition, higher cortical dysfunction is also manifested as amnesia, dementia, delirium and language disturbances.

The pathophysiological events during ischemia follow a certain timescale that have been well reviewed by Dirgnal et al. [38]

The first phase is the acute phase, during that the cells of the brain are mainly affected by excitotoxicity that arises due to lack of oxygen and glucose, which cause the loss of neuron membrane polarity and the release of neurotransmitters, i.e. glutamate. However, the duration of the acute phase is short and the most effective treatment during the acute phase is the use of thrombo agents such as recombinant tissue plasminogen activator (rtPA) in order to restore the perfusion.

Following the acute phase there is the sub-acute phase that is prolonged up to days or weeks and an inflammatory reaction starts. The brain is normally protected from components of the peripheral immune system by the blood-brain barrier (BBB). However, during a stroke, the barrier becomes more permeable to blood components. In both human and other mammals, studies shown that leukocytes cross the blood-brain barrier and migrate into the brain parenchyma early in response to ischemia. [39] The neutrophils produce several highly active substances such as hypochlorous acid and oxygen radicals which can be toxic to the cells. These substances are normally used to render pathogens harmless as a part of the innate immune response. [39] Early after an ischemic insult, leukocytes can be seen adhering to the walls of small vessels in the ischemic area. These leukocytes can subsequently transmigrate across the endothelial cells lining the vessels and into the brain parenchyma. Neutrophils are the first leukocytes to migrate across the blood-brain barrier as response to injury followed by macrophages. The neutrophils follow a certain pattern when transmigrating across an endothelial cell layer. The first step in

transmigration is rolling where the neutrophil flow rate is reduced as a consequence of an increased expression of selectins on the endothelial cells. The second step is adhesion where the neutrophils link to specific adhesion molecules, such as intercellular cell adhesion molecule 1 (ICAM-1), on the endothelial cells. The third step is the actual transmigration and chemokinesis in the extracellular space towards the site of injury. Transmigration and chemokinesis are largely directed by cytokines that play a pivotal role in the whole process. As a consequence of cell dying or being damaged by ischemic processes, proinflammatory cytokines such as TNF-α and IL1ß arereleased.[40] These cytokines can in turn increase the expression of adhesion molecules and other chemotactic cytokines (chemokines) which result in neutrophil transendothelial migration.

6.1 STROKE MODELS

There are different kind of rodent stroke models, the major ones are:

1. MIDDLE CEREBRAL ARTERY OCCLUSION (MCAO)

The most widely used model for transient focal cerebral ischemia is the middle cerebral artery occlusion (MCAO) model. In this model the middle cerebral artery (MCA) is exposed and the artery is occluded for the time desired and the occlusion could also be permanent or transient. In the MCAO model the resulting lesions are dispersed in the hemisphere and the locations are dependent upon which segment of the MCA is occluded and rendered ischemic (Fig. 34).

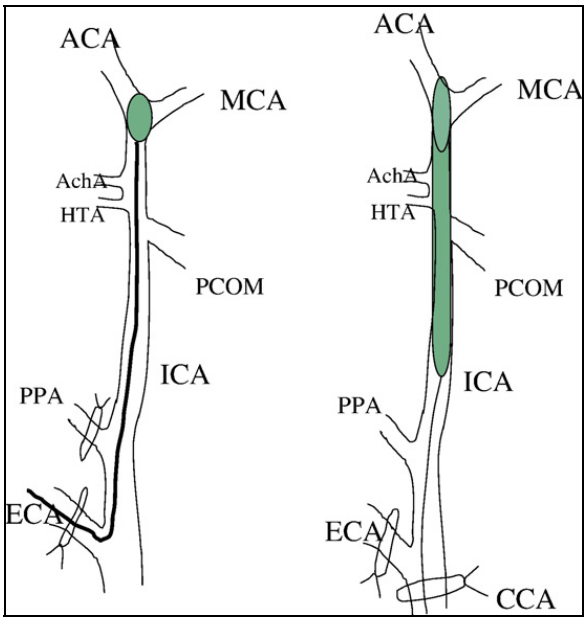

Fig. 34. Intraluminal suture middle cerebral artery occlusion technique. On the left, Longa's method, insertion of the uncoated suture into external carotid artery, where branches of internal carotid artery except MCA are kept patent; on the right Koizumi's method, insertion of the silicone-coated suture into common carotid artery, blocking MCA, AchA, and HTA. ACA, anterior carotid artery; AchA. anterior choroidal artery; CCA, common carotid artery; ECA, external carotid artery; ICA, internal carotid artery; HTA, hypothalamic artery; PPA, pterygopalatine artery; PCOM, posterior communicating artery.

1. ISCHEMIC/REPERFUSION INJURY (IRI)

Another kind of ischemic model is the ischemic/reperfusion injury (Ischemia is a state of tissue oxygen deprivation accompanied by a reduced washout of the resulting metabolites; reperfusion is the restoration of blood flow to the ischemic tissue). Despite the unequivocal benefit of reperfusion of blood to an ischemic tissue, reperfusion itself can elicit a cascade of adverse reactions that paradoxically injure tissue. Indeed, reperfusion injury has been well described in the literature to cause organ damage in the brain, heart, lungs, liver, kidneys and skeletal muscle. The pathophysiology of the IRI is complex. The inflammatory aspect of IRI includes both the cellular and humoral components (Fig. 35). Moreover, mechanisms of IRI may be organ-dependent, with similar but distinct pathways involved in different organs. During the last decade there has been an explosion of research documenting the role of leukocytes and leukocyte adhesion molecules in IRI. Multiple mechanisms have been postulated for the leukocyte-mediated tissue injury that occurs after ischemia-reperfusion. Microvascular occlusion, release of oxygen free radical, cytotoxic enzyme release, increased vascular permeability and increased cytokine release have all been demonstrated to contribute to leukocyte-induced tissue injury. [41]

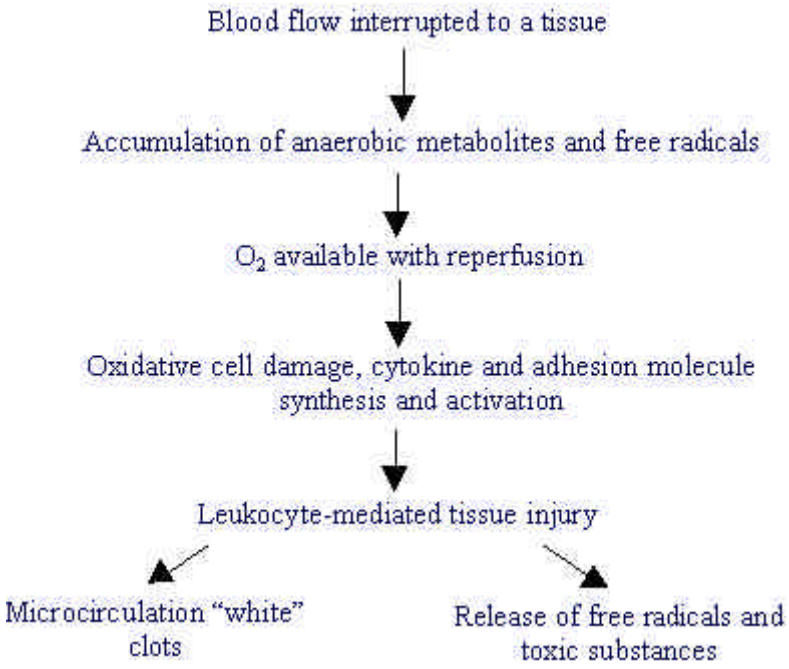

Fig. 35. Proposed inflammatory cascade in ischemia/reperfusion injury.

2. PHOTOTHROMBOTIC STROKE MODEL

The photothrombotic ring stroke (PRS or PT stroke) produces, in contrast to the MCAO model, a photochemical reaction that damages the vessel wall and results in an

occlusion of the vessel in a fashion similar to what is observed in vivo and rendering the area inside the ring ischemic. Correct concentration of the photosensitive chemical (for example: Rose Bengal) and correct tuning and positioning of the laser produces an ischemic area that is spontaneously reperfused with time (Fig. 36).

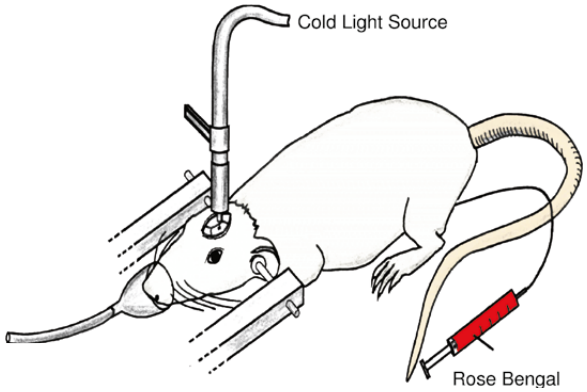

Fig. 36. Schematic drawing of the setup for induction of focal photochemical lesion in the rat brain. The brain is illuminated through the intact skull of the anesthetized rat.

Oxygen free radicals generated in the lumen of a vessel may provoke nitric oxide inactivation, lipid peroxidation of platelets and endothelial cells membranes, platelet activation, and eventually the formation of a thrombus. Free radicals are generally produced by illumination of the vessel with a filtered light, following the intravenous administration of a sensitizing compound, such as sodium fluoresceine or FITC and Rose Bengal.

It has been demonstrated that the photo activation (wavelength= 540 nm) of Rose Bengal in aqueous solution induces the formation of singlet oxygen and superoxide anion. Moreover, photonic and electronic studies failed to show the endothelial cell destruction and the extracellular matrix exposition usually found in the arterial models of thrombosis. [42]

Photochemical stroke models have a number of advantages:[42]

a- The stroke can be placed exactly and reproducibly at the desired cortical or subcortical site. Rapidly evolving ischemic cell death occurs in the irradiated cortical bed, as measured by nonselective indicators of cell death such as terminal deoxynucleotidyl transferase- mediated biotinylated uridine triphosphate nick end labeling (TUNEL) staining, or indicators of apoptotic progression such as cytoplasmic cytochrome c.

b- The size of the lesion is very reproducible.

c- The lesion can be produced without opening the skull, avoiding many artificial changes due to the operation procedure in other cortical lesion models.

d- The model is accompanied by a vessel thrombosis; the properties of the thrombus are more similar to that of a thrombus in human stroke than in some other models of embolic stroke.

However the photochemical model also has several limitations and differences compared to the stroke in humans:[42]

a- Photothrombosis is associated with a pronounced disruption of endothelial integrity and rapidly progressive infarction in a small cortical volume results in substantial local vasogenic edema. MRI of photochemical stroke shows the simultaneous development of substantial vasogenic edema and ischemic infarction. This pattern is different from that seen in human stroke, where infarcts develop with decreased diffusion of water, followed by a vasogenic edema which is delayed by several hours. A simultaneous development of both significant vasogenic and cytotoxic edema in MRI of photochemical stroke more closely resembles traumatic brain injury.

b- Induction of photochemical stroke with a ring filter provides a central area within the lesioned cortex that has not been optically thrombosed. This penumbral area is present within the evolving vasogenic edema, and it is unclear if this accurately models the human penumbra.

6.2 ROLE OF THE CANNABINOID AND ENDOCANNABINOID IN CEREBRAL ISCHEMIA

The endocannabinoid signaling system has several features that support its hypothesized involvement in ischemic injury.

First, the endocannabinoids (eCBs) and related lipids accumulate in ischemic tissues[28] supporting the hypothesis that the ECS is activated during ischemia. Second, accumulating data support a general role for ECS in the maintenance of metabolic homeostasis and responsivity of the brain to stress.[43] Third, activation of the CB1 cannabinoid receptor results a decrease in the probability of opening of voltage-operated calcium channels which could result in a reduction in intraneuronal calcium contents.

In addition, a subset of CB1 receptors are present on glutamatergic nerve terminals and their activation results in inhibition of glutamate release in response to depolarization. Together these signaling mechanisms are consistent with neuroprotection because they lead to decreased intracellular calcium. Fourth, the

CB2 cannabinoid receptor is expressed by immune cells, including brain resident microglial cells, and its activation results in a decrease in the release of pro-inflammatory mediators.[44] Fifth, the CB1 cannabinoid receptor is present in the cerebral vasculature and its activation produces vasodilation.[44, 45, 46, 47, 48]

Importantly, data suggest that activation of cerebrovascular CB1 receptors results in loss of autoregulation, which could exacerbate the effects of ischemia. To summarize, both theoretical considerations and experimental data suggest that the ECS contributes to the consequences of cerebral ischemia via multiple mechanisms. However, the role of the ECS is complex, and it can both exacerbate and reduce injury.

As reported before, two arachidonic acid derivatives, N-arachidonylethanolamine (AEA or anandamide) and 2- arachidonoylglycerol (2-AG) function as endogenous ligands of the cannabinoid receptors. The earliest studies of the family of the *N*-acylethanolamines (NAEs), of which AEA is a minor constituent, demonstrated that members of this family accumulate in tissues deprived of blood flow.

Sugiura and colleagues have reported that 2-AG increases in rat brain within the first minute after decapitation, and decreases back to baseline concentrations at 5 min.[48]

Several studies have examined the effects of controlled interruptions in cerebral blood flow on tissue eCB contents. NAE contents have been examined in brain tissue following MCA occlusion (without reperfusion) of various durations in rats. A five hour occlusion of the rat MCA increased the contents of 6 long chain NAEs in the striatum ipsilateral to the occlusion, including a 23-fold increase in PEA and a 12-fold increase in AEA. The NAEs likely accumulate earlier in the ischemic period as AEA content in the ipsilateral hemisphere was significantly increased in tissue harvested immediately following a 30 min MCA occlusion and in the ipsilateral striatum immediately following a 2 hour MCA occlusion. No changes in 2-AG content in the ischemic hemisphere were seen in rats after a 30, 60 or 120 min MCA occlusion.[49]

These findings suggest that increased biosynthesis, at the level of precursor generation, could play a role in the increase of at least some NAEs following ischemia in rats. On the other hand, the increase in AEA content in the ischemic striatum following 2 hour MCA occlusion was accompanied by a decrease in the protein content and activity of FAAH. These data suggest that increased accumulation of AEA could also be driven by a reduction in its catabolism in the ischemic region.[37]

Somewhat different results were obtained following permanent occlusion of the MCA in mice. However, it is striking that ischemia results in a significant accumulation of the NAEs in both species even though the mechanisms differ. Two studies have examined the effects of ischemia followed by reperfusion on brain NAEs. Both studies

found that the NAEs were increased after reperfusion and suggest that the addition of a reperfusion period following ischemia results in exacerbation NAE accumulation compared to ischemia alone. In a study carried out in mice by Stella and colleagues, one MCA was occluded for 20 min followed by 24 hours of reperfusion. This ischemia/reperfusion procedure resulted in a 25-fold increase in PEA; 3-fold increase in AEA and 4-fold increase in docosatetraenoylethanolamide (DEA) in the cerebral cortex compared to sham-operated controls.[50] Changes in the brain content of 2-AG in response to ischemia have been examined in a few studies. Interestingly, mice exposed to a sham surgery (which involved anesthesia and incisions but no vessel occlusions) exhibited significant increases in 2-AG content in the cerebral cortex compared to untreated controls 24 hours after the intervention. Mice in which the MCA was occluded had lower 2-AG contents than the sham surgery animals. These studies raise the intriguing possibility that one or more of the aspects of the surgical intervention itself (anesthesia or activation of stress responses) increases tissue 2-AG while ischemia itself actually decreases 2-AG.[50] There have been several studies exploring the hypothesis that ischemia alters the amount of either of the two established cannabinoid receptors (CB1 and CB2) in the brain. In the first study to tackle this question, Greenberg and colleagues used transient MCA occlusion in rats to induce ischemia/reperfusion injury. They found that CB1 receptor-like immunoreactivity was up-regulated in neuronal-type cells in the ischemic boundary zone as early as 2 hours after reperfusion. There were no changes in CB1 receptor-like immunoreactivity in the ischemic core of the infarct. these results are consistent with those of a recent study in which quantitative PCR was used to measure CB1 receptor mRNA content following transient, MCA occlusion in mice. The mRNA for the CB1 receptor in the brain ipsilateral to the occlusion was significantly elevated at 1 hour, and maximally elevated 6 hours, after the ischemia. In contrast, 5 hours of permanent MCA occlusion had no effect on CB1 receptor binding site density in male rats. Taken together, these studies suggest that reperfusion injury is associated with a rapid increase in CB1 receptor expression, possibly driven by increased mRNA. The mechanism involved in the increased expression is not clear, but it seems not be associated with excitotoxicity.

The CB2 cannabinoid receptor is found on circulating immune cells and at low levels in perivascular microglia in the uninjured brain. However, during states of neuroinflammation, CB2 receptor expression in the brain is increased in brain resident microglial cells and via migration into the brain of macrophages and T cells which express CB2 constitutively. Ashton and coworkers have recently reported that CB2 receptor expression is increased in two models of ischemia. In another study of

the effects of transient MCA occlusion in mice, CB2 receptor mRNA expression was found to be decreased in the ischemic hemisphere 1 and 3 hours after the ischemia and significantly increased 24 hours after. These studies suggest that CB2 expression increases later in the time course of the ischemia, which is consistent with its presence on macrophages or leukocytes recruited into the injured brain.[50]

CB1 receptor activation is protective

There are several *in vivo* studies that support the hypothesis that CB1 receptor activation prevents neuronal death in response to ischemia. CB1 receptor agonists have also been shown to reduce infarct volumes following permanent MCA occlusion. Win 55212-2 (a mixed CBR agonist) produced a significant reduction in infarct volume when administered either 30 min before or 30 min after the onset of occlusion but not when administered more than 60 min after occlusion. Several other studies using different compounds confirm that exogenous administration of CB1 agonists before, during, or immediately after the onset of a permanent, focal ischemic event reduce the amount of neuronal damage;[38] although none of these studies demonstrated convincingly that the CB1 receptor was involved. A protective role of the CB1 receptor is also supported by studies in CB1 receptor null mice. The knockout mice demonstrated increased mortality from permanent MCA occlusion as well as increased infarct size and neurological deficits following transient MCA occlusion. Another study found that AM404, an indirect agonist of the CB1 receptor, is protective against neuronal damage induced by transient, global ischemia in the gerbil.[50] Finally, there is other evidence demonstrating that inhibition of the CB1 receptor during ischemia can be protective.

CB1 receptor activation reduces excitotoxicity—As described above, several *in vivo* studies have demonstrated that exogenous activation of the CB1 receptor during ischemia is neuroprotective. There have been several hypotheses put forward to explain this protection at a mechanistic level. The first hypothesis is that CB1 receptor activation protects against glutamate-induced excitotoxicity. This hypothesis is supported by the effects of CB1 agonists in cell culture models. Other studies indicate that the CB1 receptor also reduces the deleterious effects of excessive glutamate by effects that are down-stream of glutamate receptor activation. The first evidence for this mechanism came from spinal cord cultures in which CB1 receptor activation was protective against neuronal death evoked by the direct application of kainic acid.[48]

A recent study using the hippocampal slice used changes in glutamatergic signaling (rather than cell death) as an end point and provided some evidence that CB1

receptor activation contributes to decreased glutamatergic signaling that occurs following oxygen and glucose deprivation (OGD).These in vitro studies are supported by in vivo studies demonstrating that activation of the CB1 receptor is protective in models of excitotoxic injury. [48]

CB1 receptor activation produces hypothermia—Hypothermia has been shown to be neuroprotective in several models of ischemia and the CB1 agonists could produce neuroprotection via their ability to reduce body temperature. Two in vivo studies support this mechanism. The cannabinoid, HU-210, significantly reduced the infarct size in rats following permanent occlusion of the MCA. [48]

HU 210 also produced a significant reduction in body temperature at 1 and 24 hours after its injection in rats with MCA occlusion

CB1 receptor activation reduces edema—Ischemia, reperfusion and other forms of brain injury are commonly accompanied by edema formation in the brain. Edema results in an expansion of brain volume resulting in an increase in intracranial pressure which can damage cells directly through compression and indirectly by impairment of cerebral perfusion. Therefore, a reduction in the degree of edema formation following ischemia is beneficial to the outcome of the injury. The CB1 agonists have been found to reduce edema following brain trauma and in a model of excitotoxicity [82]. It is not clear whether the edema-lowering effect was a consequence of reducing damage through other mechanisms or was an independent, protective mechanism. There are several possible mechanisms by which CB1 agonists could reduce edema, including decreased systemic blood pressure and increased glucocorticoid release in response to stress. [48]

Evidence that reduced endocannabinoid signaling is protective against ischemia/ reperfusion injury

There are data from multiple laboratories that pharmacologic inhibition of the CB1 receptor at the time of the ischemia results in a reduction in the injury produced. Berger, Schmid and colleagues reported that rats treated intravenously with 1 mg/kg of the CB1 receptor antagonist rimonabant (SR141716A) 30 min after permanent MCA occlusion had infarct size that was reduced by 40% compared to vehicle controls at 5 hours. In one of these studies, a second, structurally unrelated CB1 receptor antagonist, LY 320135, was also protective. Rimonabant is also protective in male gerbils exposed to transient, global ischemia. [48]

The hypothesis that decreased CB1 receptor activation is neuroprotective is inconsistent with the finding that CB1 receptor null mice exhibit increased lethality following MCA occlusion and that CB1 activation is protective in models of ischemia

and other injury. There are methodological differences between these studies and that of Nagayama and colleagues in which the CB1 agonist was shown to be neuroprotective, including different anesthetic agents; time at which damage was assessed and the route of drug administration. None of these methodological differences seems to explain the completely opposite results seen in these studies. It is possible that more subtle methodological differences have occurred and contribute to the results. For example, the degree to which the hypothermic effects of the cannabinoid agonists were counteracted with temperature regulation could contribute to differences in agonist effect. Another possibility is that the drugs, both agonists and antagonists, could be acting through non-cannabinoid receptor targets to produce neuroprotection. The eCB, AEA, has many non-cannabinoid effects, including functioning as a precursor to ethanolamine, which inhibits serum withdrawal apoptosis in cell culture at surprisingly low concentrations .[48]

There are several possible mechanisms by which decreased CB1 receptor activation could result in reduced ischemic injury. First, CB1 receptors present on terminals of GABAergic interneurons in the hippocampus inhibit the release of GABA. This mechanism of CB1 receptor activation will result in decreased inhibitory neurotransmission and could exacerbate excitotoxicity and CB1 receptor blockade would result in protection.

CB1 receptors are expressed by cerebral endothelial cells and astrocytes and there is evidence that AEA, through changes in endothelial NOS activity, alters capillary blood flow. In addition, CB1 receptors are expressed by cerebral arterial smooth muscle cells and the activation of these receptors results in vasodilation and increased blood flow. While this might seem to be a beneficial effect of CB1 receptor activation during ischemia, it is likely detrimental as it will result in a loss of the ability of the circulation to autoregulate and to provide blood flow to regions in greatest need.

This leads to the hypothesis that antagonism of the CB1 receptor during cerebral ischemia is protective because it allows for maintenance of proper autoregulation and/or neurovascular coupling.[48]

CB2 receptor activation is protective

The expression of the CB2 cannabinoid receptor increases during many types of brain injury, and the activation of CB2 receptors promotes cellular changes associated with decreased inflammation. These data lead to the hypothesis that activation of the CB2 receptor by eCBs produced during ischemia could be neuroprotective. This hypothesis is supported by several studies, although this line of research is far less developed at this stage then the CB1 receptor-related research.[48]

Among the first studies that raised the possibility that activation of CB2 cannabinoid receptors could protect against excitotoxic as well as inflammatory damage is an important study by Docagne and colleagues. These investigators found that cannabinoid agonists with affinity for both CB1 and CB2 receptors prevented AMPA-induced cell injury both in vivo and in vitro. The role of the CB2 receptor in focal ischemia/reperfusion has been examined in mice. Treatment of mice before the ischemia or immediately after reperfusion with CB2 receptor agonists significantly reduced both infarct size and the motor disability induced by the insult. These authors also explored a possible mechanism of action for the CB2 receptor agonists. They used a closed cranial window preparation to visualize leukocyte rolling and adhesion in cerebral arterioles after the insult. These vascular changes are associated with increased inflammation and edema formation following ischemia and are an important contributor to the overall damage produced. The CB2 agonists attenuated leukocyte rolling and adhesion in this model, which is an interesting and important potential mechanism of action of this class of drugs.

Therefore, it seems that ischemia can be added to the list of potential CNS disorders in which CB2 receptor activation holds promise as a therapeutic intervention. Since Win 55212-2 is a mixed CB receptor agonist, it is also possible that the neuroprotective effects ascribed to its ability to activate CB1 receptors could actually be due to its effects at the CB2 receptor. Finally, the studies of Zhang and colleagues add to the studies suggesting that CB1 receptor activation during ischemia is detrimental and that reducing this effect is also beneficial, they also observed a higher neuroprotective effect by the coadministration of a CB2 agonist and a CB1 antagonist. [48]

7. EXPERIMENTAL PART

7.1 INTRODUCTION

The primary goal of this study was to investigate whether modification of the endocannabinoid system could influence cerebral ischemia obtained using a photothrombotic stroke model.

The hypothesis that modification of the endocannabinoid system could influence outcome following ischemia was based upon prior research projects which demonstrated that this system can have direct effects on neuronal function and can also modify inflammatory responses.[51] As reported before, a variety of studies have demonstrated that there is an increase of the number of cells that express the CB2 cannabinoid receptor during many types of brain injury.[52] Furthermore, activation of CB2 receptors induces cellular changes which are associated with decreased inflammation. [53] These data lead to the hypothesis that activation of the CB2 receptor by eCBs produced during ischemia could be neuroprotective. Previous studies performed in Dr. Tuma laboratory, and in others have shown inflammatory responses after ischemia to be important contributors to secondary injury. In fact Zhang et al[54] demonstrated that selective activation of the CB2 receptor might provide protection from reperfusion injury. Futhermore in order to evaluated the role of the CB2 receptor in cerebral ischemic injury, in the same study, they performed studies using CB2 knockout mice. The results indicated that the CB2 receptor knockout mouse had larger cerebral infarction and worse neurological function compared to wild type mice. These findings provide evidence for a role of endogenous cannabinoids in protection of the brain following ischemia/reperfusion injury through the CB2 receptor.

The CB1 receptor has also been studied in cerebral ischemia/reperfusion injury. However, the results obtained by the CB1 activation by endogenous and exogenous cannabinoids in cerebral ischemic injury are controversial. Several studies using different compounds confirm that exogenous administration of CB1 agonists before, during, or immediately after the onset of a permanent, focal ischemic event reduce the amount of neuronal damage.[55, 56, 57] Other studies carried out in our laboratory [58] have provided evidence that the inhibition of the CB1 receptor was protective and to confirm this in the same study has been also showed that the combination of a CB2 agonist and a CB1 antagonist provided the greatest degree of protection.

The current study examined the effects of the ischemic damage, on CB1/CB2 receptor double knockout mice and CB2 receptors knockout mice of both sexes, obtained using a photothrombotic stroke model. Based upon findings from our laboratory that

the CB2 receptor knockout mice has larger injury volumes following stroke, and the reports from other laboratories that CB1 receptor knockout animals also had larger infarcts, we expected the double knockout animals to have much more severe strokes after ischemia. To the contrary, results of this study showed that the absence of the cannabinoid receptors leads to neuroprotective effects and that ischemic damage does not depend on the animal's sex (figure 37, figure 38). Surprisingly the CB2 receptor knockout mice also showed a reduction of the ischemic injury even if, in this case, there wasn't a significant difference between these mice and the corresponding wild type mice (figure 37, figure 38).

7.2 EXPERIMENTAL PROCEDURES

Animals

The cerebral ischemia studies were carried out in 7-8 week old C57BL/6 mice (weighing female: 20-22g, weighing male: 27-30 g), the CB1/CB2 receptor double knockout (CBR1/CB2R double KO) mice and the CB2 receptor knockout (CBR2 KO) mice were chosen based on the characteristics of the corresponding wild-type mice and were kindly provided by Dr. Kirby in the CSAR of the Temple University of Philadelphia (USA).

The experiments are conducted in accordance with the guidelines approved by the Institutional Animal Care and Use Committee at Temple University.

Materials and methods

Photothrombotic cortical lesion

Ischemia was induced by photothrombosis of the cortical microvessels. Each mouse was anesthetized with an intraperitoneal injection of ketamine (100 mg/ml)-xylane (20 mg/ml) mixture at the dose of 1 ml/kg. The rectal temperature was maintained during surgery at 37°C, 0.1 mL of a 10-mg/mL solution in normal saline of Rose Bengal (Sigma Chemical Co, St Louis, Mo) was infused intraperitoneally 7 minutes before illumination. The skull was exposed via a midline incision of the skin, the periosteum over the skull was removed completely and a cold light source was centered in the middle of the right hemisphere placed close as possible to the skull. The brain was illuminated for 20 minutes through the exposed intact skull. The incision was closed, and the mice were maintained in an incubator for 24 hours. [67]

Infarct Volume and Volume Stroke assessment

24 hours after ischemia each animal was anesthetized with intraperitoneal ketamine (100 mg/kg) and xylazine (20 mg/kg) injection, perfused with a solution of 0.9% PBS

for 5 minutes, decapitated, and then the brain was removed. The brains were sectioned into five 2-mm slices using a mouse brain matrix. The slices were immediately stained with 2% triphenyltetrazolium chloride (TTC) (Sigma Inc, St Louis, MO, USA) dissolved in saline and stained for 20 minutes at 37°C in the dark. After staining, the TTC was replaced with 4% para-formaldheyde (PFA). The cerebral infarcts in the brain were unstained and clearly delineated from normal tissue, which was stained red. The brain sections were then fixed in 4% para-formaldehyde at 4°C for 24 hours and the anterior and caudal face of each section was scanned by a flatbed color scanner (Microtek Inc, Carson, CA, USA). The resulting images were captured as JPEG files and analyzed with NIH image software. The hemispheric infarct volumes were corrected for brain edema/swelling: the hemispheric infarct volume in each section was calculated by substracting the area of normal TTC stained tissue in the hemisphere ipsilateral to the ligation from the contralateral nonischemic area to generate the infarct fraction. The infarct volumes were expressed as mm^3 as well as the percentage of the ipsilateral emisphere.

Neurological Function Evaluation

The severity of neurological deficits was evaluated 24 hours after ischemic insult using a five point deficit score (0= normal motor function; 1= flexion of torso and of contralateral forelimb upon lifting of the animal by tail; 2= circling to the contralateral side but normal posture at rest; 3= leaning to contralateral side at rest; and 4= no spontaneous motor activity).

Statistical analysis

Bonferroni's test after one way ANOVA was used for analyzing differences in infarct volume, neurological score and average. Data were presented as means ± SEM.
A statistically difference was assume at $p < 0.05$.

7.3 RESULTS

Cerebral infarct fraction and stroke volume after photothrombotic ischemia

Female

CBR1/CBR2 female double knockout mice 24 hours after stroke showed a smaller cerebral infarct fraction (10.31 ± 1.21%) and a reduction of the stroke volume (21.31 ± 2.59 mm^3) compared to the wild type mice (infarct fraction: 13.75 ± 0.69%; stroke volume: 35.09 ± 2.70 mm^3) (fig. 37). Instead for the CBR2 knockout mice we

obtained only some preliminary data because, until now, we analyzed the ischemic injury for only 3 mice. From our data is clear that 24 hours after stroke, also CBR2 KO mice, had smaller infarct fraction (9.54 ± 1.92%) and had a reduction of the stroke volume (22.38 ± 5.63 mm^3) compared to the corresponding wild type (infarct fraction: 13.75 ± 0.69%; volume stroke: 35.09 ± 2.70 mm^3) (fig. 37).

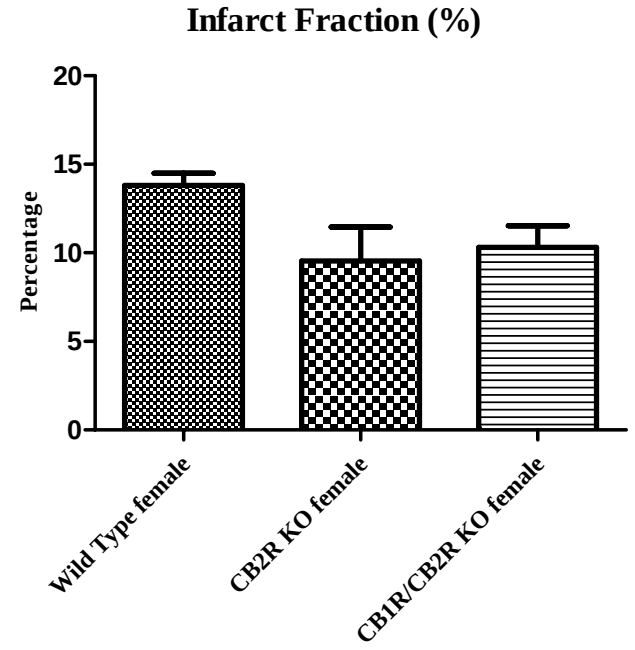

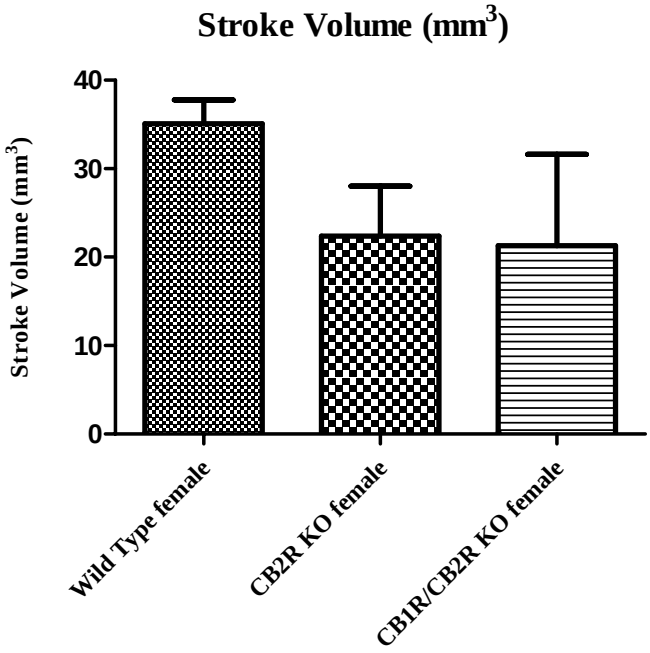

F :	Stroke Volume (mm^3)	Infarct farction (%)
WT (n=5)	35.49 ± 2.39	13.8 ± 0.69
CB2 KO (n=3) 3	22.40 ± 5.63	9.54 ± 1.92
CB1/CB2 double KO (n=5)	21.3 ± 2.59	10.31 ± 1.21

.

Stroke volume and infarct fraction of female wild type, CBR2 female KO, CBR1/CBR2R double KO mice 24 hours after the stroke (Data were expressed as mean ± SEM, n= number of mice for each group).

Male

CBR1/CBR2 male double knockout mice, 24 hours after stroke, also showed a smaller cerebral infarct fraction (7.21± 0.35%) and a reduction of the stroke volume (13.99 ± 1.53 mm^3) compared to wild type mice (infarct fraction: 12.55 ± 1.06%; volume stroke: 27.35 ± 1.76 mm^3) (fig. 38). Although not statistically significant, the CBR2 knockout mice also had smaller infarct fraction (9.24 ± 1.05%) and reduction of the stroke volume (21.81 ± 1.67 mm^3) 24 hours after stroke (fig. 38), compared to wild mice (infarct fraction: 12.55 ± 1.06%; volume stroke: 27.35 ± 1.76 mm^3).

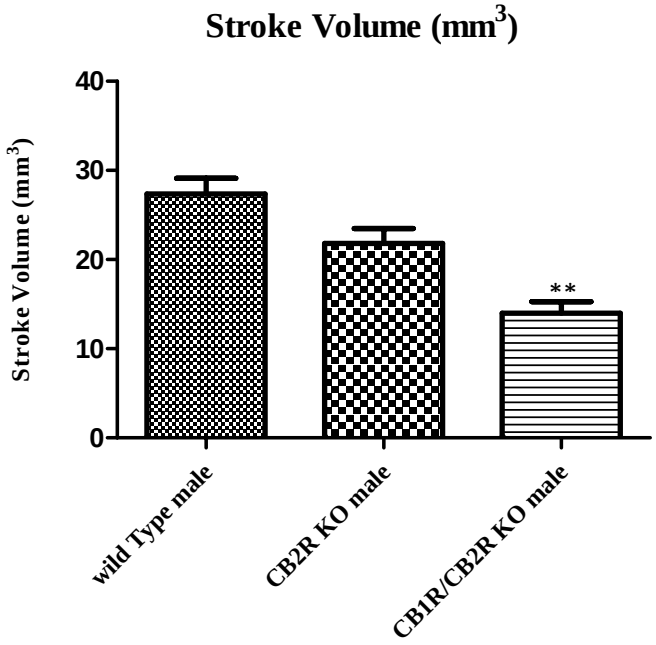

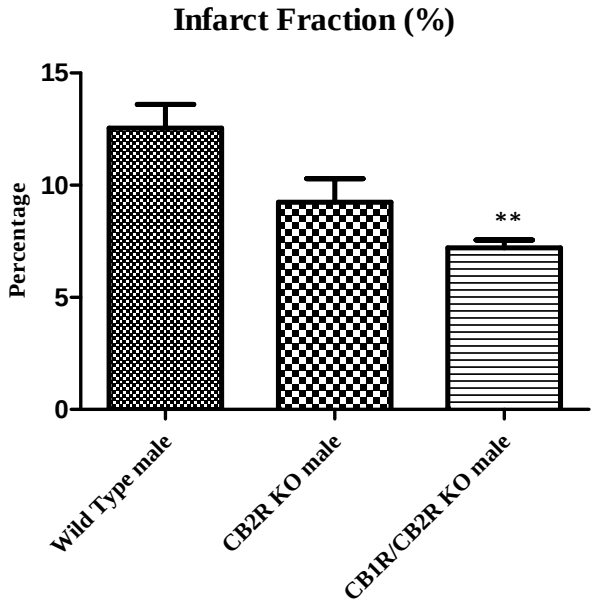

	Stroke Volume (mm^3)	Infarct farction (%)
WT (n=5)	27.42 ±1.74	12.58 ± 1.05
CB2 KO (n=5)	21.81 ± 1.67	9.24 ± 1.05
CB1/CB2 double KO (n=5)	13.99 ± 1.31	7.21 ± 0.35

Fig 38. Stroke volume (**p<0.005 vs wild type group) and infarct fraction (**p<0.005 vs wild type group) of male wild type, CBR2 male KO, CBR1/CBR2 double KO male mice 24 hours after the stroke (Data were expressed as mean ± SEM, n= number of mice for each group).

Effects on neurological function

Female / Male

In parallel with the changes in infarct size, CBR1/CBR2 receptor double KO and the CBR2 receptor KO mice of both sexes showed better neurological function after photothrombotic injury than the corresponding wild type (Fig. 39, fig. 40). As was the case for infarct size, the number of single knockout mice included in the study did not allow demonstration of statistical significance for the neurological score.

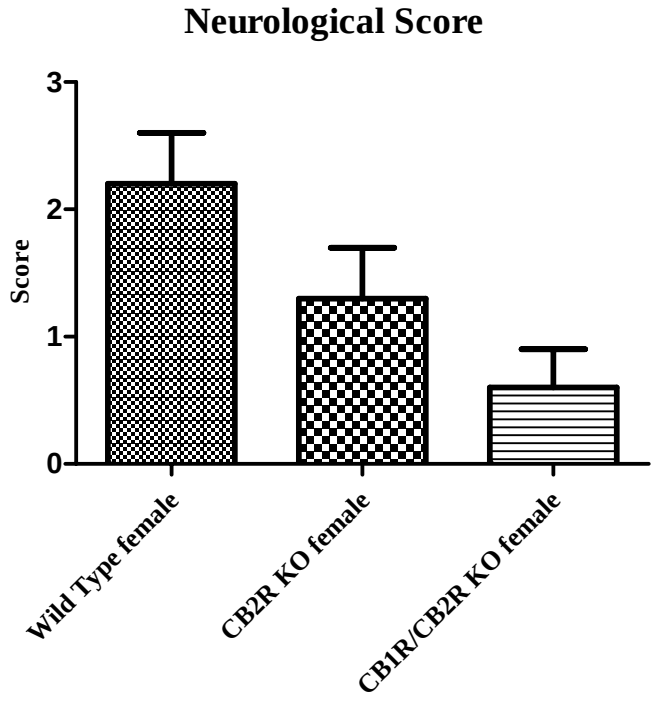

Fig 39. Neurological score of wild type, CBR2 KO, CBR1/CBR2 double KO female mice 24 hours after stroke.

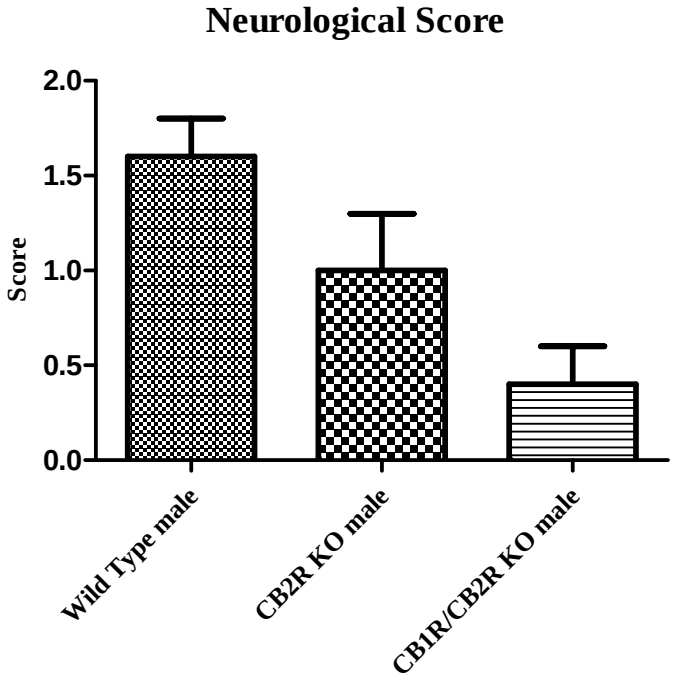

Fig 40. Neurological score of wild type, CBR2 KO, CBR1/CBR2 double KO male mice 24 hours after stroke.

7.4 DISCUSSION and CONCLUSIONS

The current study examined the effects of the ischemic damage, using a photothrombotic stroke model, on CB1/CB2 receptor double knockout and on CB2 receptor knockout mice of both sexes. The results of this study showed that the absence of the cannabinoid receptors leads to neuroprotective effects and that ischemic damage does not depend on the animal's sex. Infact both male and female CB1/CB2 receptor double knockout mice had smaller cerebral infarct fraction and had a reduction of the stroke volume compared to the wild type mice (fig. 37, Fig. 38). Surprisingly the CB2 receptor knockout mice also showed a reduction of the ischemic injury even if, in this case, there wasn't a significant difference between these mice and the corresponding wild type mice (figure 37, Figure 38).

In parallel with the changes in infarct size, CB1/CB2 receptor double KO and CB2 receptor KO mice of both sexes showed better neurological function than the corresponding wild type animals, 24 hours after photothrombotic injury(Fig. 39, fig. 40).

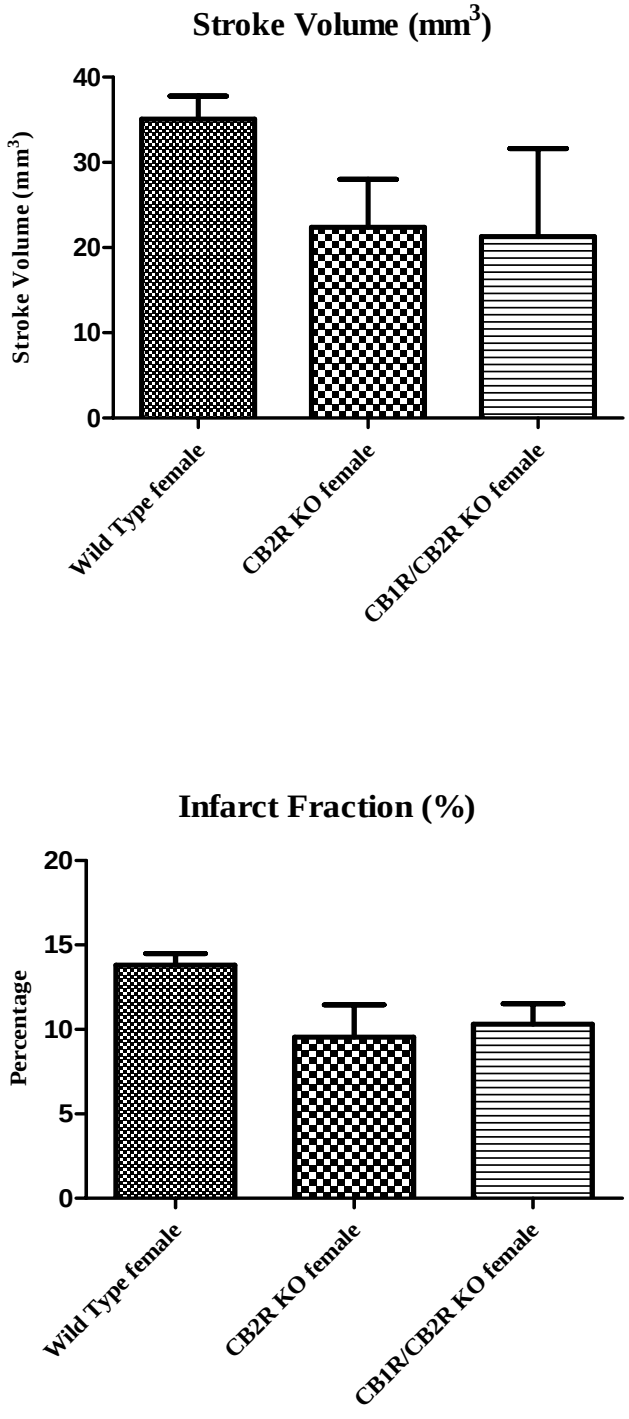

Fig 37. Stroke and infarct fraction of wild type, CBR2 KO, CBR1/CBR2R double KO female mice 24 hours after the stroke (Data were expressed as mean ± SEM, n= number of mice for each group).

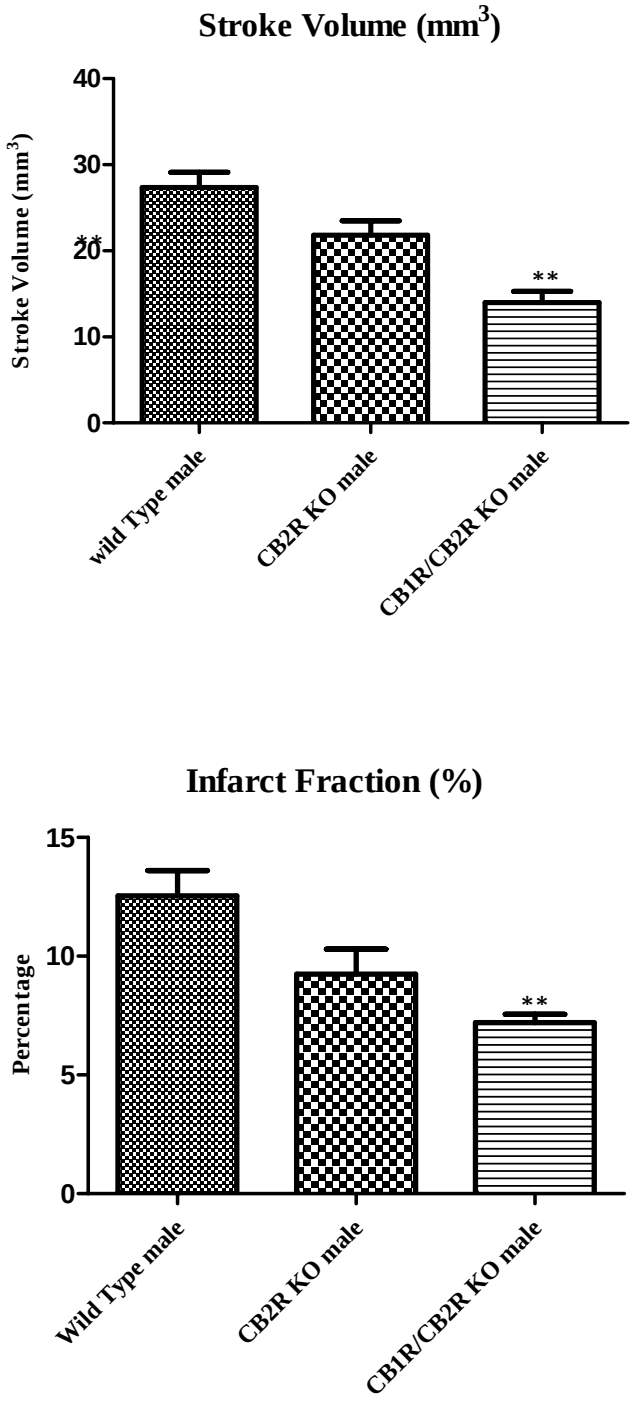

Fig 38. Stroke volume and infarct fraction of wild type, CBR2 KO, CBR1/CBR2 double KO male mice 24 hours after the stroke (**p<0.005 vs wild type group, Data were expressed as mean ± SEM, n= number of mice for each group).

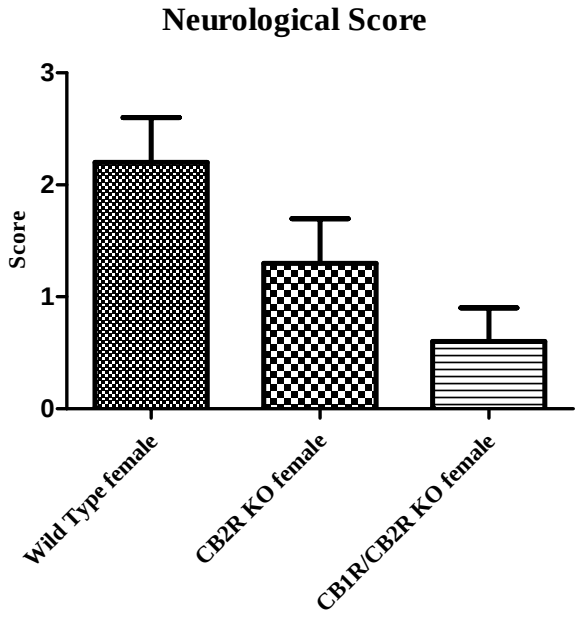

Fig 39. Neurological score of wild type, CBR2 KO, CBR1/CBR2 double KO female mice 24 hours after stroke.

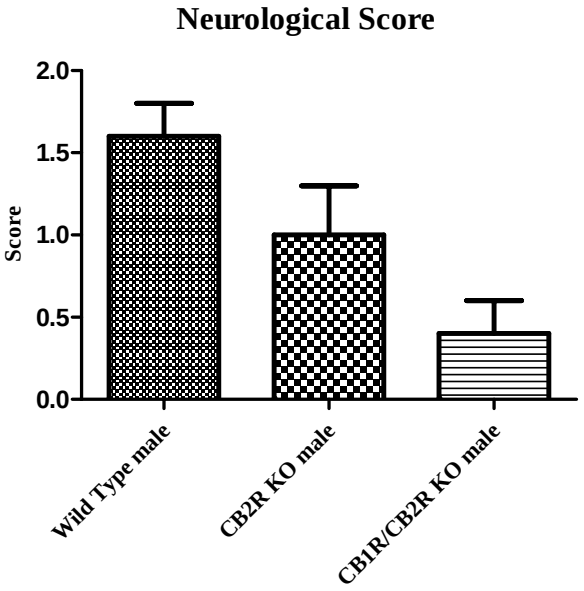

Fig 40. Neurological score of wild type, CBR2 KO, CBR1/CBR2 double KO male mice 24 hours after stroke.

In conclusion the absence of CB2 receptors or of both CB receptors contributes to neuroprotective effects. These effects could be due for multiple factors:

1- Increase of the endocannabinoids concentration (in responses of the inflammatory process due to the stroke).

Degn et al[59] have used a model of focal cerebral ischemia in young adult mice to investigate the relationship between focal cerebral ischemia and endogenous NAEs

(*N*-acetylethanolamides, family of compounds which AEA belongs to). Over the first 24 h after induction of permanent middle cerebral artery occlusion, they observed a time-dependent increase in all the investigated NAEs, except for anandamide. Moreover, they found an accumulation of 2-AG at 4 h that returned to basal level 12 h after induction of ischemia. These results suggest that NAEs and 2-AG may be involved in regulation of neuroprotection during focal cerebral ischemia in mice.

Instead Naccarato et al.[60] observed that stroke patients show an early increase in plasma AEA content which correlates with neurological disability and infarct volume. At T_0 (initial time) AEA levels were significantly higher in stroke patients compared to controls, moreover a positive correlation between T_0 AEA levels and stroke volume were found in stroke patients.

Furthermore Berger et al.[61] have shown an increase in NAEs and their precursor phospholipids during the acute phase of stroke in the adult rat brain. In the striatum, total NAE levels in the ipsilateral hemisphere exceeded those in the contralateral hemisphere by about a factor of 30 in untreated animals.

(For other studies related to the increase of the eCB concentration during or after ischemia see the introduction of this part of my PhD thesis)

The increase of the endocannabinoids concentration could also depend on the decrease of the metabolizing enzyme activity (for more details see below).

2- Decrease of the metabolizing enzyme activity.

Battista et al.[62] demonstrated that the activity of FAAH, the enzyme which degrades the anandamide, was dramatically decrease in some neurodegenerative conditions, furthermore the finding of Bergel et al.[63] that ischemia results in a combination of an increase in NAPE (*N*-Acylphosphatidylethanolamine) hydrolysis together with a decrease in FAAH expression confirm the thesis that during ischemic or neurodegenerative process there could be a reduction of the activity of some eCB metabolic enzymes.

Moreover Amantea et al.[64] measured the activity of FAAH in cortices and striata from rats with focal brain ischemia and after two hours of MCAO, with or without 1 h of reperfusion, they observed a significant decrease of FAAH activity in the ipsilateral striatum.

In conclusion we can assert that the decrease of the metabolizing enzyme activity leads to an increase of the endocannabinoids concetration which could produce a highest activation of non-CB receptors (such as GPR55, GPR18, TPRV1…). This increase of eCBs concentration could also leads to a reduction of the synthesis of arachidonic acid (Fig. 41), a precursor of prostaglandins (Fig. 42), with consequent reduction of neuroinflammation. Nomura et al.[65] in fact, have demonstrated that

endocannabinoid hydrolysis generates brain prostaglandins that promote neuroinflammation and they also claimed that the inhibition of MAGL may be a new and potentially safer way to suppress the proinflammatory cascades that underlie neurodegenerative disorders.

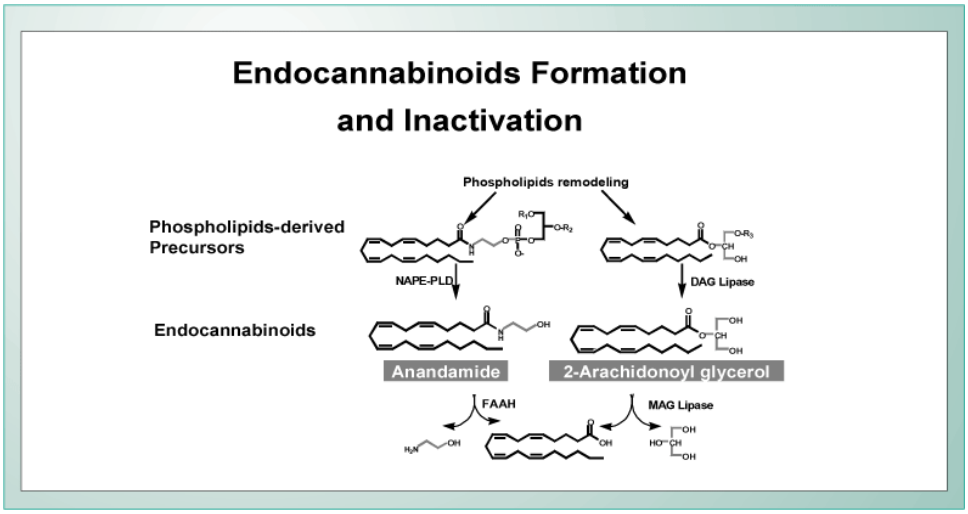

Fig. 41. endocannabinoids formation and inactivation

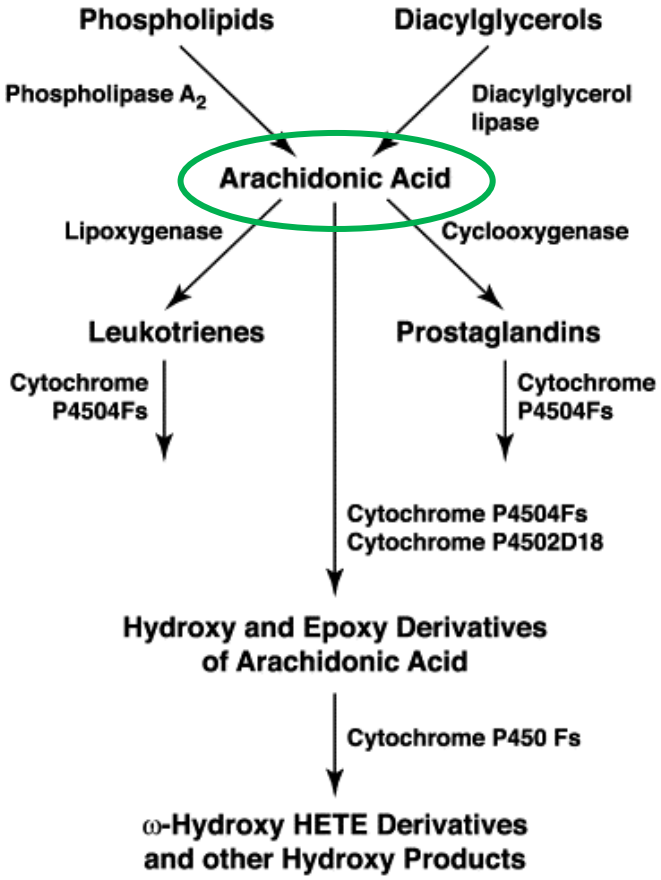

Fig 42. prostaglandin pathways

3- Interaction of the endocannabinoids with other enzymes or receptors such as GPR55, GPR18, TRPV1, serotoninergic receptors ($5HT_{1A}$).

A number of studies have demonstrated that the activation of GPR55, GPR18 and TRPV channels, by some endocannabinoids, in particular by anandamide and N-arachidonoyl glycine (a metabolite of anandamide), leads to anti-inflammatory *in vitro* effects (Journal of Cellular Biochemistry 112:3227-3233 (2011), McHugh et al. BMC Neuroscience 2010, J Neuroimmune Pharmacol 10.1007/s11481-012-9351 DOI, Pharmacology & Therapeutics 125 (2010) 181–195), and other *in vivo* studies are currently under development.

Furthermore Zhang et al.[66] have demonstrated that the combined administration of CB1R antagonist SR141716A and the CB2 agonist O-1966 cause a significant reduction in infarct size in a MCAO/reperfusion model. This protective effects involves not only the CB2R but also the $5HT_{1A}$ receptors, implicating a possible interaction of cannabinoid derivatives with the serotoninergic receptors which could contribute to neuroprotective effects.

This data suggest that the synergism between some or all of these factors could explain, at least in part, why in absence of the cannabinoid receptors we observed a neuroprotective effect (Fig. 43). These results could also mean that, after a brain injury, there might be some compensation mechanisms in order to reduce the ischemic damage.

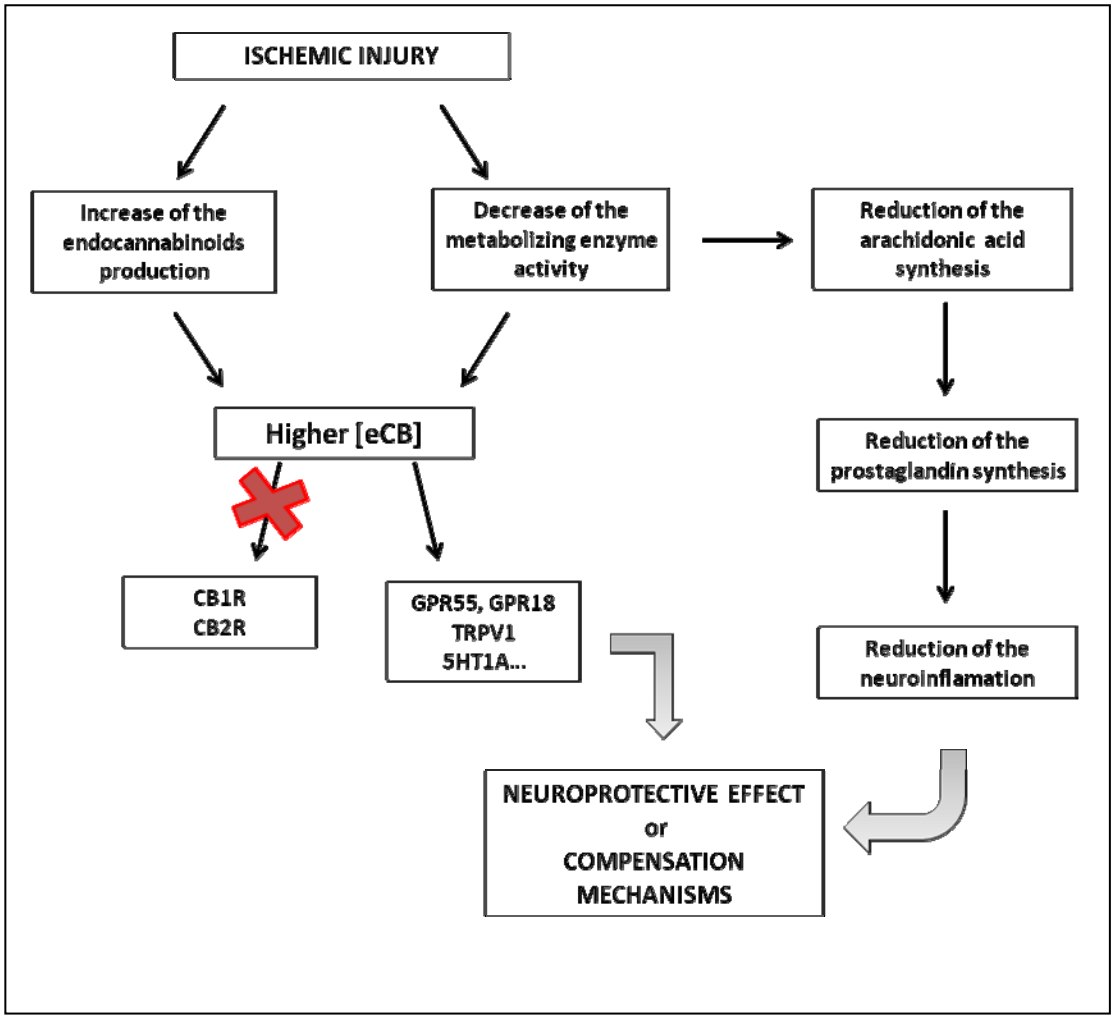

Fig. 43. Scheme of the possible mechanisms involved in the neuroprotective or compensation effect which occurs in absence of CB receptors.

8. REFERENCES

1. Katona and Freund, Annu. Rev. Neurosci. 2012; 35:529–58.
2. Matsuda LA et al. Nature 1990; 346:561–4.
3. Herkenham M al. 1990; 87:1932–6.
4. Glass M et al. Neuroscience 1997; 77 (2):299–318.
5. Munro S et al. 1993; 365: 61–5.
6. Ashton JC et al. Neurosci Lett 2006; 396 (2): 113–6.
7. Van Sickle M al. Science 2005; 310 (5746): 329–32.
8. Mukhopadhyay S et al. 2000; 57 (1): 162–70.
9. Mukhopadhyay S et al. Mol Pharmacol 2005; 67 (6): 2016–24.
10. Derkinderen P et al. J Neurosci 2003; 23 (6): 2371–82.
11. Di Marzo V et al. Nature 1994; 372: 686–91.
12. Schmid HH et al. Chem Phys Lipids 2000; 108(1–2): 71–87.
13. Devane WA et al. Science 1992; 258(5090): 1946–9.
14. Simon GM et al. J Biol Chem 2006; 281 (36): 26465–72.
15. Yu M et al. J Biol Chem 1997; 272: 21181–6.
16. Snider NT et al. Mol Pharmacol 2009; 75 (4): 965–72.
17. Dinh TP et al. Proc Nat Acad Sci USA 2002; 99: 10819–24.
18. Dinh TP et al. Mol Pharmacol 2004; 66 (5): 1260–4.
19. Acta Physiol 2012, 204, 267–276.
20. Alma Viso et al. Current Topics in Medicinal Chemistry, 2008; 8: 231-246.
21. Chem Bio Chem 2010; 11: 218-227.
22. T Bertrand et al. J. Mol. Biol. 2010; 396, 663-673.
23. Quistat et al. Tox. Appl. Pharm. 2011; 173: 48-55.
24. Quistat et al. Tox. Appl. Pharm. 2006; 211: 78-83.

25. Nomura K. et al. Nat. Chem. Bio. 2008; 4(6): 373-378.

26. Toxicology and Applied Pharmacology. Volume 211, Issue 1, 15 February 2006, 78–83.

27. Ferrarini et al. J. Het. Chem. 1983; 20: 1053-1058.

28. Lopez et al. J. Med. Chem. 2012; 55, 824–836.

28a. Cisneros, J.A. et al. J. Med. Chem. 2007; 50, 5012–5023.

29. Labar G. ChemBioChem 2010; 11, 218–227.

30. Lopez et al. J. Med. Chem. 2012; 55, 824–836.

31. Szabo et al. Bioorg. & Med. Chem. Letters. 2011; 21: 6782–6787.

32. Muccioli GG et al. Chembiochem. 2008; 9(16): 2704–10.

33. Chicca A. et al. British Journal of Pharmacology. 2012; 167: 1596–1608

34. Raduner et al. J Biol Chem. 2006; 281: 14192–14206. Gertsch et al. Proc Natl Acad Sci USA. 2008; 105: 9099–90104.

35. King et al., Br J Pharmacol. 2009; 157: 974–983.

36. Björklund et al., Br J Pharmacol. 2010;161: 1512–1526.

37. Long, J.Z. et al. Nature Chemical Biology. 2009; 5(1): 37-44.

38. Tamada T. et al. Trends Neurosci 1999; 22: 391-397.

39. Garcia JK and Kamijyo Y, J Neurop. Exp. Neurol 2006; 33: 408-421.

40. Liu Clark RK et al. Stroke 1994; 25:1481-1488.

41. Frontiers in Bioscience 2000; 5: 103-109.

42. Otto W. Witte et al. Neuromethods, vol. 47, chapter 7.

43. Natarajan V et al. Biochim Biophys Acta 1981; 664: 445–8.

44. Gorzalka BB et al. Neurosci Biobehav Rev. 2008.

45. Carrier EJ et al. Curr Drug Targets CNS Neurol Disord 2005; 4: 657–65.

46. Gebremedhin D et al. Am J Physiol 1999;276: 2085–93.

47. Chen Y et al. Circ Res 2000; 87: 323–7.

48. Wagner JA et al. Eur J Pharmacol 2001; 423: 203–10.

49. Rademacher DJ et al. Am J Physiol Heart Circ Physiol 2005; 288: H2694–701.

50. Sugiura T et al. Neurosci Lett 2001; 297: 175–8.

51. Baker et al., 2001. Eur J Pharmacol 2008; 586: 203–10.

52. Arevalo-Martin et al. Br J Pharmacol. 2008; 153:216–25.

53. Carrier et al. Curr Drug Targets CNS Neurol Disord. 2005; 4: 657–65.

54. Zhang et al. J Cereb Blood Flow Metab. 2007; 27(7): 1387–1396

55. Mauler et al. J Pharmacol Exp Ther. 2002; 302: 359–68.

56. Leker et al. Stroke 2003; 34: 2000–6.

57. Hayakawa et al. Life Sci. 2007; 80: 1466–71.

58. Zhang et al. Neuroscience. 2008; 152: 753–760.

59. Lipids in Health and Disease 2010; 9:47

60. Neurobiology of disease 2007; 27, 108-116

61. Journal of Neurochemistry, 2004; 88, 1159–1167

62. FEBS Journal. 2007; 274 :4464–4475.

63. Science. 2011, VOL 334.

64. Zhang et al. J Cereb Blood Flow Metab. 2012; 27(7): 1387–1396.

65. Lee et al. Surgical Neurology. 2007;67: 620– 625